NASA Contractor Report 4394

The NASA Aircraft Noise Prediction Program Improved Propeller Analysis System

L. Cathy Nguyen
Lockheed Engineering & Sciences Company
Hampton, Virginia

NASA

National Aeronautics and
Space Administration

Office of Management

Scientific and Technical
Information Program

1991

ABSTRACT

This report describes the improvements and the modifications of the NASA Aircraft

Noise Prediction Program (ANOPP) and the Propeller Analysis System (PAS).

Comparisons of the predictions and the test data are included in the case studies for the flat

plate model in the Boundary Layer Module, for the effects of applying compressibility

corrections to the lift and pressure coefficients, for the use of different weight factors in the

Propeller Performance Module, for the use of the improved retarded time equation solution,

and for the effect of the number of grids in the Transonic Propeller Noise Module. The

DNW tunnel test data of a propeller at different angles of attack and the Dowty Rotol data

are compared with ANOPP predictions. The effect of the number of grids on the Transonic

Propeller Noise Module predictions and the comparison of ANOPP TPN and DFP-ATP

codes are studied. In addition to the above impact studies, the transonic propeller noise

predictions for the SR-7, the UDF front rotor, and the support of the enroute noise test

program are included.

PRECEDING PAGE BLANK NOT FILMED

INTENTIONALLY BLANK

TABLE OF CONTENTS

1. Introduction

The NASA Aircraft Noise Prediction Program (ANOPP) Propeller Analysis System (PAS) is a set of computational modules for the prediction of the aerodynamics, performance, and noise of subsonic and transonic propellers. The theoretical manual for the ANOPP-PAS was published as NASA TM-83199, Part 3 in June 1986. This report documents the additions and improvements that have been made to the modules in this system.

Three additional functional modules are available in the ANOPP-PAS for the aerodynamic prediction analysis. They are the Improved Blade Shape Module (IBS), the Improved Blade Section Aerodynamics Module (IBA), and the Improved Blade Section Boundary Layer Module (IBL). These modules are modified versions of functional modules RBS, RBA, and BLM in the original system. The IBS module includes a revised blade geometry input format and an additional output table for the maximum thickness location and trailing edge thickness. The IBA module includes options to use compressibility corrections to compute section lift coefficients and local pressure coefficients. The IBL module includes an option to use a zero pressure gradient flat plate model to compute the boundary layer and a separation of section lift and drag coefficient output tables. Also, the boundary-layer thickness is added to the thickness table to match with the Rotor Broadband Noise Module (RBN) input table.

Modifications have also been made to some of the original functional modules in the ANOPP-PAS. The Transonic Propeller Noise Module uses a revised method for solving the retarded time equation. The Performance Module, the Propeller Loads Module, the

1

Subsonic Propeller Noise Module, and the Transonic Propeller Noise Module have been modified to include an option to use the output created by the improved blade aerodynamics modules, IBS, IBA, and IBL. A detailed theoretical description of the new functional modules and the revisions in each original functional module are presented in Chapter 2.

Impact studies on the changes to the ANOPP-PAS are documented in Chapter 3. The Subsonic Propeller Noise Comparison of the Flat Plate and the Integral Formulation Boundary Layer Models presents the thickness and loading noise for each model using test case AN5 for the "N" propeller from the FAA DNW Test (reference 1). The effects of different combinations of compressibility corrections for pressure loading and lift coefficients on total noise and the effect of using different weighing factors on the Propeller Performance Module are presented using test case AN5 for the "N" propeller from the FAA DNW Test. Loading noise comparisons were made using the output of both the original and improved blade aerodynamics modules and TPN with and without the new retarded time solver. Subsonic propeller noise predictions are made for the R212 propeller (NACA 16 series blade sections) and compared with the Dowty Rotol data (reference 2). In addition to the subsonic propeller noise study, the comparisons of ANOPP predictions and the FAA DNW test data are presented for the propellers at different angles of attack. Transonic propeller noise predictions are made to study the noise effect of the chosen number of grids. The chosen grid combinations are then used for the ANOPP TPN prediction and compared with the DFP-ATP (now called ASSPIN) predictions. Further use of the grid combinations is made in support of the SR-7 propeller, the UDF front rotor, and the enroute noise test program.

The conclusions from these validation studies are presented in the final chapter.

SYMBOLS

b   Joukowski transformation parameter, re R

C   chord length, re R

C_f skin friction coefficient

C_l section lift coefficient

C_{l_o} incompressible lift coefficient

C_∞ ambient speed of sound, m/s (ft/s)

C_p pressure coefficient

C_{p_c} corrected pressure coefficient

$C_{p_{lim}}$ limiting pressure coefficient

g   function defining blade surface S

M   local Mach number

M_∞ ambient Mach number

R   blade length measured from axis to tip, m(ft)

R_{inf} Reynold's number based on blade length, speed of sound, and kinematic viscosity

r_l leading edge radius, re C

R_n Reynold's number

t	time at which noise signal is received by observer, s
t_{max}	maximum thickness, re C
t_{te}	trailing edge bluntness, re C
U_∞	free stream velocity, m/s (ft/s)
x, y	surface coordinate, re C
x_t	maximum thickness location, re C
$x_{2, tr, \ell}$	lower trip location, re C
$x_{2, tr, u}$	upper trip location, re C
α	angle of attack, deg
δ	boundary layer thickness, re C
δ_1	displacement thickness, re C
δ_2	momentum thickness, re C
γ	ratio of specific heats
ν	kinematic viscosity, m^2/s (ft^2/s)
Ω	angular velocity of blade, rad/s
ϕ	solution of retarded time equation as solved by Newton's method $\Omega (\tau - t)$
ψ	blade surface elliptical radial coordinates, rad
τ	time at which noise signal is emitted at source position, s

ξ_1	spanwise surface coordinate, $0 \le \xi_1 \le 1$
ξ_2	chordwise surface coordinate, $0 \le \xi_2 \le 1$
$\xi_{2,s}$	leading edge stagnation point, rad

Subscripts

l	lower surface
te	trailing edge
tr	trip location
u	upper surface
∞	ambient

2. Functional Modules

2.1 Improved Blade Shape Module

INTRODUCTION

The Improved Blade Shape Module generates a functional representation of the airfoil surface using the same methods as the Blade Shape Module (reference 3), with input and output table modifications. The improved module incorporates a more concise blade section input table and produces an additional output table containing maximum thickness location and trailing edge thickness.

SYMBOLS

C	chord length, re R
R	blade length measured from axis to tip, m (ft)
t_{max}	maximum thickness, re C (η_2)
t_{te}	trailing edge bluntness, re C (η_2)
x,y	surface coordinates in complex z - plane
x_t	maximum thickness location, re C (η_2)

Subscripts:

ℓ	lower surface
u	upper surface

INPUT

This module requires a description of the airfoil surface using the same methods as the Blade Shape Module (reference 3).

Blade Section Table

The description of the airfoil is entered as a sequence of cross sections defined in a Cartesian coordinate system (reference 3). For each cross section, a description array containing the spanwise coordinate, leading edge abscissa, leading edge ordinate, chord length, leading edge radius, and number of (x,y) pairs on the upper and lower surfaces is entered. In the Improved Blade Shape Module, the first four entries in this description array are entered normalized with respect to blade length. If the (x,y) coordinates of the upper and lower surfaces of a cross section are not identical to the coordinates of the next cross section, then the (x,y) coordinates are entered directly after the description array. (i.e. upper and lower surface (x,y) coordinates for adjacent identical cross sections are not repeated.)

OUTPUT

The outputs for this module include all of the outputs produced by the Blade Shape Module (reference 3) and an additional table containing the maximum thickness location and the trailing edge thickness for each cross section.

Blade Thickness Table

ξ_1 array of spanwise coordinates, re R

$x_t(\xi_1)$ chordwise location where maximum thickness occurs, re $C(\xi_1)$

$t_{te}(\xi_1)$ thickness of the airfoil cross section at the trailing edge, re $C(\xi_1)$

METHOD

Maximum Thickness Location and Trailing Edge Thickness Table

The maximum thickness of an airfoil section is given by

$$t_{max} = (y_u - y_\ell)_{max}$$

The maximum airfoil thickness location x_t is the chordwise location where maximum thickness occurs. The trailing edge thickness t_{te} is the thickness of the airfoil cross section at the trailing edge (i.e. $x = 1$).

2.2   Improved Blade Section Aerodynamics Module

INTRODUCTION

The Improved Blade Section Aerodynamics Module is a modified version of the Blade Section Aerodynamics Module (reference 4).

The improved module includes the following modifications:

- The number of Fourier series terms used in evaluating the conformal mapping coefficients has been increased.

- An option to use the Glauert compressibility correction, the Karman-Tsien compressibility correction (reference 5), or no correction when computing the pressure coefficients has been added.

- An option to use the Glauert compressibility correction (reference 5) or no compressibility correction when computing the lift coefficient has been added.

- A limiting pressure coefficient check for high negative pressure coefficients based on the Carlson and Walkley method has been added (reference 6).

- Separate tables for the lift coefficients and stagnation points are produced.

SYMBOLS

C   chord length, re R

C_p pressure coefficient

C_{pc}	corrected pressure coefficient
$C_{p_{lim}}$	limiting pressure coefficient
C_{l_0}	incompressible lift coefficient
C_l	section lift coefficient
C_{p_0}	incompressible pressure coefficient
C_∞	ambient speed of sound, m/s (ft/s)
M_∞	ambient Mach number
M	local Mach number
R	blade length, m (ft)
R_n	Reynold's number
R_{inf}	Reynold's number based on blade length, sound speed, and kinematic viscosity
x_t	maximum thickness location, re C (η_2)
γ	ratio of specific heats
ν	kinematic viscosity, m^2/s (ft^2/s)
ξ_1	spanwise surface coordinate, $0 \le \xi_1 \le 1$
ξ_2	chordwise surface coordinate, $0 \le \xi_2 \le 1$

INPUT

This module requires the airfoil elliptical coordinates produced by the Improved Blade Shape Module (IBS) and arrays of Mach numbers and angles of attack. It requires all of the user parameters required by the Blade Section Aerodynamics Module (reference 4) and the following additional user parameters.

C_∞ ambient speed of sound, m/s (ft/s)

γ ratio of specific heats

R_{inf} Reynold's number, based on blade length, speed of sound, and kinematic viscosity

OUTPUT

This module produces the same output as the Blade Section Aerodynamics Module (reference 4) but creates a separate lift coefficient table and separate stagnation point table.

ξ_1 array of spanwise surface coordinates, $0 \leq \xi_1 \leq 1$

α array of angles of attack, deg

M array of Mach numbers

$C_\ell(\xi_1,\alpha,M)$ section lift coefficient

$\xi_{2,s}(\xi_1,\alpha,M)$ leading edge stagnation point, rad

11

METHOD

Coefficient of Pressure

Three options are now available for applying compressibility effects adjustments to the pressure coefficients C_p found from Bernoulli's equation (equation 26 in reference 4). The first option is to use equation 26 with no compressibility correction. The second option applies Glauert's pressure correction formula

$$C_p = \frac{C_{p_0}}{\sqrt{1 - M^2}} \tag{1}$$

where M in the equation is set at 0.7 if the actual Mach number is greater than 0.7, because the Glauert compressibility correction is not valid at Mach numbers greater than 0.7.

The third option applies the Karman-Tsien pressure correction formula (equation 27 in reference 4).

Limiting Pressure Coefficient

The limiting pressure coefficient is applied to replace extremely high negative pressure coefficients on the upper surface of an airfoil. The Reynold's number based on the maximum thickness location is

$$R_n = 2\, x_t\, C\, M_\infty\, R_{inf}$$

The relation of the limiting pressure coefficient, Mach number and Reynold's number is

12

$$C_{p_{lim}} = \frac{-2}{\gamma M_\infty^2} \left[\frac{R_n \times 10^{-6}}{R_n \times 10^{-6} + 10^e} \right]^E \tag{2}$$

where $\qquad e = 4 - 3M_\infty + 4(1 - M_\infty)^{15}$

and $\qquad E = 0.05 + .35 (1 - M_\infty)^2$

If the pressure coefficient is negative and less than $2C_{p_{lim}}$ then

$$C_{pc} = 2C_{p_{lim}}$$

The method for calculating the pressure coefficients continues as described for the Blade Section Aerodynamics Module (reference 4).

Coefficient of Lift

The coefficient of lift for the section is calculated as described in reference 4. There are now two options for applying compressibility effects adjustments to the lift coefficients C_l (equation 25 in reference 4). The first option is to use the lift coefficient with no compressibility correction, C_{lo}. The second option applies Glauert's compressibility correction formula

$$C_l = \frac{C_{lo}}{\sqrt{1 - M^2}}$$

where M in the equation is set at 0.7 if the actual Mach number is greater than 0.7, because the Glauert compressibility correction is not valid at Mach numbers greater than 0.7.

2.3   Improved Blade Section Boundary-Layer Module

INTRODUCTION

The Improved Blade Section Boundary-Layer Module is a modified version of the Blade Section Boundary-Layer Module (reference 7). The improved module computes the two-dimensional boundary-layer on airfoil sections using either the integral formulations for the boundary-layer thickness (reference 7) or the zero pressure gradient flat plate model (reference 8). The user-designated trip locations which locate the transition points are input in x coordinates normalized by chord length instead of the elliptical coordinates required by the original module. The improved module creates a separate table which contains the section drag coefficients.

SYMBOLS

b	Joukowski transformation parameter, re R
C	chord length, re R
C_f	skin friction coefficient
C_∞	ambient speed of sound, m/s (ft/s)
R	blade length, m (ft)
R_n	Reynold's number
r_l	leading edge radius, re C
U_∞	free stream velocity, m/s (ft/s)

14

x	chordwise transition point location, re C
$x_{2,tr,l}$	lower trip location, re C
$x_{2,tr,u}$	upper trip location, re C
ψ	blade surface elliptical radial coordinates, rad
δ	boundary-layer thickness, re C
δ_1	displacement thickness, re C
δ_2	momentum thickness, re C
ν	kinematic viscosity, m^2/s (ft^2/s)
ξ_1	spanwise surface elliptical coordinate, $0 \leq \xi_1 \leq 1$
ξ_2	chordwise surface elliptical coordinate, $0 \leq \xi_2 \leq 1$

Subscripts:

l	lower surface
tr	trip location
u	upper surface
∞	ambient

INPUT

This module requires the same input as the Blade Section Boundary-Layer Module (reference 7). If the trip locations are required, the x coordinates for the upper surface and the lower surface of the trip locations normalized by chord length are input.

ξ_1 array of spanwise surface coordinates, $0 \leq \xi_1 \leq 1$

$x_{2,tr,u}(\xi_1)$ upper trip location, re C

$x_{2,tr,\ell}(\xi_1)$ lower trip location, re C

OUTPUT

This module creates the same output as the Blade Section Boundary-Layer Module (reference 7). The section drag coefficients are stored in a separate table.

ξ_1 array of spanwise surface coordinates, $0 \leq \xi_1 \leq 1$

α array of angles of attack, deg

M   array of Mach numbers

$C_d(\xi_1,\alpha,M)$ profile drag coefficient

METHOD

Boundary-Layer Equation

There are two methods that may be used to compute the boundary-layer thickness: the integral formulations method described in reference 7 and the zero pressure gradient flat plate model.

Zero Pressure Gradient Flat Plate Model

For a zero pressure gradient flat plate model, the skin friction coefficients C_f increase with the distance from the leading edge x (normalized by chord length) and are computed

16

from the Reynold's number

$$C_f = 0.0576 \left(\frac{U_\infty x}{v}\right)^{-1/5} \tag{4}$$

or $\qquad C_f = 0.0576 \, (R_n \cdot x)^{-1/5}$

At the trailing edge, the turbulent boundary layer thickness

$$\delta(x) = 0.37 \left(\frac{U_\infty x}{v}\right)^{-1/5}$$

or $\qquad \delta(x) = 0.37 \, (R_n x)^{-1/5}$

the displacement thickness

$$\delta_1(x) = \frac{\delta(x)}{8}$$

and the momentum thickness

$$\delta_2(x) = \frac{7}{72} \delta(x)$$

are computed using the Reynold's number

$$R_n = \frac{U_\infty C}{v}$$

or $\qquad R_n = R_{inf} MC$

where $\qquad R_{inf} = \frac{C_\infty R}{v}$

Trip Locations in x Coordinates Normalized by Chord

For convenience, the trip locations are input in x coordinates normalized by chord

and converted to elliptic coordinates ξ_2.

With the input trip location in x coordinates normalized by chord and the assumption

that the initial elliptical radial coordinates are equal to 0, the elliptic coordinates are

17

computed using

$$x = (2b \cdot \cosh \psi \cdot \cos 2\pi \, \xi_2 + 2b + r_l \, /2)/C \qquad (5)$$

The new value of the elliptical radial coordinate is then interpolated for the calculated elliptic coordinate. The x coordinate is obtained using equation (5) and the whole procedure is repeated until the computed x coordinate is equal to the input trip location.

2.4   Transonic Propeller Noise Module

INTRODUCTION

The Transonic Propeller Noise Module has been modified to include an improved retarded time equation solution method developed by Dunn (reference 9). The module also includes an option to use the output from the original blade geometry and aerodynamics modules, RBS, RBA, and BLM or the improved blade geometry and aerodynamics modules, IBS, IBA and IBL.

SYMBOLS

g	function defining blade surface S
t	time at which noise signal is received by observer, s
τ	time at which noise signal is emitted at source position, s
ϕ	solution to retarded time equation as solved by Newton's method, $\Omega (\tau\text{-}t)$
Ω	angular velocity of blade, rad/s

METHOD

Roots of the Retarded Time Equation

The retarded time equation is written as

$$g\,(\phi) = A\phi^2 + B\phi + C + \cos\,(\phi + D) = 0 \qquad\qquad (6)$$

where $\phi = \Omega(\tau - t)$ and only the roots $(\phi/\Omega) < 0$ are of interest. In order to solve numerically for the roots by Newton's method, the number of roots and a close approximation for each root must be determined.

Step 1 - Define the interval $[\phi_0, \phi_1]$ containing all solutions (Bracket the roots):

Figure 1.1 illustrates that the roots of equation (6) are the points of intersection of the parabola $A\phi^2 + B\phi + C$ and the sinusoidal curve $-\cos(\phi + D)$. Since $|\cos(\phi + D)| \leq 1$, then the roots of g are bounded by the negative roots of $A\phi^2 + B\phi + C = \pm 1$, defined to be ϕ_0 and ϕ_1.

Step 2 - Determine the inflection points of g that lie in $[\phi_0, \phi_1]$:

Subintervals $[\phi_i, \phi_{i+1}]$ are formed by the endpoints and/or the adjacent inflection points in $[\phi_0, \phi_1]$. In each subinterval the curvature of g does not change sign, therefore g exhibits parabolic behavior.

The inflection points $\phi_i, \phi_{i+1} \ldots \phi_N$ are found by solving

$$g''(\phi) = 2A - \cos(\phi + D) = 0,$$
$$\phi = \begin{cases} \cos^{-1}(2A) - D \pm 2n\,\pi \\ -\cos^{-1}(2A) - D \pm 2m\,\pi \end{cases}, \ (\phi_0 \leq \phi \leq \phi_1), \ (n, m = 1, 2, 3 \ldots) \tag{7}$$

Step 3 - Determine the number of roots that exist in each subinterval $[\phi_i, \phi_{i+1}]$:

Several tests are made to determine if there are 1, 2, or no roots in each

subinterval $[\phi_i, \phi_{i+1}]$.

(1) if $g(\phi_i) \cdot g(\phi_{i+1}) = 0$ then check the end points of the interval $[\phi_i, \phi_{i+1}]$ for roots

   if $g(\phi_i) = 0$, there is a root at ϕ_i

   if $g(\phi_{i+1}) = 0$, then there is a root ϕ_{i+1}

(2) if $g(\phi_i) \cdot g(\phi_{i+1}) < 0$, then there is exactly one root in $[\phi_i, \phi_{i+1}]$

(3) if $g(\phi_i) \cdot g(\phi_{i+1}) > 0$, then more work has to be done to find roots in $[\phi_i, \phi_{i+1}]$:

   (a) if $g'(\phi) \cdot g'(\phi_{i+1}) > 0$, then there are zero roots in $[\phi_i, \phi_{i+1}]$, if not:

   (b) on $[\phi_i, \phi_{i+1}]$, $g(\phi)$ is approximated by a parabola, $p(\phi)$, with extreme point ϕ_{ext}^*

   (c) find the root of g' in $[\phi_i, \phi_{i+1}]$, ϕ_{ext}, by the hybrid Newton/Bisection method using ϕ_{ext}^* as the initial guess

   (d) if $g(\phi_{ext}) = 0$, then there is exactly one double root in $[\phi_i, \phi_{i+1}]$

   (e) if $g(\phi_i) \cdot g(\phi_{ext}) < 0$, then there are two roots in $[\phi_i, \phi_{i+1}]$:

      (i.e. 1 root in $[\phi_i, \phi_{ext}]$ and

      1 root in $[\phi_{ext}, \phi_{i+1}]$)

if $g(\phi_i) \cdot g(\phi_{ext}) > 0$ then no roots.

Step 4 - Determine an initial guess for each root:

If roots are detected in $[\phi_i, \phi_{i+1}]$, then $g(\phi)$ is approximated by a parabola $p(\phi)$, in the subinterval, and the roots of $p(\phi)$ are used as an initial guess for the roots of g.

Step 5 - Test each initial guess for stability in Newton's method:

Newton's method can be unstable if $\dfrac{dg}{d\phi}$ is small in some neighborhood of a root.

If $g'(\phi)$ is less than a given tolerance at the initial estimate of a root then the Bisection method is used to further refine the estimate.

Step 6 - Newton's method is used to determine the roots:

The roots of equation (6) are determined through an iterative process,

$$\phi_{n+1} = \phi_n - \frac{\left[A\phi_n^2 + B\phi_n + C + \cos\left(\phi_n + D\right)\right]}{\left[2A\phi_n + B - \sin\left(\phi_n + D\right)\right]}$$

which terminates when $|\phi_{n+1} - \phi_n|$ is smaller than a user-specified convergence criterion or if the number of iterations exceeds a limit set by the user.

2.5   Additional Modifications in ANOPP-PAS Functional Modules

The Propeller Performance Module (PRP), the Propeller Loading Module (PLD), the

Subsonic Propeller Noise Module (SPN), and the Propeller Trailing Edge Module (PTE)

each include an option to use the output from the original blade geometry and

aerodynamics modules, RBS, RBA, and BLM, or the output from the improved blade

geometry and aerodynamics modules, IBS, IBA, and IBL.

3. Impact Studies

3.1 Impact Study of Boundary Layer Models

Predictions using the Subsonic Propeller Noise Module for the test case AN5 from the FAA DNW test, as described in reference 1, were made with the following parameters:

Pitch Angle	=	20.8 deg
RPM	=	2700
Flow Velocity	=	77.0 m/s
Power	=	184.6 kW
Thrust	=	1907 N
Attitude Angle	=	0.0 deg
Flow Temp	=	16°C
Flow Pressure	=	99480 Pa
Flow Density	=	1.194 kg/m^3
Advance Ratio	=	0.2680
Angle of Attack	=	1.134 deg
Power Coefficient	=	0.0490
Thrust Coefficient	=	0.0463
Helical Tip Mach No.	=	0.8720

The "N" propeller, used in the FAA DNW test case, is the F8475 D-4 Hartzell, 2-bladed, 2.03 m diameter propeller with Clark Y airfoil sections, identical to the propeller used on the Piper Cherokee Lance aircraft, and has a thin round tip with a thickness ratio of 6.4 percent at the 3/4 radius position. The two observer coordinates are shown in figure 2.1 following the ANOPP convention and the DNW tunnel convention.

The predictions were made using both the flat plate zero pressure gradient boundary-layer model and the integral formulation boundary-layer model. The thickness noise and loading noise predictions using each model were compared. The predictions at two observer positions are presented in table 1. Figures 3.1 and 3.2 show comparisons of flat plate and integral formulation data with the DNW data. The results show that the predictions using the two models are almost identical and very good in comparison with the DNW data. The CPU times required for each of the two models in the Improved Boundary-Layer Module are quite different. On MicroVAX, the CPU times required for the execution of the Boundary-Layer Module using the integral formulation model is approximately about 30 minutes. Functional module IBL executes 70 times faster when using the flat plate model than it executes when using the integral formulation model. The results of this study indicate that the zero pressure gradient flat plate model can be used to decrease execution time with little or no loss of accuracy.

3.2   Impact Study of the Effects of Applying Compressibility Corrections to Pressure and Lift Coefficients

The Improved Blade Section Aerodynamics Module (IBA) has an option to include the effects of Mach number on the lift coefficients using the Glauert theories or to use the lift coefficient independent of Mach number. The variation of the pressure coefficients with Mach number can be expressed in terms of Glauert or Karman theories, or the pressure coefficient can be determined independent of Mach number. For Mach numbers greater than 0.7, the Glauert compressibility correction is not valid and the correction for 0.7 Mach number is used.

Predictions for test case AN5 using the "N" propeller from the DNW test were made for all possible option combinations. Table 2 provides a summary of the total noise predications made for two observer positions using the following option combinations:

CASE	Lift Coefficient	Pressure Coefficient
CASE A	CONSTANT (ICL=0)	CONSTANT (ICP=0)
CASE B	CONSTANT (ICL=0)	Glauert theory applied (ICP=1)
CASE C	CONSTANT (ICL=0)	Karman theory applied (ICP=2)
CASE D	Glauert theory applied (ICL=1)	CONSTANT (ICP=0)
CASE E	Glauert theory applied (ICL=1)	Glauert theory applied (ICP=1)
CASE F	Glauert theory applied (ICL=1)	Karman theory applied (ICP=2)

The two observer positions are at 60 ° and 90° polar directivity angles as shown in figure 2.1. Figure 4.1 and figure 4.2 show the total noise comparisons of the six cases and DNW data for the two observers. Figure 4.3 and figure 4.4 present the overall noise of observer 1 when the Glauert theory is used for the lift coefficients (figure 4.3) and no compressibility correction is used for the lift coefficients (figure 4.4). The same for observer 2 is shown in figure 4.5 and figure 4.6.

The Glauert compressibility correction applied to the lift coefficients provided lower noise levels compared to the results from using the lift coefficients independent of the Mach number (figures 4.3 and 4.4 for observer 1; figures 4.5 and 4.6 for observer 2). For the pressure coefficients, the Karman theory provided higher noise compared to the noise results from using the Glauert theory. The variation of pressure coefficients with Mach number may be expressed by either theory. The Karman correction is more accurate than the Glauert correction; however, it is more cumbersome in application.

3.3   Impact Study of the Propeller Performance Module

The Newton iteration method for the induced axial and tangential velocity components in the Propeller Performance Module did not always converge when Glauert compressibility correction was applied for the lift coefficient.

The following modifications of the Propeller Performance Module have been accomplished:

- The interval of the derivatives of the lift and drag coefficients with respect to the angle of attack and Mach number is reduced to a smaller interval (from 0.1 to 0.01) for better accuracy.

- The induced axial velocity component a_1 and the induced tangential velocity component a_2 are initialized for each spanwise station when originally a_1 and a_2 were initialized only for the first spanwise station.

- The weighting factor for the Newton iteration was initially set to 0.5 for the first iteration and set to 1.0 for the next iteration. Now the weighting factor is set as a user parameter and can be varied from 0.1 to 0.8 with a default value of 0.25.

The effect of using different weighting factors in the functional module is studied using the test case AN5 and "N" propeller for observer 1. Several weighting factors, wt, are used for the convergence of the induced velocity. The reference power coefficient, Cp, is 0.049. The thrust coefficient C_T, power coefficient Cp, efficiency η, and advanced ratio J values are listed in table 3 for comparison. Table 4 presents overall noise in dB for the use of different weighting factors.

28

The results show that the effects of the weighting factor are insignificant on the convergence of power and thrust coefficients and on the predicted noise levels. Therefore, the weighting factor can be varied for the convergence of Newton's iteration without affecting the results. Convergence has been achieved in problems with the Glauert compressibility correction applied to the lift coefficient.

3.4 Impact Study of the Improved Retarded Time Equation Solution

Predictions were done to study the effects of using the improved retarded time equation solution. The pressure coefficients in terms of Glauert and Karman theories were also used to provide variable test cases.

Predictions for the study used the SR-3 propeller which has 4 blades with a 45° tip sweep distribution tailored for noise reduction. It also showed the lowest noise level, about 5 decibels less than the straight-blade SR-2 at Mach 0.8 cruise, and yielded the highest propulsive efficiency, 78.7 percent - an improvement of approximately 3 percent over the straight-blade SR-2 (reference 10).

ANOPP coordinates for the two observers located just behind the disk plane in meters are as follows:

X_1	X_2	X_3	
0.806	0.00	-0.01	OBSERVER 1
0.806	0.00	-0.806	OBSERVER 2

The following prediction test case combinations were used:

Case	Pressure Coefficient	Retarded Time Equation Solution
A	Glauert theory applied	Old
B	Karman theory applied	Old
C	Glauert theory applied	New
D	Karman theory applied	New

and the following operating conditions:

Flight Mach Number, M_z = 0.80

Helical Tip Mach Number, M_h = 0.854

RPM   = 7878.4

The total noise results for the two observers are shown in table 5. There is less than a 0.5 dB difference in the first 6 harmonics comparing case A and case C of observer 1, a 1.5 dB difference in the seventh harmonic, and a 4 dB difference in the eighth harmonic. For other cases of the two observers, the results from using the old Transonic Propeller Noise Module (TPN) and from the modified TPN are identical. The solutions from the improved retarded time equation solution method have been successfully achieved in all demonstration problems.

Newton's method usually converges in 3 to 5 iterations. The example function is shown in figure 5.1. For the function which is flat as shown in figure 5.2 and has a first derivative as shown in figure 5.3, more than 10 iterations were required. Therefore, a call to the Bisection method was added before a call to Newton's method, and the number of permitted iterations was increased to 20 to solve for the flat functions.

3.5 A Comparison of ANOPP Predictions with Dowty Rotol Data

Predictions were made for the 4-bladed Dowty Rotol R212 propeller having NACA 16-series blade sections. The Improved Blade Shape Module (IBS), the Improved Blade Section Aerodynamic Module (IBA), the Improved Boundary-Layer Module (IBL), the Propeller Performance Module (PRP), the Propeller Loading Module (PLD), and the Subsonic Propeller Noise Module (SPN) were used for the predictions.

The propeller is 3.66 meters in diameter and the blade chord, thickness/chord ratio, and the blade twist distributions are show in figure 6.1. Predictions were done for the operating conditions as follows:

Parameter	Case 1	Case 2	Case 3
RPM	1250	1401	1400
Flow velocity, m/s	48	48	30
Power coefficient	.024	.036	.024
Thrust coefficient	.023	.044	.036
Helical Tip Mach	.71	.794	.787
3/4 span blade pitch, deg.	14.03	14.03	8.68

The near-field microphone is 2.44 m from the propeller hub and the far-field microphone is 5.49 m from the propeller hub.

The Dowty Rotol data were from experiments run in the RAE 24-foot anechoic wind tunnel (reference 2). Predictions are compared with the experimental data in figure 6.2 for case 1, figure 6.3 for case 2 where the near field and far field microphones are included, and figure 6.4 for case 3. Figure 6.2 shows the test case where the propeller helical tip

Mach number is moderate and the rpm is low. The first two harmonics show good agreement, and a difference of 4 dB is shown at higher harmonics. Only the first eight harmonics are presented since the data does not extend beyond the frequency of 672 Hz for this case. The overall agreement of prediction is good over the range of available experimental data. Figure 6.3 shows the case where the helical tip Mach number and rotational speed are higher than case 1. Agreement is good between experimental data and prediction across all harmonics. The third case has a higher propeller speed and a lower power coefficient than the first case. Figure 6.4 shows good agreement at lower harmonics and fair agreement at higher harmonics.

3.6   Impact Study of Propellers at Different Angles of Attack

Noise predictions were done using the Subsonic Propeller Noise Module (SPN) to study the effects of noise for a propeller at different angles of attack. The angles of attack are in terms of the propeller shaft inclination and are those from the nacelle axis which were tested in the DNW tunnel.

The "N" propeller was used for this test case. The two microphone positions at 60° and 90° polar directivity angles according to ANOPP convention, and the nacelle attitudes are shown in Figure 7.1.

The operating conditions for the DNW tunnel test cases are as follows:

Parameter	Case 1	Case 2	Case 3	Case 4	Case 5
RPM	2700	2700	2700	2700	2700
Flow velocity, m/s	77.3	76.9	77.2	77.0	77.3
Power, kW	152.1	145.9	151.6	149.9	154.9
Thrust, N	1500	1422	1432	1476	1530
Nacelle Attitude Angle, deg	0	-3.8	3.6	-7.4	7.3
3/4 span blade pitch, deg	19.9	19.9	19.9	19.9	19.9

The results are compared with the experimental DNW data. For the microphone at 90° polar directivity angle, figures 7.2 and 7.3 present the total noise at 0°, -3.8°, 3.6°, -7.4°, and 7.3° nacelle attitudes. Similarly, figure 8.1 and figure 8.2 present the total noise for the 60° polar directivity angle microphone at the same above nacelle attitudes. Case 1 is the case where the propeller shaft is at 0°. The agreement is good for the first six harmonics with the exception of the second harmonic where there is a slight overprediction for both mi-

crophones. For the 90° microphone, underprediction appears to be less than 3 dB for the higher harmonics. Furthermore, predictions seem to agree better with data for the 90° microphone than for the 60° microphone. Cases 2 and 4 are those where the propeller shaft is at -3.8° and -7.4°, respectively. In the above two cases for the 90° microphone, with the exception of overprediction for the second harmonic, the overall agreement is excellent for the first 13 harmonics. For higher harmonics, the agreement is still good for the -7.4° attitude, and less than 5 dB overpredicted for -3.8° attitude. For both the 60° and 90° microphones, the prediction and the DNW data are in good agreement. For the cases where the propeller shaft is at 3.6° and 7.8°, the DNW data are higher than the predictions for all harmonics for both microphone positions. This significant diference may due to the non-uniform inflow calculations which is not included in ANOPP. Further study needs to be done to determine the possible causes of this underprediction.

3.7 Impact Study of the Effect of the Number of Grids on Transonic Propeller Noise Module (TPN) Predictions

The pressure time history is affected by the number of propeller blade computation grid points and the number of time points per revolution. It is important that a large number of propeller grid points near the leading edge be used and enough time points be used to give sufficient accuracy of the pressure time history.

Sixteen combinations of propeller blade computation grids and number of time points per revolution were selected for the study as follows:

	Spanwise Stations	Chordwise Stations	Time Points			
Case 1	8	21	100	200	500	1000
Case 2	12	31	100	200	500	1000
Case 3	19	41	100	200	500	1000
Case 4	25	51	100	200	500	1000

The two observer coordinates were chosen as follows:

	X_1	X_2	X_3
Observer 1	3.06	0.0	0.833
Observer 2	3.06	0.0	0.000

The SR-7 propeller, one of the propellers used in the Advanced Turboprop Project (ATP), was used for these preliminary studies. This propeller is similar to the SR-3 but has less sweep (41° versus 45°). The flight conditions for this study were a Mach number of 0.8, a flight altitude of 35000 feet, and a propeller speed of 1692 RPM.

In order to determine the minimum required number of time points for accuracy, the first three harmonics of each observer with the four grid cases for each time point number were compared. Figures 9.1 to 9.3 and figures 10.1 to 10.3 show that for the time points of 500 and 1000, the difference in the total noise is insignificant. For the four cases, especially cases 1 and 2 where there are less propeller grid points, the same noise levels are produced. Therefore, the minimum required number of time points for the analysis was chosen to be 500.

A large number of propeller grid points in the regions where the blade is highly curved is recommended. In the combination grid cases, the difference in amplitude between cases 3 and 4 is fairly small compared to that between cases 1 and 2. Therefore, case 3, where there are 19 spanwise and 41 chordwise grid points, was selected as having the optimum number of grid points to save computation time.

3.8　The Comparison of ANOPP TPN and ASSPIN Codes

The ASSPIN code is the latest theoretical acoustic result for the transonic/supersonic sources developed by Mark H. Dunn, F. Farassat, and Sharon L. Padula (reference 9). For the noise comparison of the two codes, the same aerodynamic loads generated from Adamczyk's Euler code are used for input to ANOP TPN code. The propeller grid combination of 19 grid points for the span and 41 grid points for the chord with 500 time points was used for ANOPP TPN.

A comparison of the ANOPP TPN and the ASSPIN codes was done for the SR-7 at l=1 and k=1-20 grid points (figure 11.1). The flight conditions for this study are a Mach number of 0.8, a flight altitude of 35000 feet, and a propeller speed of 1692 RPM. The first harmonic of the ANOPP TPN and ASSPIN (figure 12.1) shows that the maximum difference of 1.5 dB is in the area behind the propeller plane. However, in figure 12.2, for the second harmonic, the noise from ASSPIN prediction is about 2 dB higher than the noise from ANOPP TPN in the area in front the propeller plane. The opposite effect is shown in the area behind the propeller. For the third harmonic, ASSPIN produces almost 5dB higher noise in the aft area of the propeller (figure 12.3). The noise difference seems to be greater at higher harmonics. Since there is not a great difference in the sound pressure level between ANOPP TPN and ASSPIN especially for the first harmonic, either ANOPP TPN or ASSPIN can be chosen for transonic noise prediction. Further study should be done for the noise comparison at higher harmonics.

3.9 Impact Study of the Improved TPN Using the SR-7 on the ATP and the UDF Front Rotor on the 727

The pressure amplitude and phase data for the exterior noise levels were computed using the ANOPP predictions. The area of interest was $k=5$ to 20 and $l=1$ to 10 (figure 11.1) for the SR-7. The predictions were used for input to the Propeller Aircraft Interior Noise (PAIN) program. A propeller grid having 19 grid points spanwise and 41 grid points chordwise combined with 500 time points was used for computation.

The grid is specified by coordinates x_1, x_2, and x_3 as shown in figure 11.1. The coordinate positions are then given by the following relations for $k=1,20$ and $l=1,10$:

$$x_1 = (r_p - a) = a \{1 - \cos [(l-1) \pi/18]\}$$

$$x_2 = -a \sin [(l-1) \pi/18]$$

$$x_3 = (\pi a/18) [k_p - k]$$

where

k_p is the k index of the grid point $(k, l) = (k_p, 1)$, that is, where the coordinate x_1 penetrates the fuselage

r_p is the radial distance from the center of the fuselage cylinder to the axis of rotation of the propeller

a is the radius of the fuselage

$$k_p = 8$$

$$r_p - 4.25615 \text{ m}$$

$$a = 1.1938 \text{ m}$$

The operating conditions were:

Flight Mach Number	Flight Altitude(ft)	Propeller RPM	Power Coefficient
0.8	35,000	1692	1.787
0.8	25,000	1777	1.560
0.5	15,000	1692	1.33

The refined grid, which is the mid-point of the space between the two grid points, is again used in the prediction for the first flight case.

The same grid point combination is used for the prediction of the UDF front rotor with the following flight conditions:

Flight Mach Number	Flight Altitude(ft)	Propeller RPM	Thrust lbf
0.8	35,000	1267.5	2100
0.72	35,000	1275	2100

The coordinate positions (figure 14.1) are given by the following relations for k=1 to 16 and l=1 to 10:

$$x_1 = r_p - a \cos[(l-1)\pi/18]\left[1 - \frac{z_p}{a}\cot\alpha\right]\left[1 + \frac{\pi}{18}(k_p - k)\cot\alpha\right]$$

$$x_2 = a \sin[(l-1)\pi/18]\left[1 - \frac{z_p}{a}\cot\alpha\right]\left[1 + \frac{\pi}{18}(k_p - k)\cot\alpha\right]$$

$$x_3 = (\pi a/18)\left[k_p - k\right]\left[1 - \frac{z_p}{a}\cot\alpha\right]$$

$$\alpha = \cos^{-1}(a/s_2)$$

where

r_p is the radial distance from the center of the fuselage cylinder to the axis of rotation of the propulser

a is the radius of the fuselage

40

s_2 is the meridian distance to the apex of the frustum

$$r_p = 3.3782 \text{ m}$$

$$a = 1.880 \text{ m}$$

$$z_p = 3.91 \text{ m}$$

$$s_2 = 9.40 \text{ m}$$

The first harmonics for the 3 cases of the SR-7 at $L = 1$ are shown in figure 13.1. Case 1, with a power coefficient greater than that of case 2, provides higher amplitude. Case 3, which is the subsonic case, has the lowest amplitude compared to cases 1 and 2. The overall predictions for case 1 (figure 13.2), case 2 (figure 13.3), and case 3 (figure 13.4) show that moving from $L = 1$ (closest to the propeller) to $L = 10$ (further away from the propeller), result in amplitude decreases in front the propeller plane. However, in the area aft of the propeller (starting at $k=12$), the amplitude increases going from $L = 1$ to 10.

For the UDF (figure 15.1) at longitudinal positions $k = 1$ to 9, the amplitude is low at $L = 1$ and progressively increases at $L = 10$. The trend is opposite from position $k = 9$ to the plane of the propeller and continues aft to $k = 13$. Aft of $k = 13$ the trend with changing L returns to that found forward of $k = 9$. Case 2 (figure 15.2) has the same trends with L as seen in figure 15.1 but shifted to different longitudinal positions.

The amplitude and phase trends seen in figures 15.1 and 15.2 have an impact on results from the Interior Noise Prediction Program (PAIN).

3.10   Impact Study from the Support of the Enroute Noise Test Program

Predictions of the PTA propfan noise to be used as input to the ray tracing propagation code were made. These predictions used the same propeller computation grid and the same number of time points per revolution as were used for the predictions of the PTA noise for the Propeller Interior Noise Program (PAIN) study.

The propeller speed is 1697.65 RPM for all of the following flight conditions:

Case	Altitude (ft) (Above Sea Level)	Mach Number	Power Coefficient
1	7,000	0.5	1.28
2	14,000	0.5	1.34
3	20,000	0.5	1.37
4	20,000	0.7	1.55
5	35,000	0.7	1.48

An atmospheric absorption table was built (using the ATM and ABS modules) with a reference altitude of 5,000 feet and 70% relative humidity for the White Sands standard day meteorological conditions. The flight altitudes were therefore set relative to the White Sands test level.

For each flight condition, the PTA propfan predictions were done for 25 observer positions starting at a polar directivity angle of 30° with 5° intervals and at a source-to-observer distance of 500 ft (figure 16.1).

The first and the second harmonics of the eight requested harmonics were examined for the above five cases as shown in figures 17.1 to 17.5. Cases 1, 2, and 3, where the flight Mach number was 0.5, provide smooth curves compared to cases 4 and 5, where the flight Mach number was 0.7. First harmonic noise comparisons for each of the five flight

42

conditions are presented in figure 18.1 and those for the second harmonic are presented in figure 18.2. For the first harmonic, the first three cases show very similar noise levels (figures 17.1, 17.2, and 17.3).

4. Example Problem

Usually, the predictions are made in two steps for the use of the subsonic propeller or in three steps for the use of the transonic propeller. If the computation requires a large number of chordwise and spanwise stations for the airfoil sections, a large number of grid points or observers, and a large number of time points per revolution; then the prediction should be made in three steps.

The first step is to build the blade library from the execution of IBS, IBA, and IBL as illustrated below:

```
CREATE GRID    $
UPDATE NEWU=GRID SOURCE=* $
   -ADDR OLDM=* NEWM=PSI FORMAT=4H*RS$ MNR=1 $
   0.0$
   -ADDR OLDM=* NEWM=XI2 FORMAT=4H*RS$ MNR=1 $
   0.0 0.0417 0.0833 0.1250 0.1667 0.2083 0.2500
   0.2917 0.3333 0.37509 0.41667 0.45804 0.50000
   0.54167 0.58333 0.62500 0.66667 0.70833 0.75000
   0.79167 0.83333 0.87500 0.91667 0.95833 1.00000 $
END* $
PARAM    IUNIT=2HSI   $
   CREATE GEOM $
   UPDATE NEWU=GEOM SOURCE=* $
   -ADDR NEWM=BLADE OLDM=* FORMAT=0 $
      10 $
      1,1,1,1,1,1,2,2 $
.3     -.0324  .1762  .340    6.85E-3  79.6   24    23 $
      1.000000  0.000000 $
      .990000    .002020 $
      .980000    .004044 $
         !
         !
         !
         !
         !
      .980000    .000660 $
      .990000    .000356 $
      1.000000  0.000000 $
.4     -.0571  .2159  .374    2.50E-3  75.2   24    23 $
      1.000000  0.000000 $
      .990000    .001677 $
      .980000    .003347 $
```

44

```
          !
          !
          !
          !
          !
    .980000      .001357 $
    .990000      .000699 $
   1.000000     0.000000 $
.5  -.0806  .2350  .400     9.42E-4   71.0   50     49 $
   1.000000      .000000 $
    .990000      .002505 $
    .980000      .004825 $
          !
          !
          !
          !
          !
    .980000     -.000152 $
    .990000     -.000144 $
   1.000000     -.000000 $
.6  -.0874  .2054  .4       5.63E-4   66.9   50     49 $
   1.000000      .000000 $
    .990000      .002210 $
    .980000      .004265 $
          !
          !
          !
          !
          !
    .980000      .000407 $
    .990000      .000150 $
   1.000000     -.000000 $
.7 -.0730  .1438      .376  3.29E-4   63.1   50     49 $
   1.000000      .000000 $
    .990000      .001972 $
    .980000      .003814 $
          !
          !
          !
          !
          !
    .980000      .000855 $
    .990000      .000386 $
   1.000000     -.000000 $
.8  -.0350  .0588  .332     2.36E-4   59.2   50     49 $
   1.000000      .000000 $
    .990000      .001852 $
    .980000      .003588 $
          !
          !
          !
          !
          !
    .980000      .001080 $
```

```
         .990000     .000506 $
        1.000000    -.000000 $
  .85   -.0066  .0106  .304    2.15E-4   57.9    50      49 $
  .9    .0312   -.0468  .258   2.15E-4   56.3    50      49 $
        1.000000     .000000 $
         .990000     .001822 $
         .980000     .003531 $
            !
            !
            !
            !
            !
         .980000     .001136 $
         .990000     .000536 $
        1.000000    -.000000 $
  .95   .0748   -.1063  .204   1.95E-4   54.9    50      49 $
  .99   .1143   -.1568  .154   1.95E-4   53.9    50      49 $
        1.000000     .000000 $
         .990000     .001792 $
         .980000     .003474 $
            !
            !
            !
            !
            !
         .980000     .001192 $
         .990000     .000566 $
        1.000000    -.000000 $
    END* $


EXECUTE IBS   $
PARAM IPRINT=3  NORDER=4   $
PARAM ICL=0       $ NO  COMPRESSIBILITY CORRECTION FOR
                  $ LIFT COEFFICIENT
PARAM ICP=2       $ KARMAN COMPRESSIBILITY CORRECTION
$  FOR PRESSURE COEFFICIENT
CREATE IBA   $
UPDATE NEWU=IBA   SOURCE=*   $
-ADDR NEWM=MACH   OLDM=*  FORMAT=4H*RS$    MNR=1$
     .1  .3  .5  .7  .9  $
-ADDR NEWM=ALPHA   OLDM=*  FORMAT=4H*RS$    MNR=1  $
     -1.  1.  3.     $
   END* $
PARAM CA = 309.7073 $  SPEED OF SOUND IN M/S
PARAM VNU = .000028026   $  VISCOSITY IN M**2/S
PARAM B = 1.3716         $  BLADE LENGTH IN M
EVALUATE  RINF = CA*B/VNU $
EXECUTE IBA   $
$
$

EXECUTE IBL     $
UNLOAD /SR3LIB1/    $
PARAM ICL=1    ICP=2   $ GLAUERT CORRECTION FOR LIFT,
                       $ KARMAN CORRECTION FOR PRESSURE
```

```
EXECUTE IBA $
EXECUTE IBL $
UNLOAD / SR3LIB2 / $
ENDCS $
```

- The second step is to use the libraries built in the first step to build the Loads

library for the noise calculation.

```
LOAD/SR3LIB1 / $ LOAD IN THE GEOM LIBRARY BUILT IN THE FIRST STEP
PARAM EPSILON=0.01                      $ ERROR CRITERION FOR
$                                         STOPPING THE ITERATION
$                                         ON THE INDUCED ANGULAR
$                                         AND AXIAL VELOCITIES
PARAM OPTION=1, UNIFORM=.TRUE.          $ OPTION, METHODOLOGY
$                                         OPTION
$                                         = 0:BLADE ELEMENT-
$                                              MOMENTUM THEORY
$                                         = 1:PRANDTL TIP RELIEF
$                                              CORRECTION
$                                         UNIFORM, INFLOW OPTION
$                                              = TRUE :UNIFORM INFLOW
$                                                      SPECIFIED BY MZ
$                                              = FALSE:RADIALLY VARYING
$                                                      INFLOW SPECIFIED
$                                                      BY RBF(FLOW)
     PARAM IMPROV = .TRUE. $ FLAG TO USE THE IMPROVED VERSION
                           $ OF ANOPP
CREATE GRIDA  $
UPDATE NEWU=GRIDA SOURCE=*  $
-ADDR NEWM=PSI OLDM=* FORMAT=4H*RS$ $
     0.0  $
-ADDR NEWM=XI1 OLDM=* FORMAT=4H*RS$  MNR=1  $
     .300   .3380  .4334  .4669
     .5004 .5980 .6956  .7337  .7718  .8060
     .8402 .8706 .9010  .9277  .9544  .9772   .99  $
-ADDR NEWM=XI2 OLDM=* FORMAT=4H*RS$ MNR=1   $
     .0000   .0933  .1602  .2337  .2836  .3225  .3536  .3789
     .3940   .4002  .4186  .4267  .4348  .4421  .4494  .4562
     .4629   .4693  .4757  .4819  .4880  .4940  .5000  .5060
     .5120   .5182  .5243  .5307  .5371  .5439  .5506  .5652
     .5814   .6211  .6464  .6775  .7164  .7663  .8302  .9096
     1.000 $
     END* $
  $
     PARAM B=1.3716,IUNITS=2HSI IPRINT=3  $
     PARAM ALPHAP = 0.              $ SET PROPELLER ANGLE OF
                                    $ ATTACK IN DEGREES
     PARAM  IDPDT = 0               $ PROPELLER LOADING IS STEADY
     PARAM BETA75 = 60.31           $ INITIAL GUESS FOR PROPELLER
                                    $    3/4 SPAN
```

```
                                    $  PITCH ANGLE IN DEGREES
       PARAM      RPM = 1777.       $  PROPELLER RPM
       PARAM NBLADE = 4             $  NUMBER OF PROPELLER BLADES
       PARAM     ORIG = 61.15       $  BLADE TWIST FROM ROOT TO 3/4
                                    $     SPAN
       EVALUATE RHOA=.149616E-2*32.1726*16.02 $ DENSITY IN KG/M**3
       PARAM IUNITS = 2HSI          $  SI UNITS
       PARAM IPRINT = 3             $  REQUEST INPUT AND OUTPUT
                                    $     PRINT
       $
       $   EVALUATE CONTROL STATEMENTS ARE USED TO COMPUTE
       $   ADDITIONAL REQUIRED QUANTITIES
       $
       $


       EVALUATE     RPS = RPM / 60.
                             $   COMPUTE REVOLUTIONS PER SECOND
       PARAM          PI = 3.1415926
                             $   SET VALUE OF PI
       PARAM CPREF = 1.56       $
       EVALUATE    BETA = BETA75 - ORIG
                             $   COMPUTE ROOT PITCH IN DEGREES
       EVALUATE THETAR = BETA * PI / 180.
                             $   CONVERT ROOT PITCH TO RADIANS
       EVALUATE ALPHAP = ALPHAP * PI / 180.
                             $   CONVERT PROPELLER ANGLE OF
                             $   ATTACK TO RADIANS
       PARAM       CA = 309.70728
                             $   SPEED OF SOUND IN M/S
       PARAM          VF = 247.766
                             $   VELOCITY IN M/SEC
       EVALUATE     MZ = VF / CA
                             $   COMPUTE FORWARD MACH NUMBER
       EVALUATE   OMEGA = 2. * PI * RPS
                             $   COMPUTE ANGULAR VELOCITY
       EVALUATE MACHRF = B * OMEGA / CA
                             $   COMPUTE ROTATIONAL TIP MACH
                             $   NUMBER
       $
       $   ADDITIONAL OUTPUT CONTROL PARAMETERS ARE
       $
       $
       $

$ THE 3/4 SPAN BLADE PITCH MUST BE ADJUSTED SO THAT THE
$ COMPUTED POWER COEFFICIENT MATCHES THE MEASURED
$ POWER.   THIS REQUIRE AN ITERATIVE SOLUTION OF THE
$ PROPELLER PERFORMANCE (PRP) MODULE.   THE SECANT
$ METHOD IS USED TO FIND THE ROOT TO THE EQUATION F(Z) =
$ CPREF - CP.   CONVERGENCE IS ASSUMED COMPLETE WHEN THE
$ COMPUTED VALUE IS WITHIN ONE PERCENT OF THE MEASURE
$ VALUE.
$
$
```

```
 PARAM Z1 = THETAR $
 EXECUTE PRP  GRID=GRIDA    $
 EVALUATE FZ1 = CPREF - CP $
 EVALUATE THETAR = THETAR + PI / 180. $
 PARAM Z2 = THETAR $
 PARAM COUNT = 1 $
LAB1 CONTINUE $
 EXECUTE PRP  GRID=GRIDA    $
 EVALUATE FZ2 = CPREF - CP $
 EVALUATE DIFF = FZ2 / CPREF $
 EVALUATE DIFF=ABS(DIFF)    $
      EVALUATE COUNT = COUNT + 1 $
      IF ( DIFF .LT. 0.01 ) GOTO LAB2 $
      EVALUATE Z = Z2 - FZ2 * ( Z2 - Z1 ) / ( FZ2 - FZ1 ) $
      PARAM Z1 = Z2 $
      PARAM Z2 = Z $
      PARAM FZ1 = FZ2 $
      PARAM THETAR = Z $
      EVALUATE COUNT = COUNT + 1 $
      IF ( COUNT .GT. 10 ) GOTO LAB3 $
      GOTO LAB1 $
LAB2 CONTINUE $
 EXECUTE PLD  GRID=GRIDA    $
LAB3 CONTINUE   $
 UPLIST   $
 UNLOAD /PRPLIB1/  PLD   $
```

• Finally, the third step is where the noise is calculated. The blade geometry library

which is built in the first step and the load library which is built in the second step are used

in this step as shown:

```
      LOAD /SR3LIB1/   $
      LOAD /PRPLIB1/   $
      PARAM IMPROV=.TRUE. $
      EVALUATE Z = 25000.*0.3048    $
      EVALUATE RHOA = .106626E-2 * 32.1726 * 16.02   $
      PARAM PI=3.1415926, REV=1777.,IPRINT=3 $
      EVALUATE CA=1016.10 * .3048    $
      EVALUATE OMEGA=2. *PI * REV / 60.   $
      PARAM MZ = 0.8 $
      EVALUATE B=4.5 * 0.3048    $
      EVALUATE MACHRF = B * OMEGA / CA $
      PARAM THETAR=0.0, EPSILON=0.001, NBLADE=4 $
         CREATE TPN $
             UPDATE NEWU=OBSERV SOURCE=*   $
               -ADDR NEWM=COORD OLDM=* FORMAT=4H3RS$ $
                     3.34      -.77     1.46    $
                           END* $
   $
```

```
$        BLADE SECTIONS USE A GRID WITH EXTRA POINTS NEAR
$            THE LEADING EDGE (IE   WHERE XI2 = PI    )
$
         CREATE GRIDA$
    UPDATE   NEWU=GRIDA   SOURCE=*    $
         -ADDR   OLDM=GRID(XI1) $
         -ADDR   OLDM=GRID(PSI) $
         -ADDR     NEWM=XI2 OLDM=* FORMAT=4H*RS$ MNR=1 $
    0.0000 0.0933 0.1602 0.2337 0.2836 0.3225 0.3536 0.3789
    0.4002 0.4186 0.4348 0.4494 0.4629 0.4757 0.4880 0.5000
    0.5120 0.5243 0.5371 0.5506 0.5652 0.5814 0.5998 0.6211
    0.6464 0.6775 0.7164 0.7663 0.8302 0.9096 1.0000   $
         END* $
$
         PARAM  PSIO=0., NT=200   $
         PARAM NTIME = 500 $
         PARAM NHARM=8,  IPRES=1   $
         PARAM TRANS=0.98,FRACDT=1.0 $
$
         EXECUTE TPN        GRID=GRIDA $
```

If the job is small and there is no need to reuse the blade geometry library and load

library then the second and the third step can be combined, or all three steps can be

combined into one job.

5. Conclusions

The modified version of ANOPP contains three additional modules which are improved versions of the Blade Shape Module (IBS), the Rotating Blade Aerodynamic Module (IBA), and the Boundary-Layer Module (IBL). In addition, the Propeller Performance Module, the Propeller Loading Module, and the Subsonic Propeller Noise Module have been modified and improved.

For the Blade Shape Module, there is no repetition for airfoil sections with the same coordinates. For the Rotating Blade Aerodynamic Module, more options are available for the compressibility correction of the lift and the pressure coefficients. For the Boundary-Layer Module, the addition of the flat plate model option provides no loss in accuracy and less amount of computation time. Due to the modification of the Propeller Performance Module, the convergence of the Newton method in the Propeller Performance Module is fairly rapid, including the case where the Glauert theory is applied for the lift coefficient. As a result, the Propeller Loading Module, the Subsonic Propeller Noise Module, and the Transonic Propeller Noise Module with the changed retarded time solver work properly now.

Besides having more options, the improved version of ANOPP can also give the same results as the original version if the compressibility correction of the lift coefficient is set to 0, and that of the pressure coefficient is set to 2.

The study comparing the predictions of the improved version of ANOPP, the old version of ANOPP, and the available test data shows good agreement between predictions and test data. Therefore, the improved version of ANOPP should be used to save execution time when necessary with no loss in accuracy.

References

1. Dobrzynski, W. M.; Heller, H. H.; Powers, J. O.; and Densmore, J. E. : DFVLR/FAA Propeller Noise Tests in the German-Dutch Wind Tunnel DNW. Executive Data Report No. AEE 86-3, 1986.

2. Trebble, W. J. G. : Investigation of the Aerodynamic Performance and Noise Characteristics of a Dowty Rotol R212 Propeller at Full-Scale in the 24-foot Wind Tunnel. Aeronautical Journal, June/July 1987, pp.275-284.

3. Rawls, John W., Jr. : 10.2 Blade Shape Module. Aircraft Noise Prediction Program Theoretical Manual - Propeller Aerodynamics and Noise, William E. Zorumski and Donald S. Weir, eds., NASA TM-83199, Part 3, June 1986, pp. 10.2-1 - 10.2-25.

4. Zorumski, William E. : 10.3 Blade Section Aerodynamics Module. Aircraft Noise Prediction Program Theoretical Manual - Propeller Aerodynamics and Noise, William E. Zorumski and Donald S. Weir, eds., NASA TM-83199, Part 3, June 1986, pp. 10.3 - 1 10.3-13.

5. Dommasch, E. E. et al, : Airplane Aerodynamics, Third Edition. Pitman Publishing Corporation, 1961.

6. Carlson, H. W. and Walkely, K. B. : An Aerodynamic Analysis Computer Program and Design Notes for Low Speed Wing Flap Systems. NASA CR3675, March 1983.

7. Weir, Donald S. : 10.4 Blade Section Boundary-Layer Module. Aircraft Noise Prediction Program Theoretical Manual - Propeller Aerodynamics and Noise, William E. Zorumski and Donald S. Weir, eds., NASA TM-83199, Part 3, June 1986, pp. 10.4-1 — 10.4-18.

8. Schlichting, Herman (J. Kestin, transl.): Boundary-Layer Theory, Seventh Edition. McGraw-Hill Book Co., 1979.

9. Dunn, M. H. and Tarkenton, G. M.: User's Manual for the Langley High Speed Propeller Noise Prediction Program (DFP-ATP). NASA CR-4208, January 1989.

10. Hager, R. D. and Vrabel, D.: Advanced Turboprop Project. NASA SP-495, 1988.

Table 1. Subsonic Propeller Noise Comparison of the Zero Pressure Gradient Flat Plate and the Integral Formulations for the Boundary-Layer of Thickness Models

OBSERVER 1 - $\theta = 90°$, $\phi = 0°$, r = 4 m

OBSERVER 2 - $\theta = 60°$, $\phi = 0°$, r = 4 m

| | OBSERVER NUMBER 1 | | | | OBSERVER NUMBER 2 | | | |
| | FLAT PLATE | | NON-FLAT PLATE | | FLAT PLATE | | NON-FLAT PLATE | |
HARMONIC NUMBER	THICKNESS NOISE dB	LOADING NOISE dB	THICKNESS NOISE dB	LOADING NOISE dB	THICKNESS NOISE dB	LOADING NOISE dB	THICKNESS NOISE dB	LOADING NOISE dB
1	104.02	115.23	104.02	114.98	101.10	110.68	101.10	110.89
2	108.40	114.51	108.40	114.25	103.41	109.86	103.41	110.06
3	109.79	112.96	109.79	112.68	102.82	107.96	102.82	108.13
4	110.19	111.24	110.19	110.96	101.32	105.53	101.32	105.69
5	110.14	109.49	110.14	109.21	99.40	102.82	99.40	102.96
6	109.81	107.75	109.81	107.47	97.23	99.93	97.23	100.06
7	109.28	106.02	109.28	105.75	94.87	96.92	94.87	97.05
8	108.60	104.30	108.60	104.03	92.38	93.83	92.38	93.94
9	107.80	102.59	107.80	102.33	89.77	90.67	89.77	90.77
10	106.90	100.88	106.90	100.64	87.06	87.45	87.06	87.55
11	105.91	99.17	105.91	98.95	84.26	84.19	84.26	84.27
12	104.84	97.47	104.84	97.26	81.37	80.88	81.37	80.95
13	103.69	95.76	103.69	95.58	78.40	77.53	78.40	77.59
14	102.46	94.06	102.46	93.90	75.35	74.15	75.35	74.19
15	101.17	92.35	101.17	92.22	72.22	70.73	72.22	70.77
16	99.81	90.64	99.81	90.54	69.01	67.29	69.01	67.31
17	98.39	88.93	98.39	88.87	65.72	63.82	65.72	63.84
18	96.89	87.22	96.89	87.19	62.35	60.34	62.35	60.34
19	95.33	85.50	95.33	85.51	58.89	56.85	58.89	56.84
20	93.69	83.79	93.69	83.82	55.35	53.35	55.35	53.34

Table 2. Subsonic Propeller Noise Comparison from the use different theories for the computations of Lift and Pressure Coefficients: Karman-Tsien (ICL=2, ICP=2), Glauert (ICL=1,ICP=1), and Independent of Mach number (ICL=0, ICP=0).

	ICL = 0 ICP = 0 CASE A	ICL = 0 ICP = 0 CASE B	ICL = 0 ICP = 2 CASE C	ICL = 1 ICP = 0 CASE D	ICL = 1 ICP = 1 CASE E	ICL = 1 ICP = 2 CASE F	DNW Data
HARMONIC NUMBER	OBSERVER 1	$\theta = 90°$,	$\phi = 0°$,	$r = 4m$			
1	112.150	114.210	115.430	110.400	112.330	113.380	115.0
2	112.370	114.070	115.390	111.170	112.610	113.670	113.1
3	112.020	113.330	114.620	111.230	112.240	113.190	115.1
4	111.570	112.540	113.710	111.030	111.730	112.530	113.5
5	111.030	111.750	112.770	110.660	111.150	111.800	113.2
6	110.410	110.940	111.810	110.150	110.500	111.010	111.2
7	109.690	110.100	110.830	109.510	109.770	110.150	113.0
8	108.890	109.200	109.800	108.760	108.950	109.230	110.0
9	108.000	108.240	108.730	107.900	108.050	108.240	109.9
10	107.040	107.220	107.610	106.960	107.070	107.190	109.4
11	105.990	106.130	106.440	105.940	106.010	106.070	107.3
12	104.880	104.980	105.210	104.830	104.890	104.890	106.3
13	103.690	103.770	103.930	103.660	103.690	103.650	106.2
14	102.440	102.490	102.600	102.410	102.430	102.340	102.7
15	101.120	101.150	101.200	101.100	101.100	100.960	103.1
16	99.740	99.750	99.750	99.710	99.700	99.530	102.0
17	93.290	98.280	98.230	98.260	98.240	98.020	99.5
18	96.770	96.750	96.650	96.740	96.700	96.440	97.8
19	95.180	95.140	95.000	95.140	95.090	94.790	97.3
20	93.510	93.470	93.270	93.480	93.410	93.060	95.7

	CASE A	CASE B	CASE C	CASE D	CASE E	CASE F	DNW Data
	OBSERVER 2	$\theta = 60°$,	$\phi = 0°$,	$r = 4m$			
1	107.350	109.170	111.850	106.180	107.730	109.910	111.9
2	107.210	108.690	111.250	106.410	107.600	109.550	108.2
3	105.650	106.940	109.380	105.100	106.100	107.890	109.0
4	103.530	104.660	107.000	103.180	104.050	105.710	106.2
5	101.160	102.140	104.340	100.980	101.740	103.260	104.4
6	98.620	99.480	101.520	98.590	99.270	100.650	100.0
7	95.970	96.710	98.590	96.070	96.670	97.930	101.1
8	93.230	93.860	95.570	93.440	93.980	95.110	100.0
9	90.410	90.940	92.480	90.710	91.200	92.230	93.9
10	87.510	87.960	89.320	87.910	88.350	89.270	94.4
11	84.550	84.910	86.100	85.020	85.420	86.240	91.9
12	81.520	81.810	82.810	82.060	82.430	83.160	85.5
13	78.410	78.640	79.460	79.030	79.360	80.010	85.4
14	75.240	75.400	76.050	75.930	76.230	76.810	82.0
15	72.000	72.100	72.570	72.750	73.030	73.530	78.1
16	68.680	68.720	69.010	69.500	69.760	70.200	76.2
17	65.290	65.270	65.380	66.180	66.410	66.790	80.5
18	61.810	61.730	61.660	62.770	62.990	63.310	72.6
19	58.240	58.110	57.850	59.280	59.480	59.760	65.4
20	54.580	54.390	53.930	55.710	55.890	56.130	70.3

Table 3. Power Coefficients C_p, Thrust Coefficients C_T, Advanced Ratio J, and Efficiency η at Variable Weighting Factors

wt.	0.25	0.3	0.4	0.5	0.6	0.7	0.8
C_p	0.0490039	0.0490023	0.0490006	0.0490060	0.0490076	0.0490083	0.0490083
C_T	0.0496741	0.0496339	0.0495821	0.0495703	0.0495497	0.0495405	0.0495358
J	0.843905	0.843905	0.843905	0.843905	0.843905	0.843905	0.843905
η	0.855446	0.854782	0.853920	0.853623	0.853240	0.853069	0.852989
No. of Iterations	3	3	3	3	3	3	3

Table 4. Overall Noise Comparison for the Use of Variable Weighting Factors

Wt = .25	Wt = .3	Wt = .4	Wt = .5	Wt = .6	Wt = .7	Wt = .8
115.38	115.39	115.40	115.40	115.41	115.41	115.41
115.36	115.36	115.37	115.37	115.38	115.38	115.38
114.59	114.59	114.60	114.60	114.60	114.60	114.60
113.68	113.68	113.69	113.69	113.70	113.70	113.70
112.75	112.75	112.76	112.76	112.76	112.76	112.76
111.79	111.79	111.80	111.80	111.80	111.81	111.81
110.81	110.81	110.81	110.81	110.82	110.82	110.82
109.78	109.78	109.79	109.79	109.79	109.79	109.79

Table 5. Transonic Propeller Noise (dB) Comparison of the Old and Improved Retarded Time Equation Solutions

Harmonic Number	OLD Case A	Case B	NEW Case C	Case D
Observer 1 ($x_1 = .806$ m, $x_2 = 0.0$ m , $x_3 = -0.01$m)				
1	142.63	143.45	142.59	143.45
2	128.66	130.61	128.69	130.61
3	117.54	118.79	117.62	118.79
4	124.07	124.86	124.22	124.86
5	116.24	117.58	116.16	117.58
6	116.18	114.90	116.28	114.90
7	106.50	105.99	108.44	105.99
8	107.29	102.56	103.33	102.56
Observer 2 ($x_1 = .806$ m, $x_2 = 0.0$ m , $x_3 = -.806$ m)				
1	137.46	138.29	137.46	138.29
2	129.65	130.47	129.65	130.47
3	122.64	123.44	122.64	123.44
4	116.38	117.12	116.38	117.12
5	110.29	110.99	110.29	110.99
6	104.99	105.57	104.99	105.57
7	101.37	101.83	101.37	101.83
8	96.72	97.17	96.72	97.17
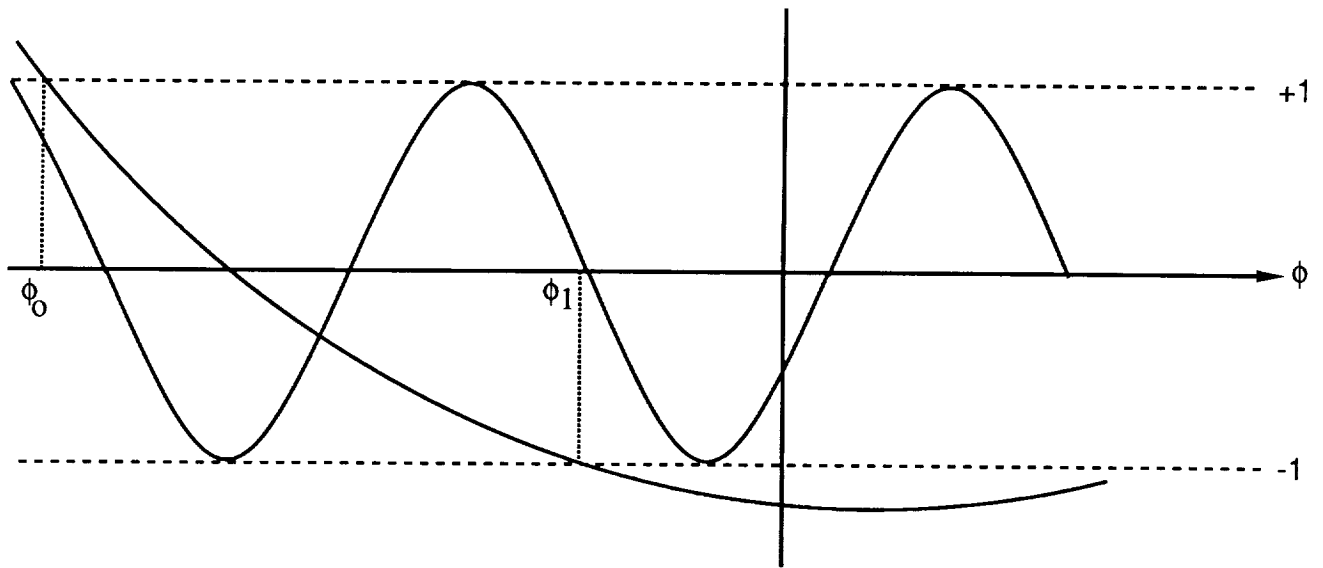
Figure 1.1 Example of the roots of the retarded time equation
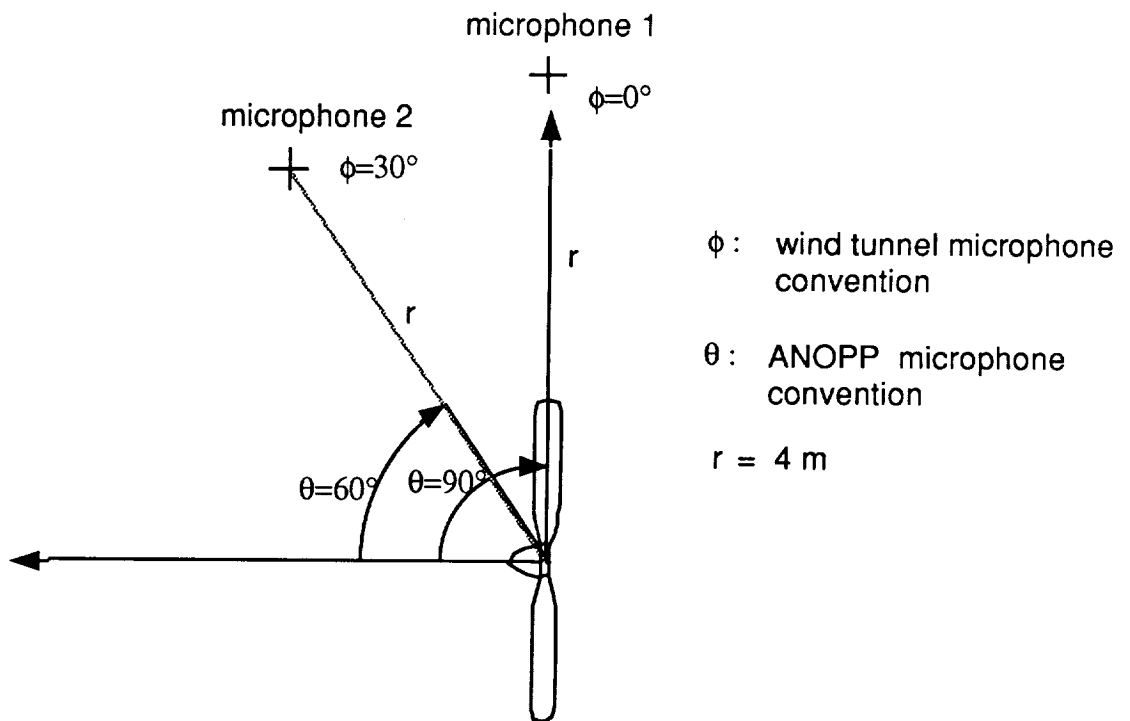
Figure 2.1 ANOPP microphone convention and DNW microphone convention for the
test case AN5 and N propeller.
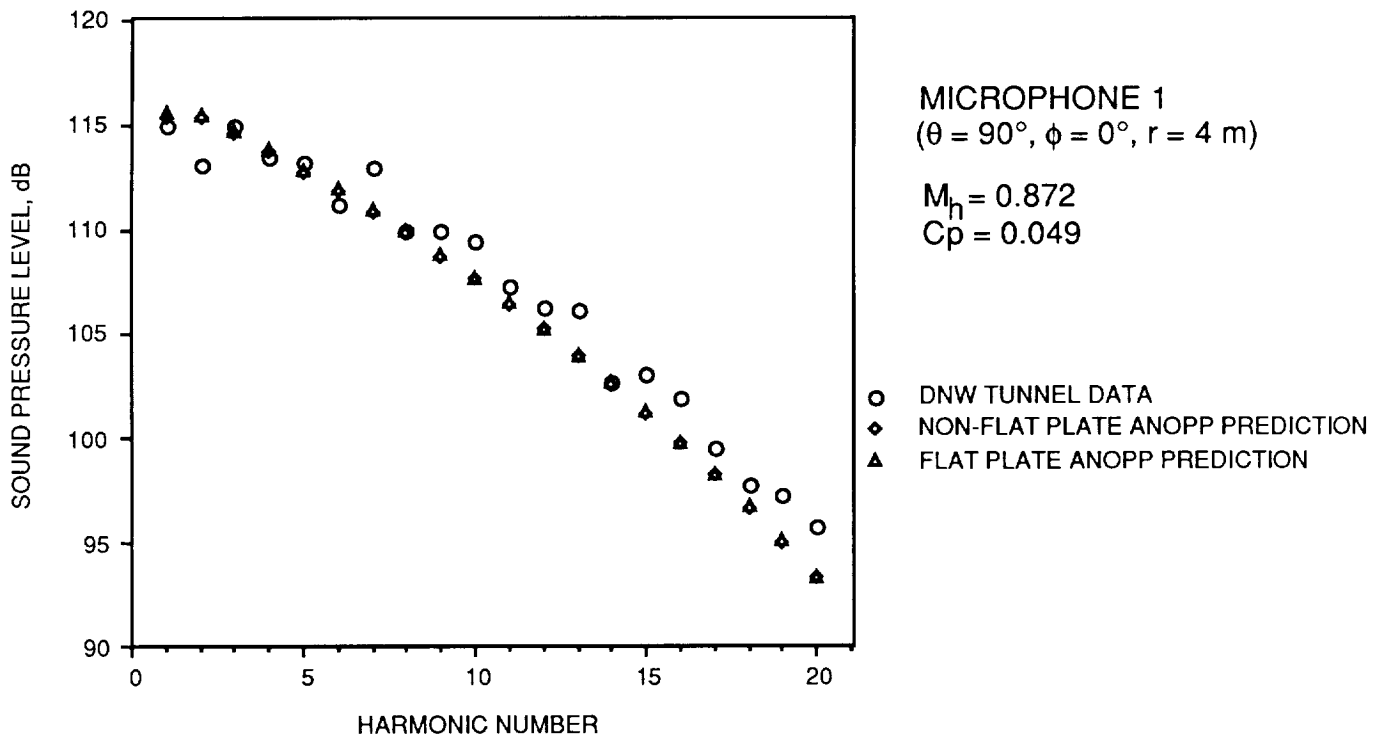
Figure 3.1   Noise comparison of ANOPP and DNW data for N propeller - test AN5. ANOPP predictions include the integral formulations for the boundary-layer thickness and the zero pressure gradient flat plate model.
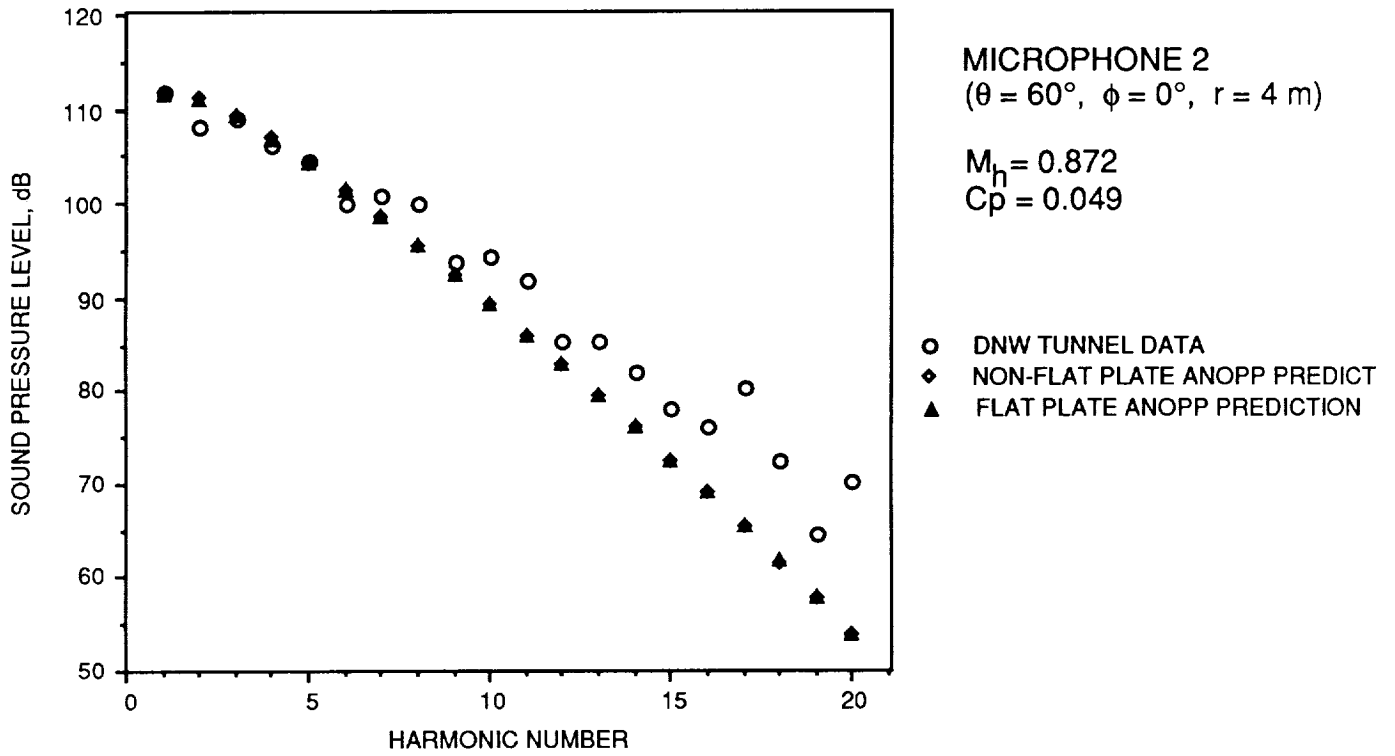
Figure 3.2 Noise comparison of ANOPP an DNW data for N propeller - test case AN5.
ANOPP predictions include the integral formulations for the boundary-
layer thickness and the zero pressure gradient flat plate model.
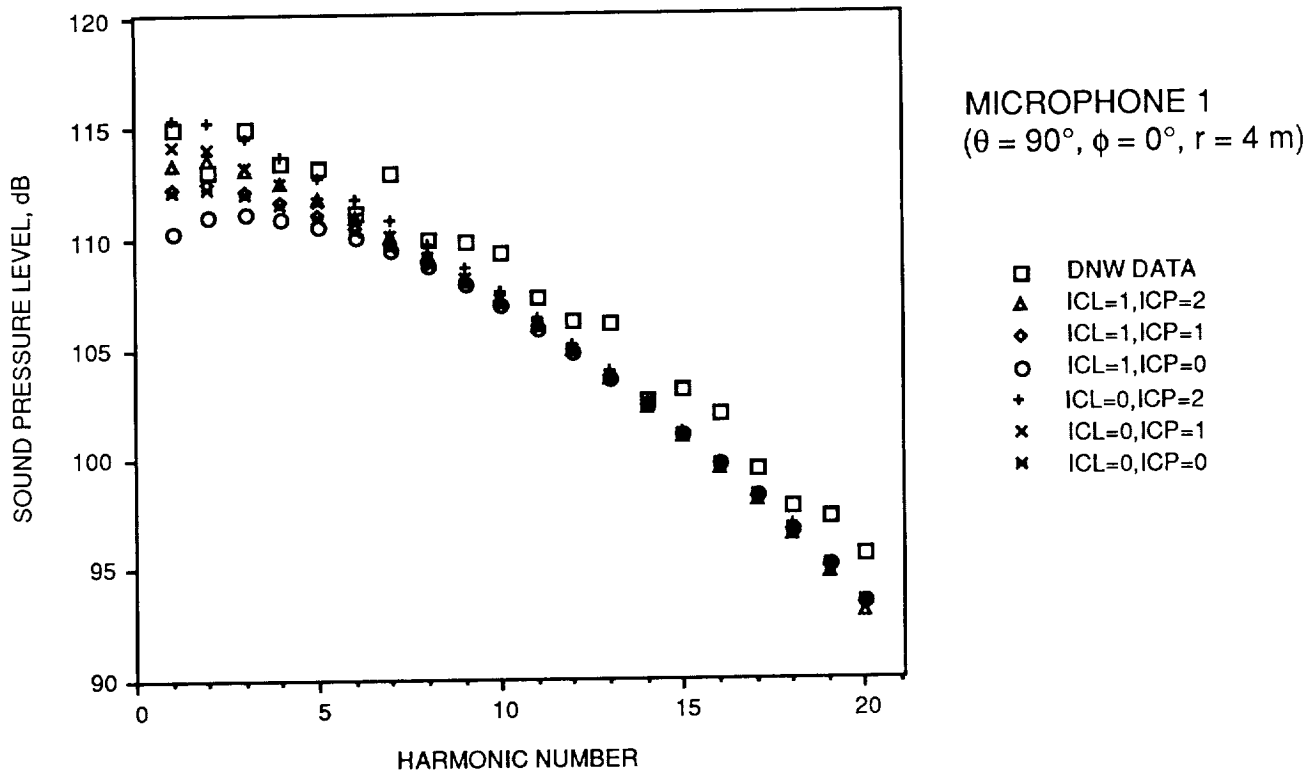
Figure 4.1 Noise comparison of different compressibility correction options of ANOPP predictions and DNW data for the test case AN5 and N propeller.

ICL - Compressibility option for the lift coefficient
= 0 - no compressibility correction
= 1 - Glauert compressibility correction

ICP - Compressibility option for the pressure coefficient
= 0 - no compressibility correction
= 1 - Glauert compressibility correction
= 2 - Karman-Tsien compressibility correction

MICROPHONE 2

($\theta = 60°$, $\phi = 0°$, $r = 4$ m)

□   DNW DATA
▲   ICL=1,ICP=2
◆   ICL=1,ICP=1
○   ICL=1,ICP=0
+   ICL=0,ICP=2
✳   ICL=0,ICP=1
✕   ICL=0, ICP=0
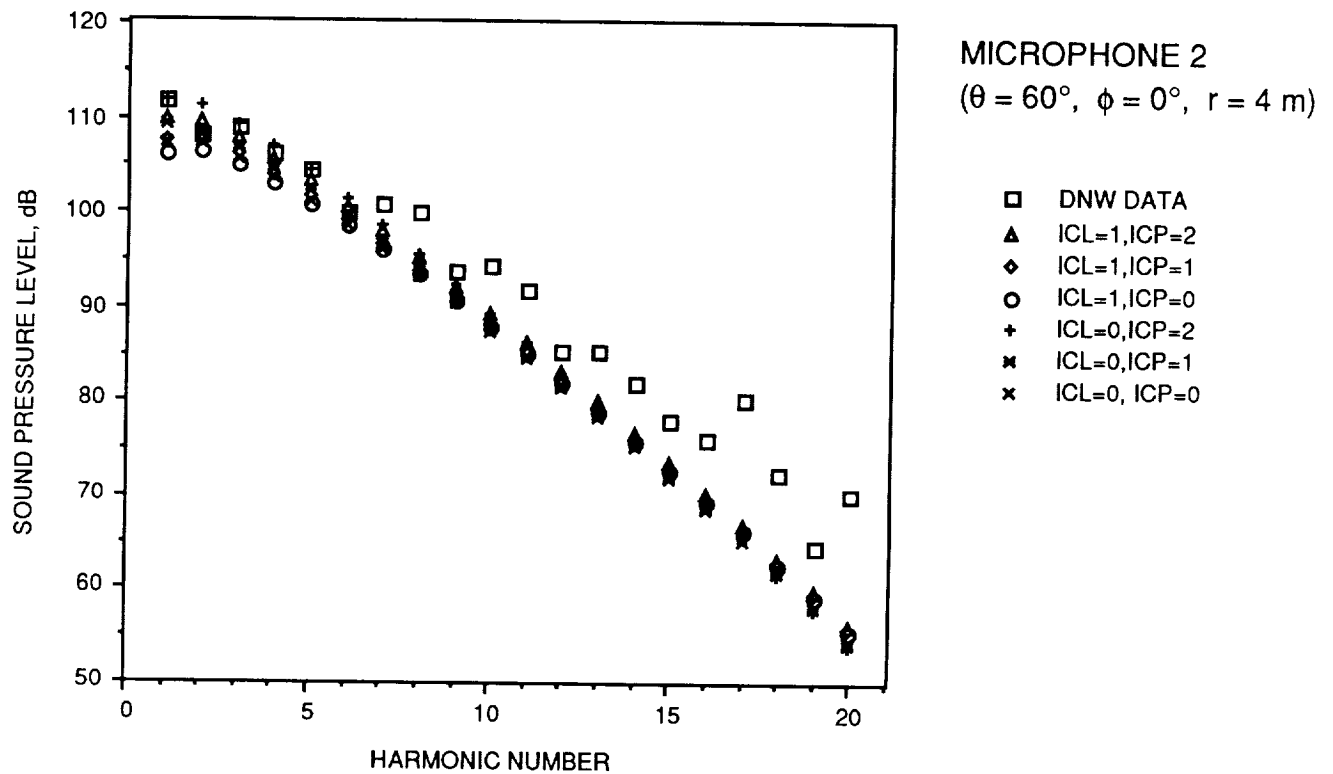
Figure 4.2 Noise comparison of different compressibility correction options of ANOPP predictions and DNW data from the test case AN5 for N propeller.

ICL - Compressibility option for the lift coefficient
= 0 - no compressibility correction
= 1 - Glauert compressibility correction

ICP - Compressibility option for the pressure coefficient
= 0 - no compressibility correction
= 1 - Glauert compressibility correction
= 2 - Karman-Tsien compressibility correction
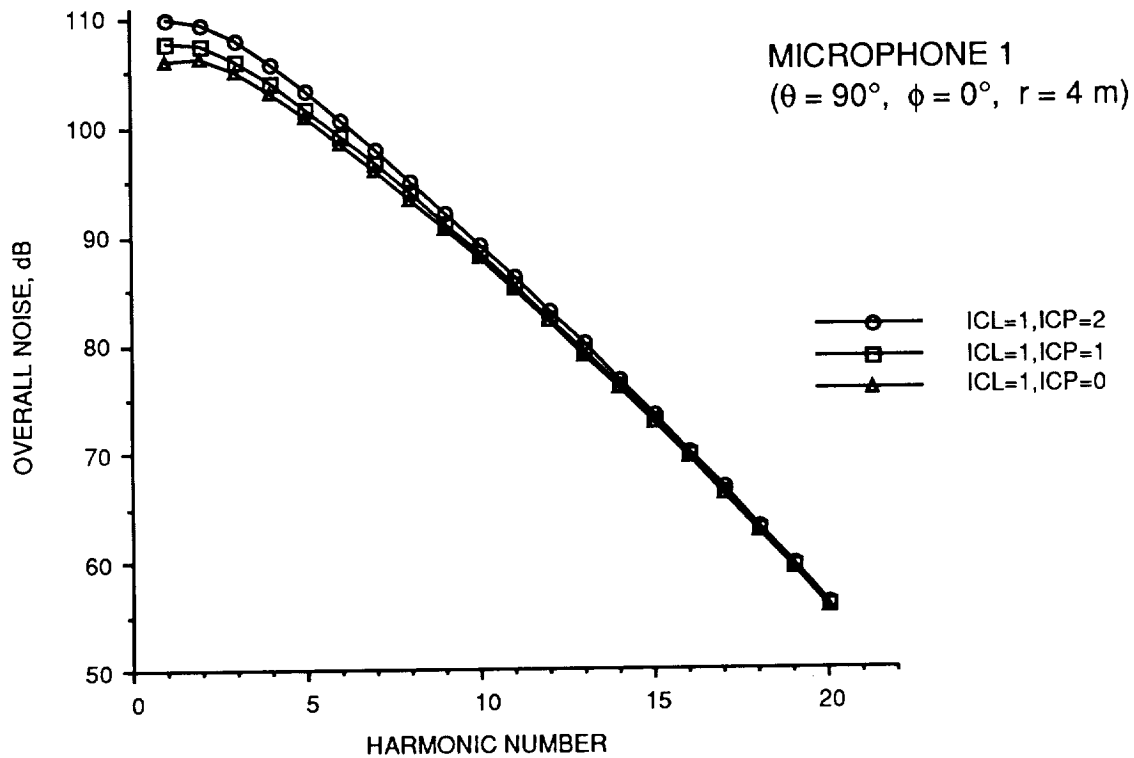
Figure 4.3 Noise comparison for different compressibility options for the pressure coefficient.

ICL - Compressibility option for the lift coefficient
    = 0 - no compressibility correction
    = 1 - Glauert compressibility correction

ICP - Compressibility option for the pressure coefficient
    = 0 - no compressibility correction
    = 1 - Glauert compressibility correction
    = 2 - Karman-Tsien compressibility correction
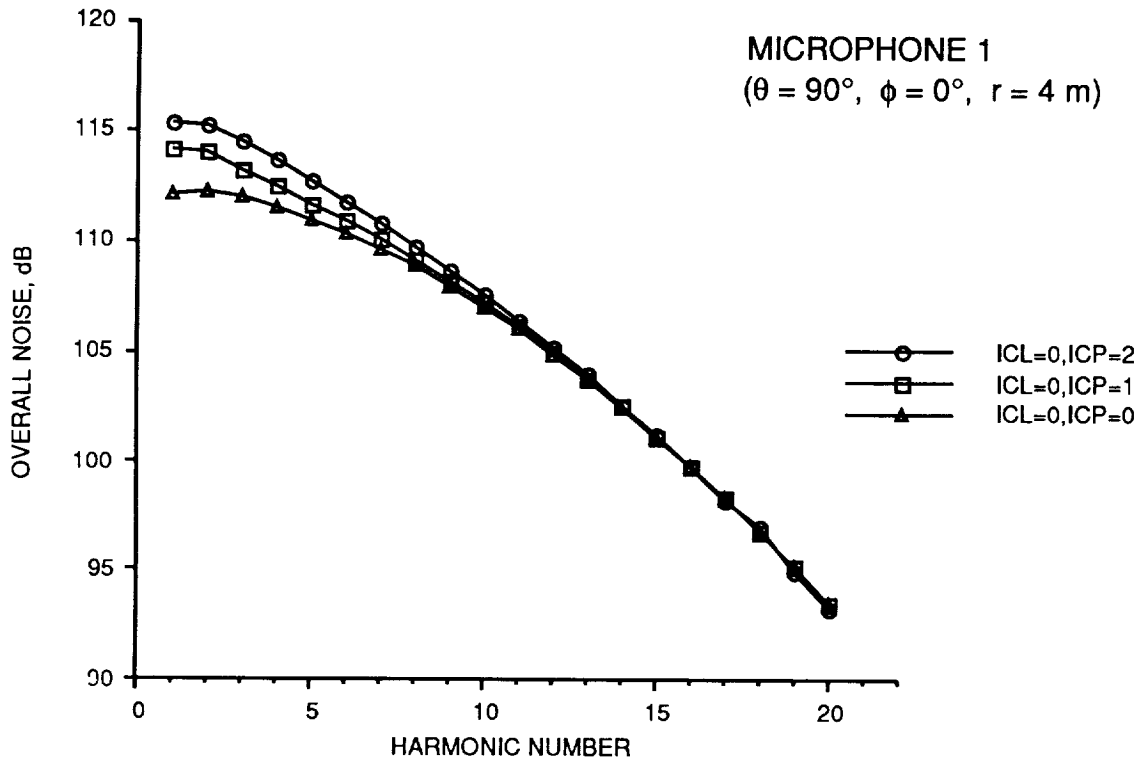
Figure 4.4 Noise comparison for different compressibility correction options for pressure coefficient - no correction applied for lift coefficient.

ICL - Compressibility option for the lift coefficient
= 0 - no compressibility correction
= 1 - Glauert compressibility correction

ICP - Compressibility option for the pressure coefficient
= 0 - no compressibility correction
= 1 - Glauert compressibility correction
= 2 - Karman-Tsien compressibility correction

MICROPHONE 2
($\theta = 60°$, $\phi = 0°$, $r = 4$ m)

ICL=1,ICP=2
ICL=1,ICP=1
ICL=1,ICP=0
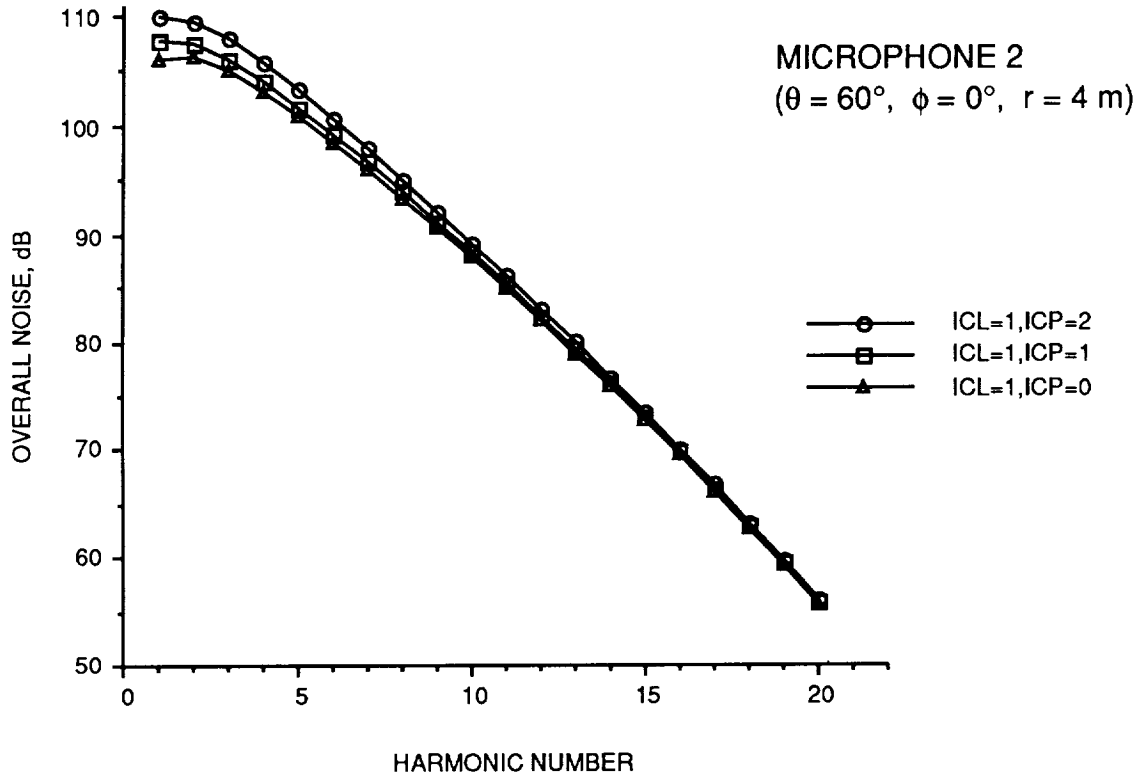
Figure 4.5 Noise comparison for different compressibility correction options for pressure coefficient.

ICL - Compressibility option for the lift coefficient
= 0 - no compressibility correction
= 1 - Glauert compressibility correction

ICP - Compressibility option for the pressure coefficient
= 0 - no compressibility correction
= 1 - Glauert compressibility correction
= 2 - Karman-Tsien compressibility correction
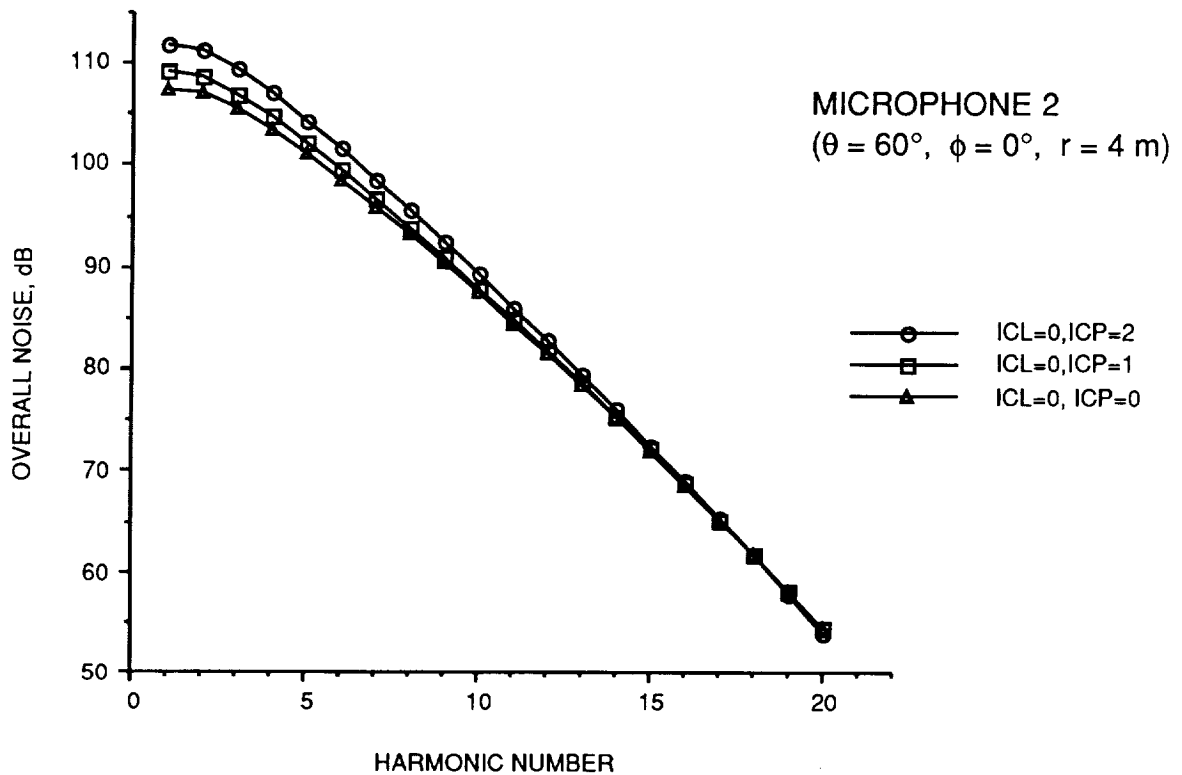
Figure 4.6 Noise comparison for different compressibility correction options of pressure coefficient - Glauert theory applied for lift coefficient.

ICL - Compressibility option for the lift coefficient
    = 0 - no compressibility correction
    = 1 - Glauert compressibility correction

ICP - Compressibility option for the pressure coefficient
    = 0 - no compressibility correction
    = 1 - Glauert compressibility correction
    = 2 - Karman-Tsien compressibility correction

$$F(X) = AX^2 + BX - C + COS(X+D)$$
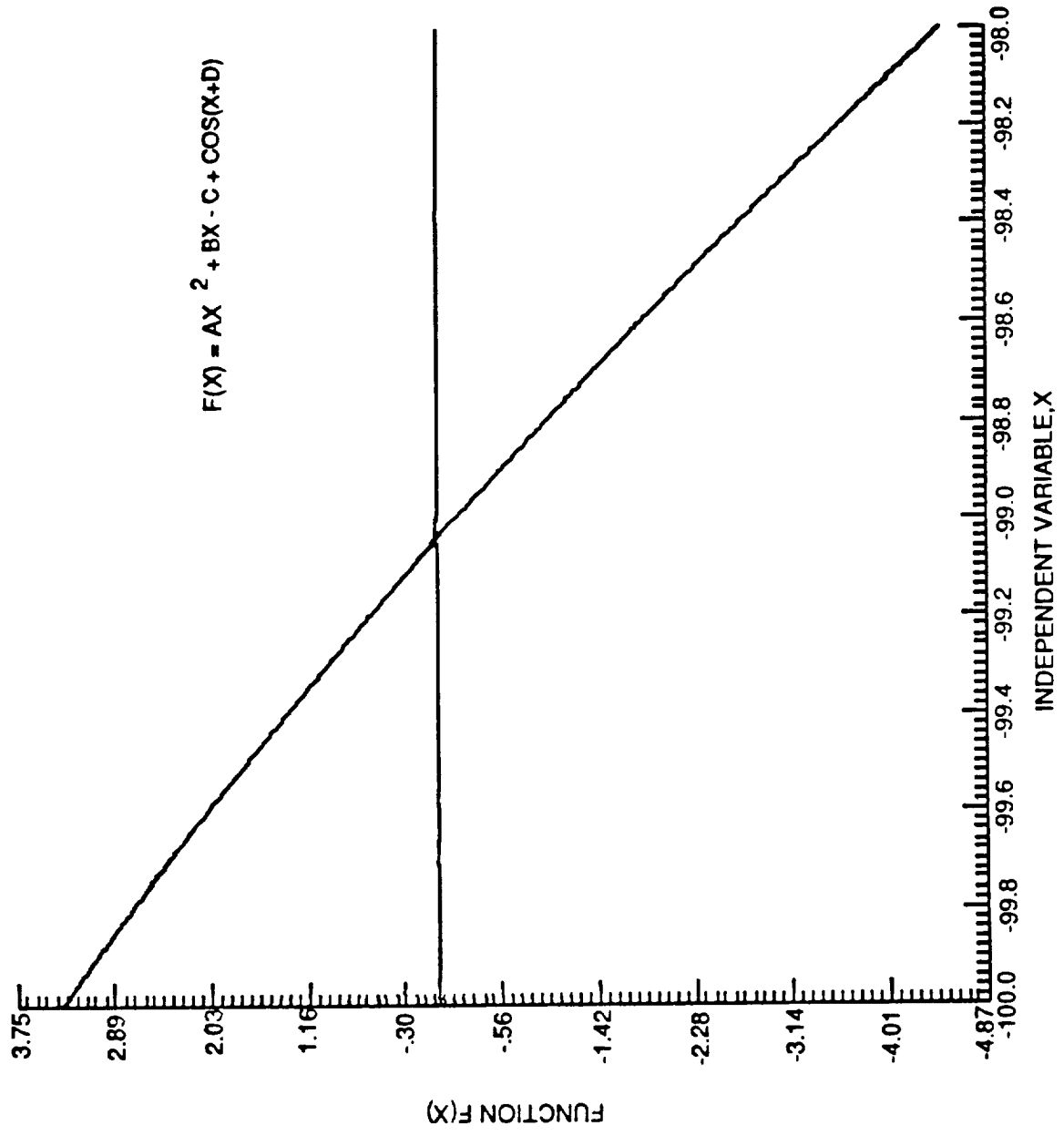
Figure 5.1   Function f(x) for the case where the root is found in two iterations.
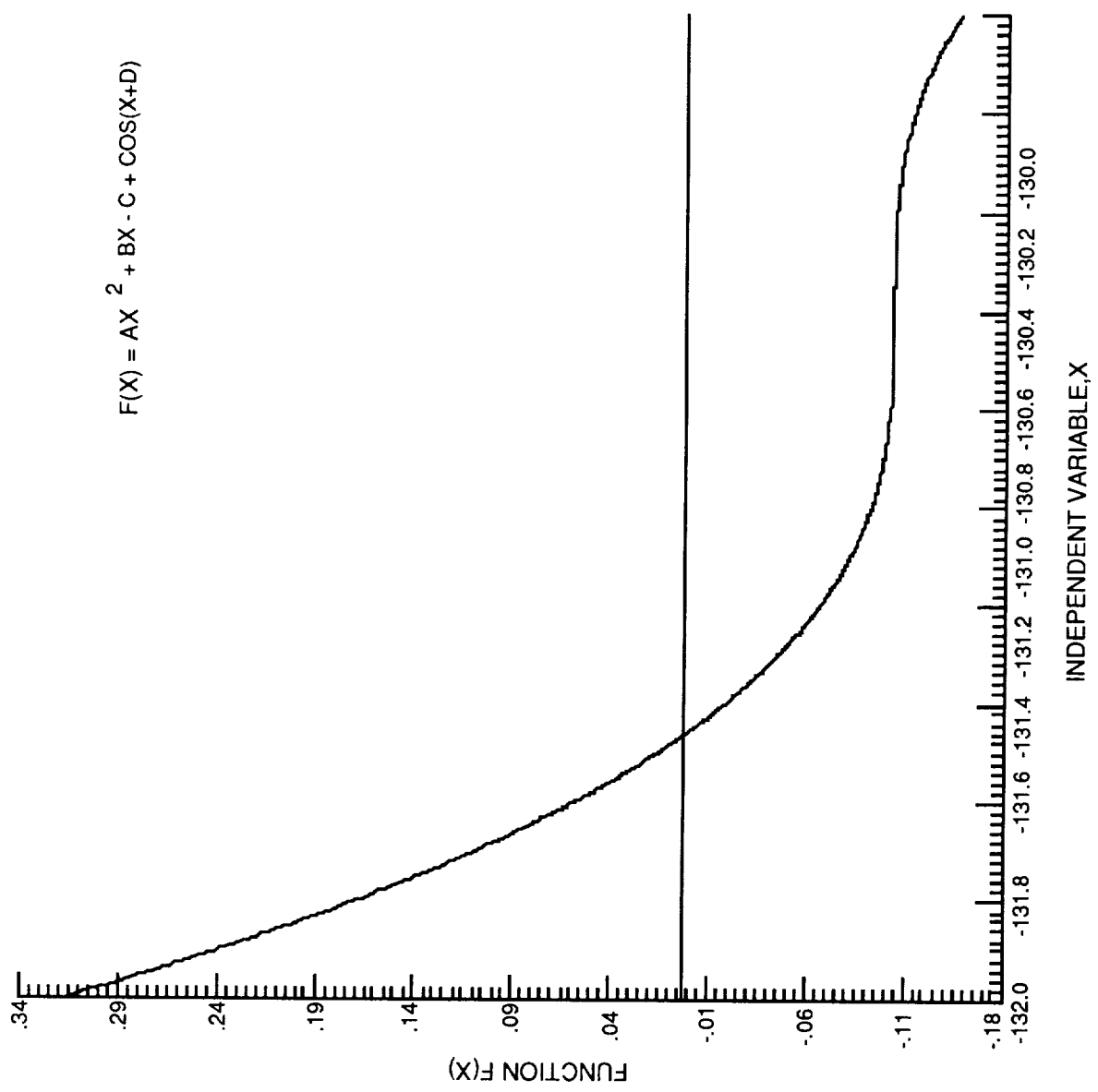
Figure 5.2   Function f (x) for the case where the root is found in 11 iterations.

F'(X) = 2AX + B - SIN(X+D)

INDEPENDENT VARIABLE,X

DERIVATIVE FUNCTION F(X)
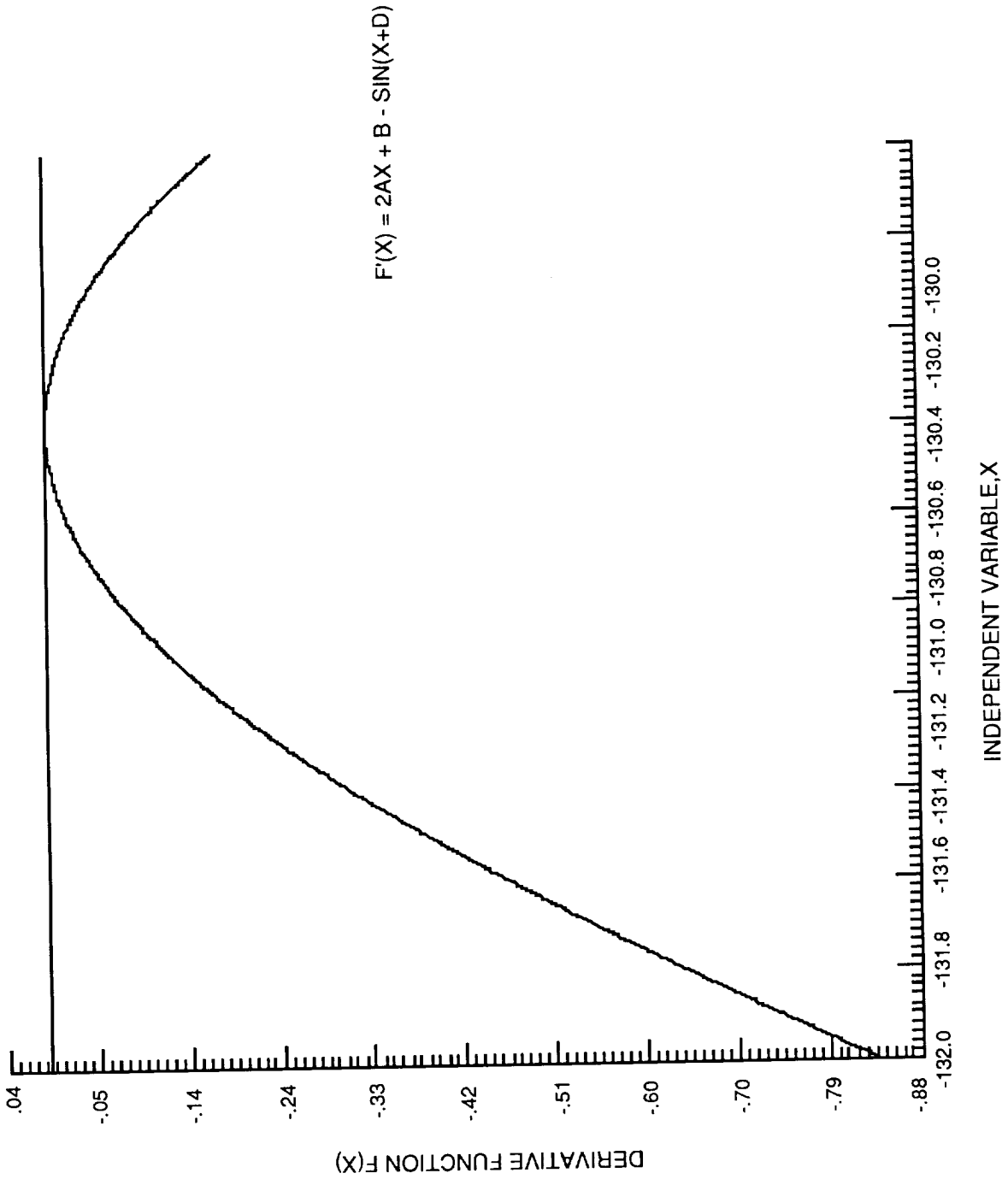
Figure 5.3   Derivative for function f(x) of the case where the root is found in 11 iterations.

Front view
Diam. = 3.66 m

Wind tunnel
nozzle diameter = 7.32 m

Far-field traversing
microphone positioned
in propeller plane

90°

2.44 m

0.6 m   0°

Near-field fixed microphone
positioned in propeller plane

5.49 m
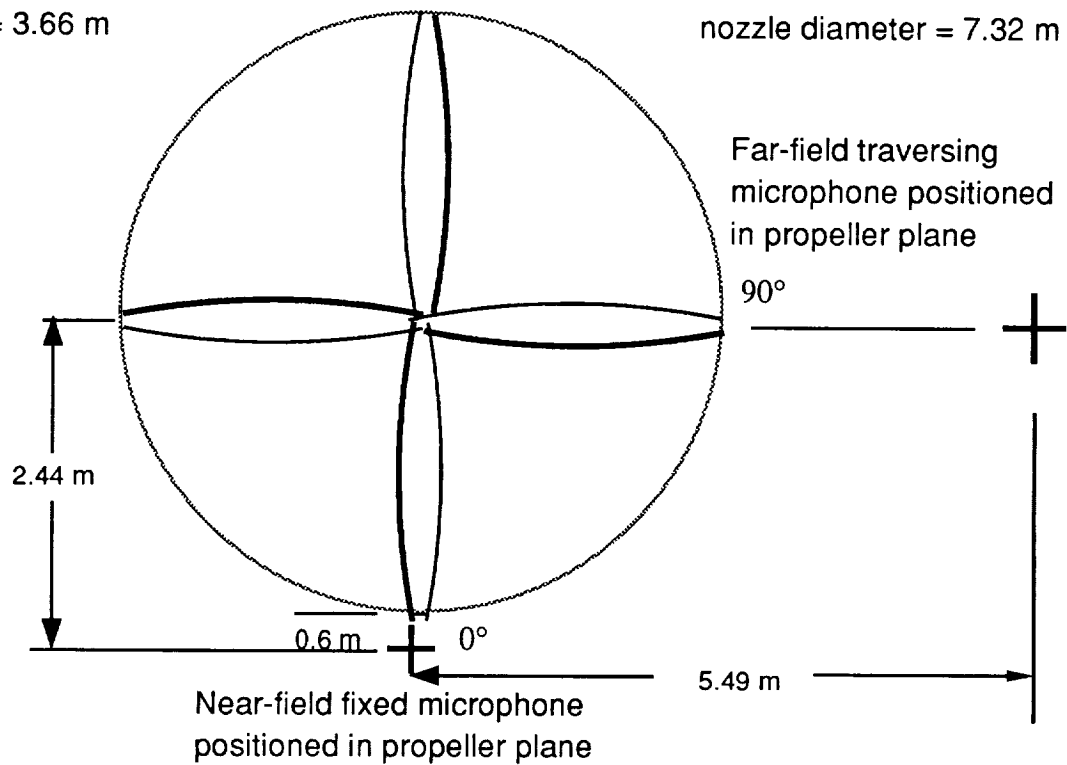
Figure 6.1   Microphone positions in 24-foot Wind Tunnel tests used for
comparisons with the ANOPP predictions.

Near field microphone

RPM = 1250

Helical tip Mach number = 0.71

Power coefficient = 0.024

O   24 -foot wind tunnel data
I   ANOPP PAS prediction

Sound pressure level, dB

Harmonic number
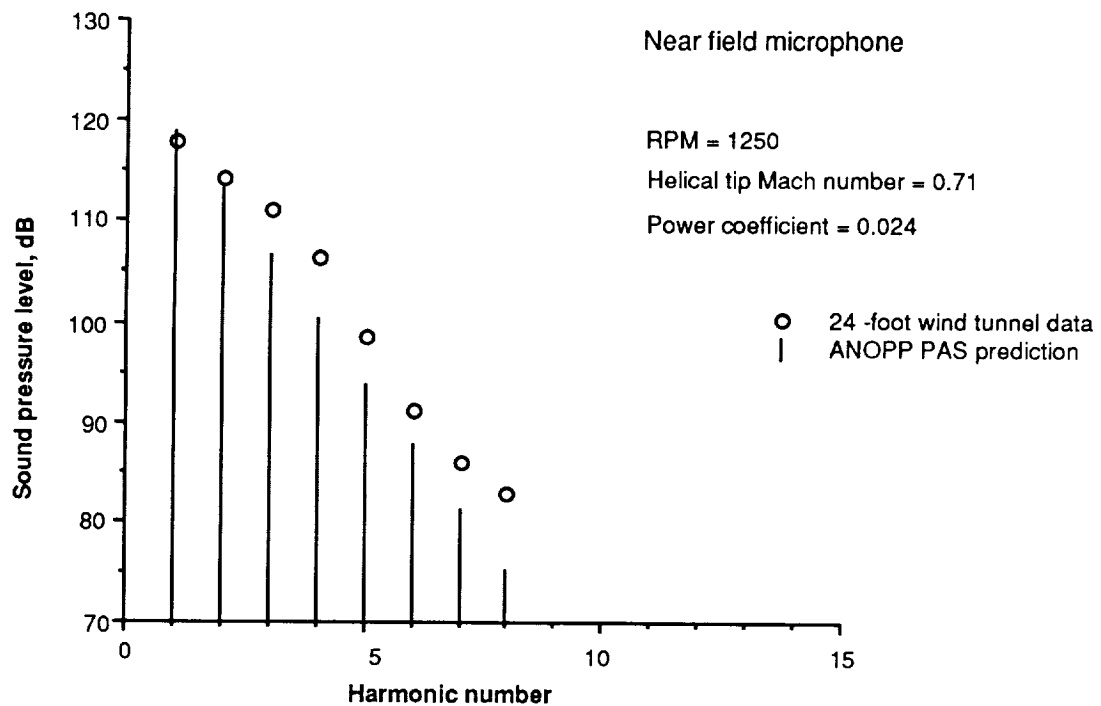
Figure 6.2   Comparison of prediction with data for the 24-foot
wind tunnel first test case (Dowty Rotol R212 propeller).
(see Fig. 6.1 for microphone position)

70
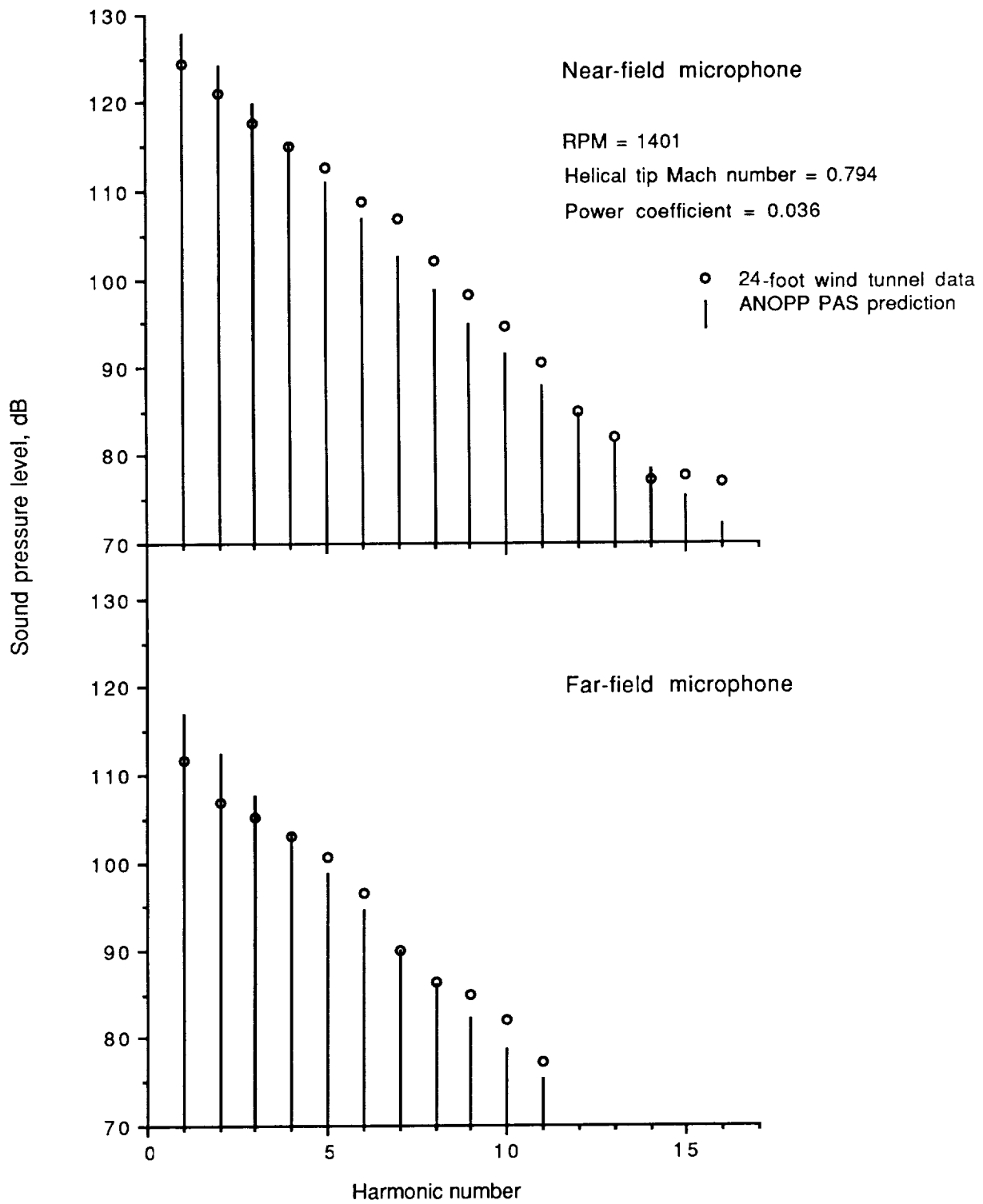
Figure 6.3   Comparison of prediction with data for the 24-foot wind
tunnel second test case (Dowty Rotol R212 propeller).
(see Fig 6.1 for microphone positions)
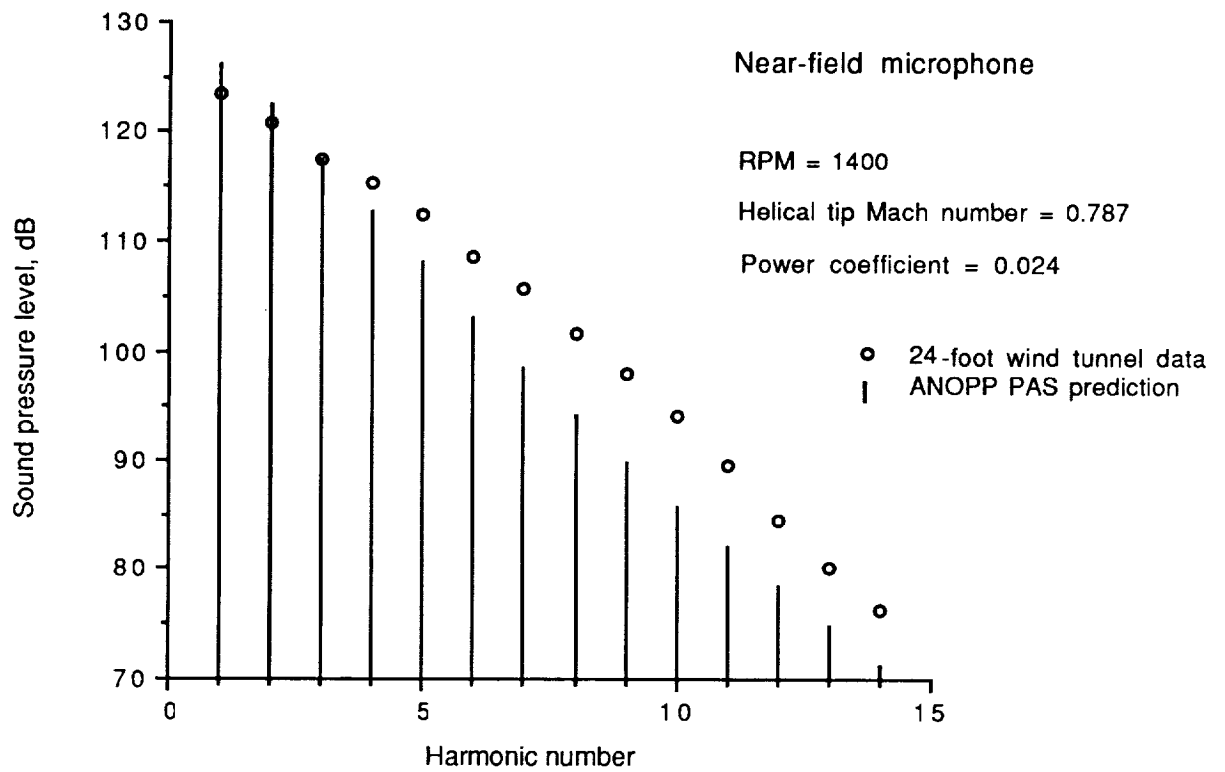
Figure 6.4 Comparison of prediction with data for the 24-foot wind tunnel third test case (Dowty Rotol R212 propeller). (see Fig. 6.1 for microphone position)
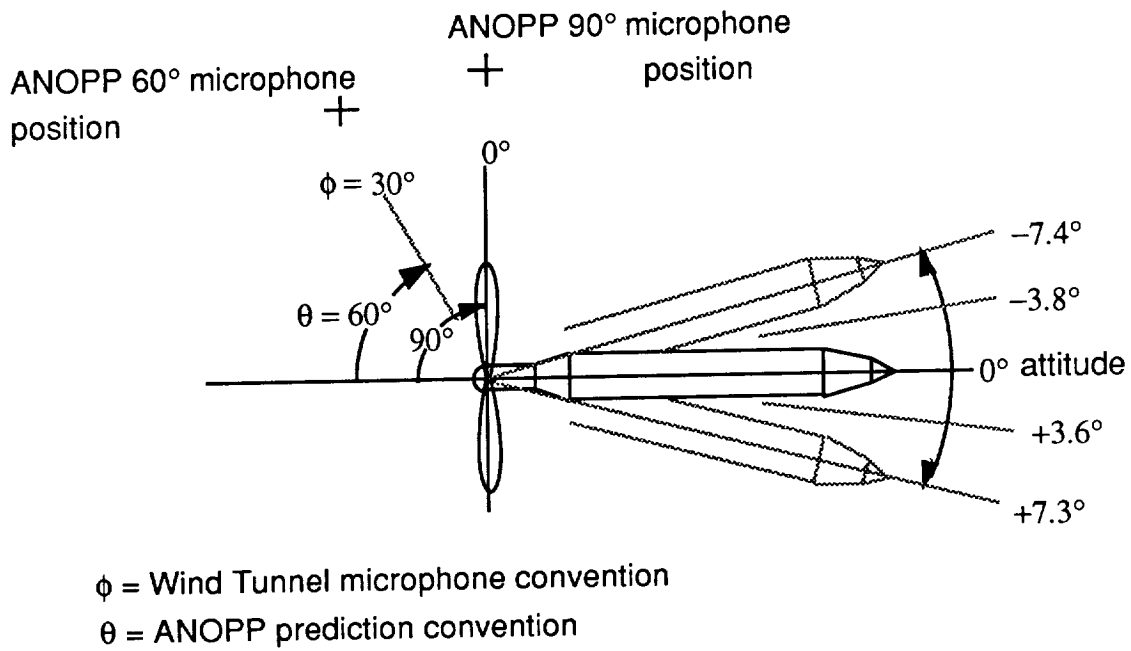
Figure 7.1   Microphone and nacelle positions in the DNW used for
comparisons with the ANOPP predictions.
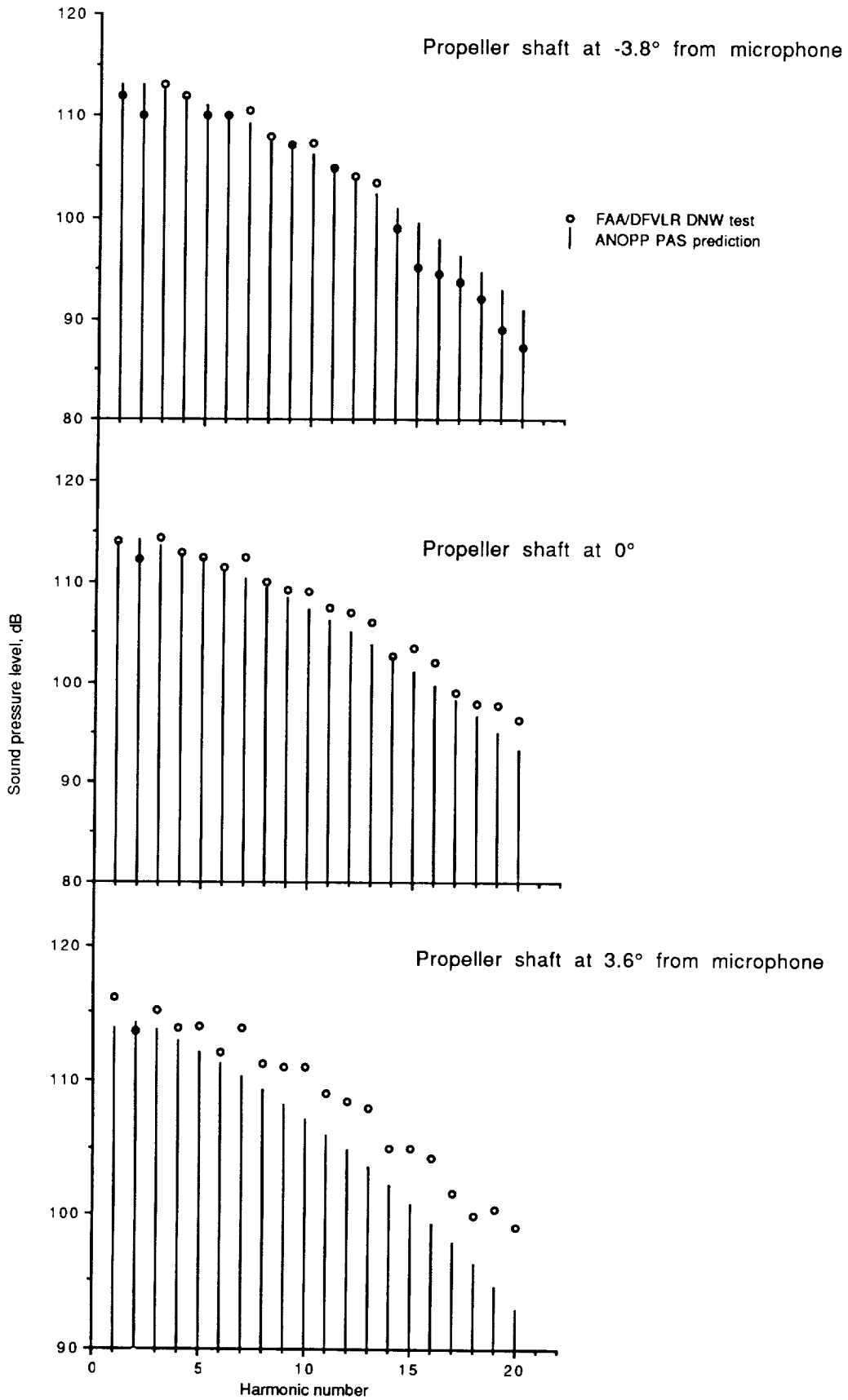
Figure 7.2   Comparison of prediction and data from 90° directivity angle
microphone for the DNW tunnel test.

74
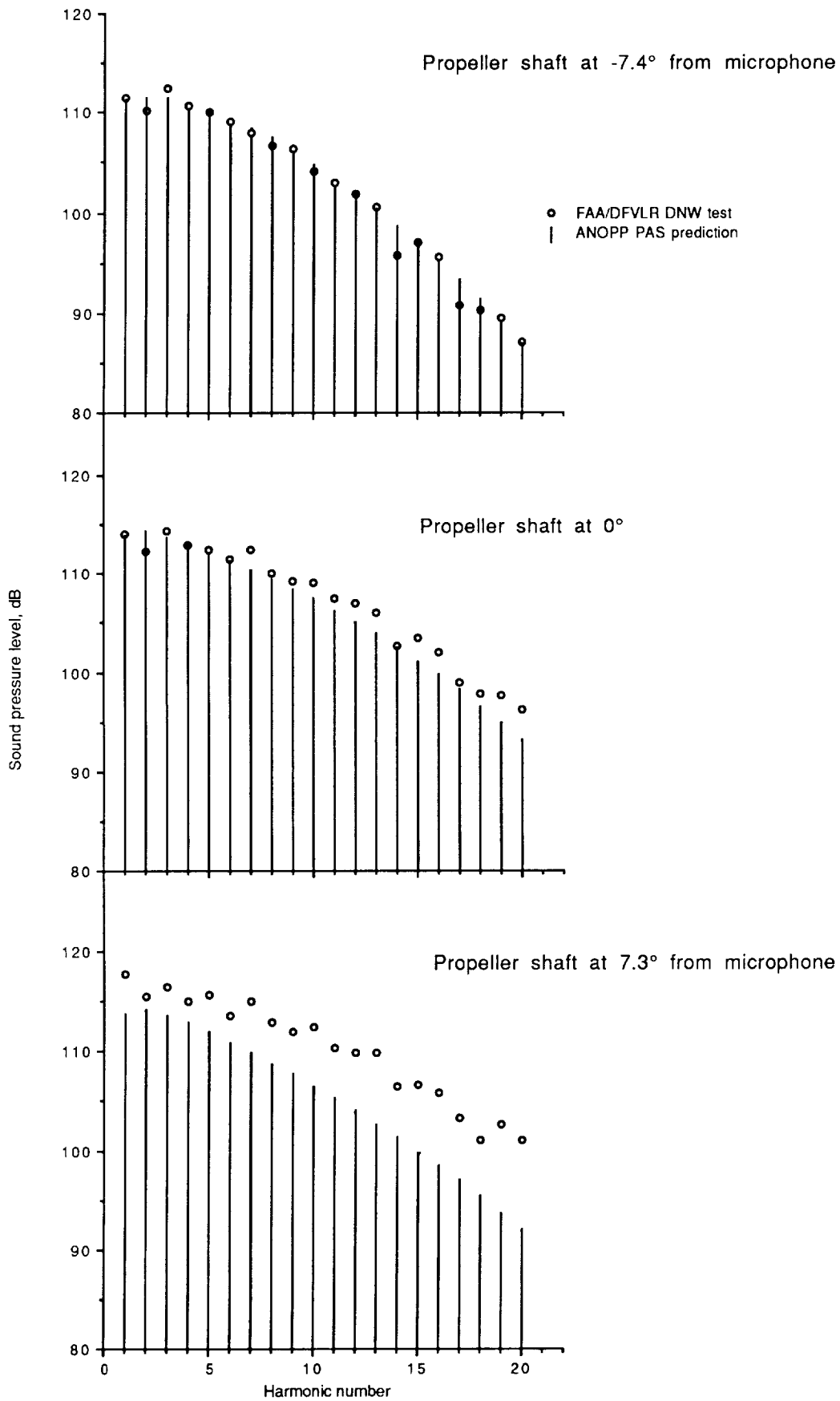
Figure 7.3 Comparison of prediction and data from 90° directivity angle
microphone for the DNW tunnel test.
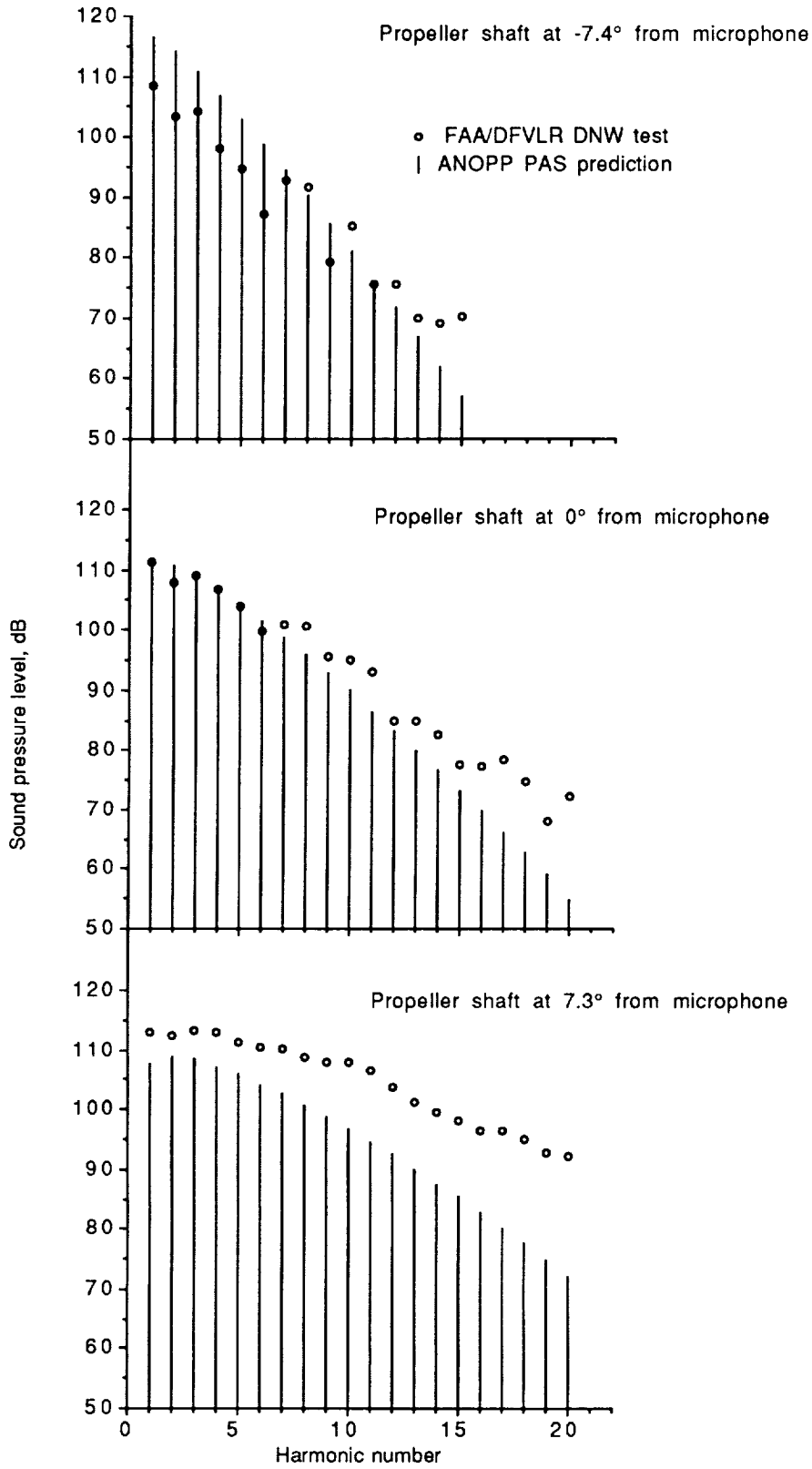
Figure 8.1   Comparison of prediction with data from   60° directivity
angle microphone for the DNW tunnel test.
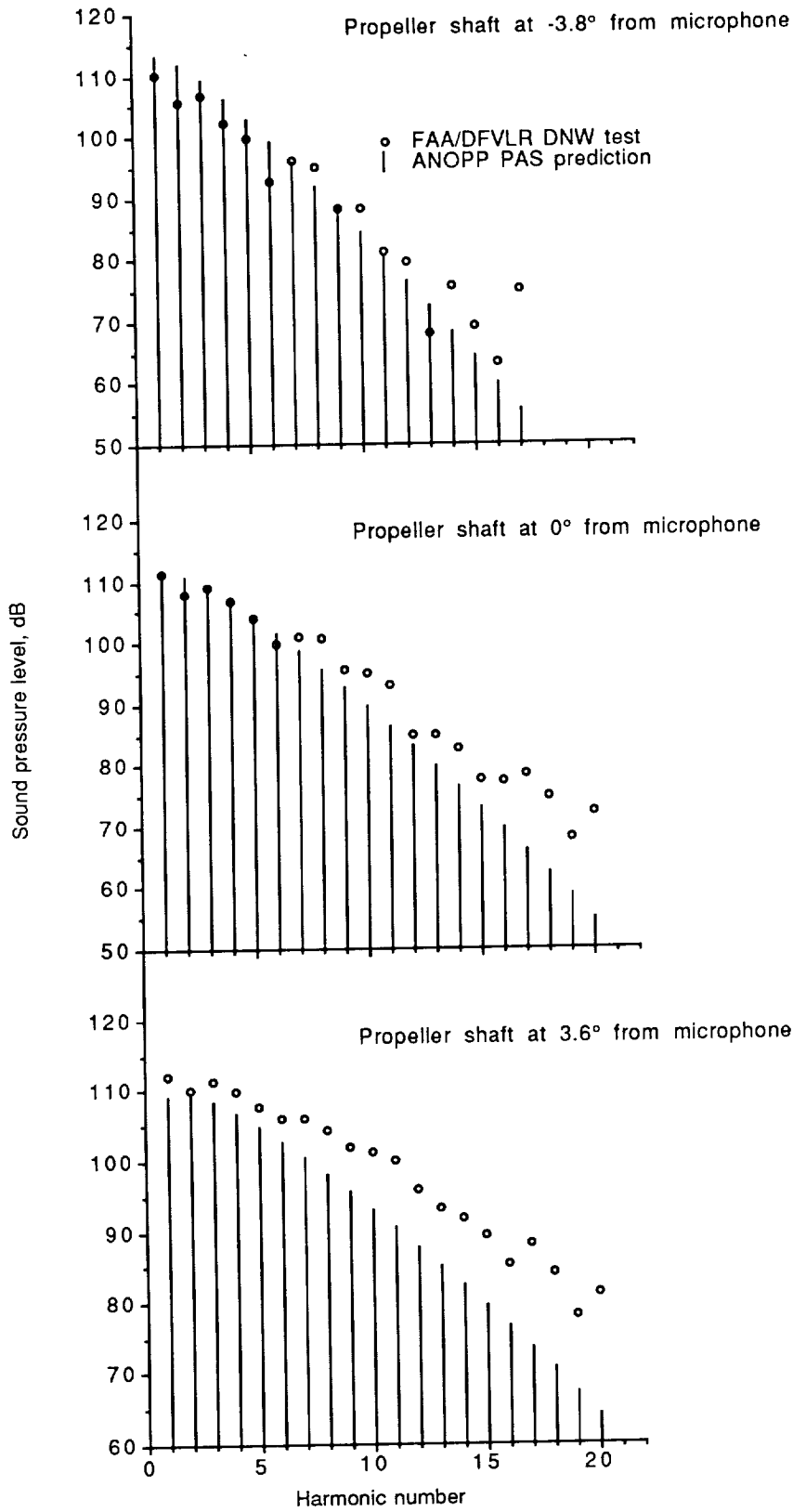
Figure 8.2   Comparison of prediction with data from 60° directivity angle microphone for the DNW tunnel test.
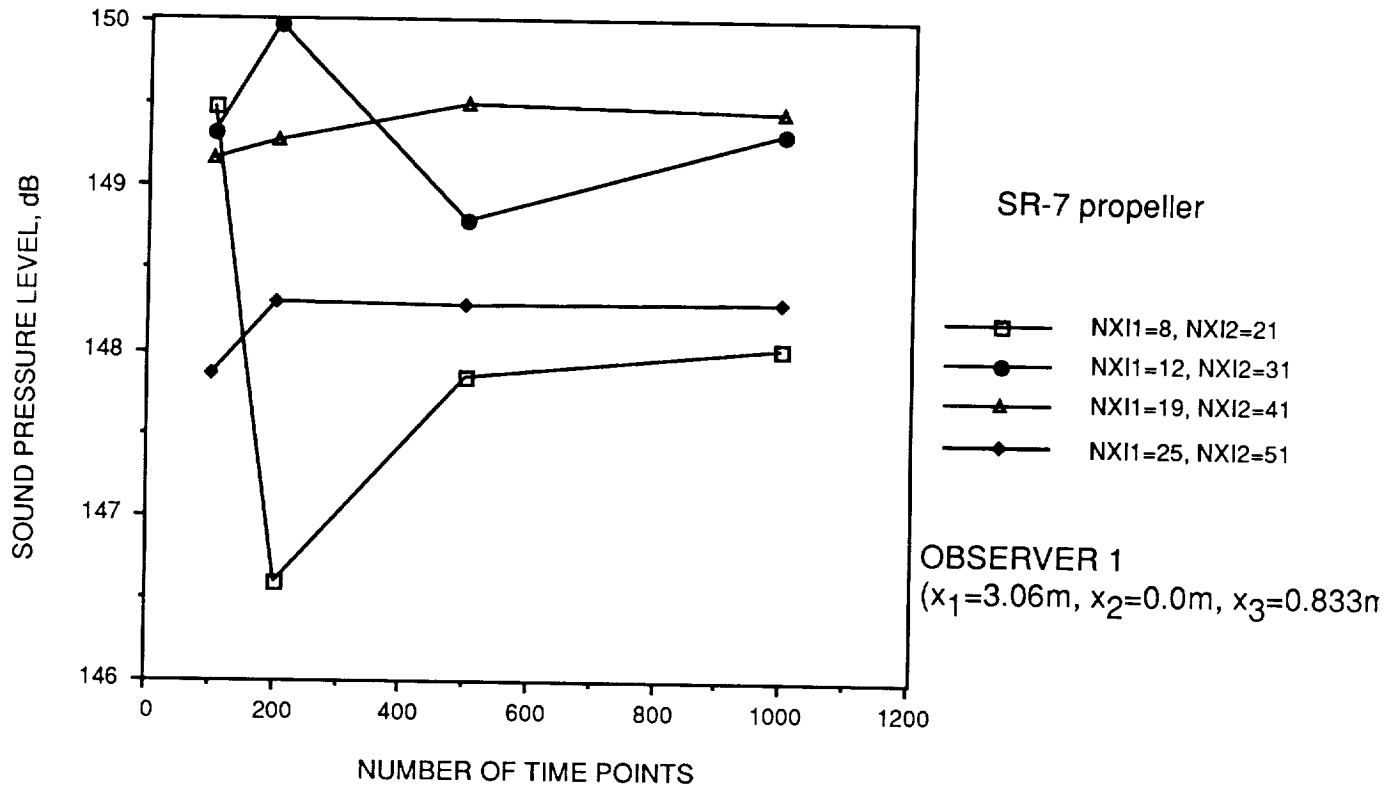
Figure 9.1 Noise comparison of the **first** harmonic for grid combinations.
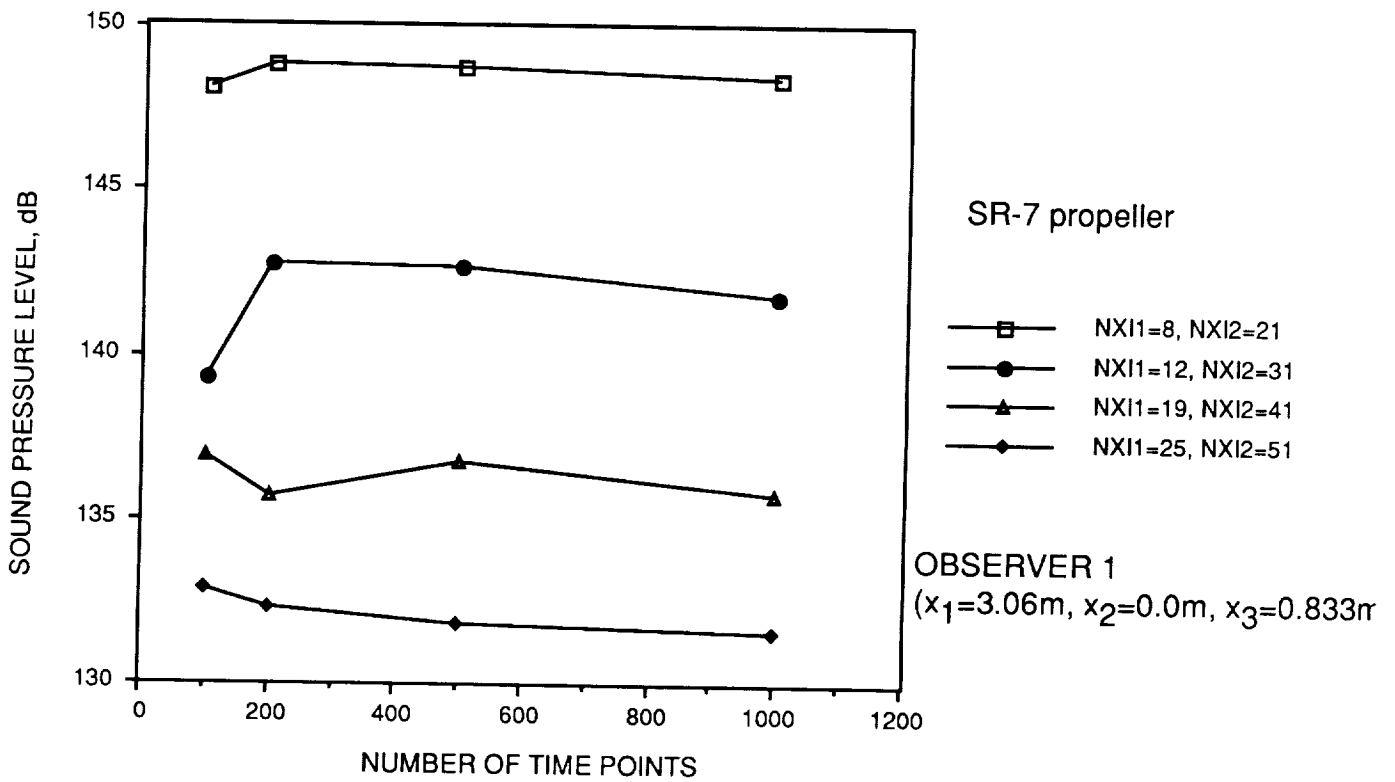
Figure 9.2 Noise comparison of the **second** harmonic for grid combinations.

78
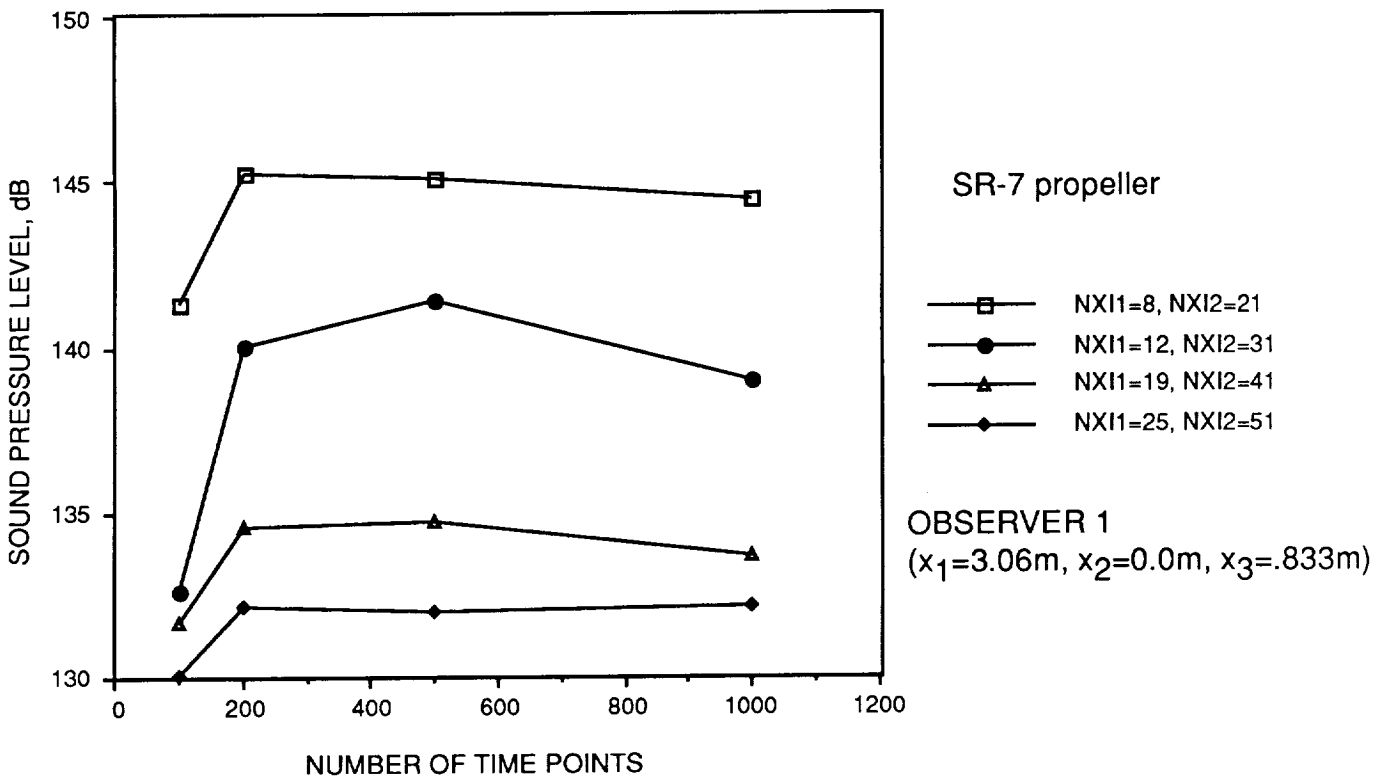
Figure 9.3 Noise comparison of the **third** harmonic for grid combinations.
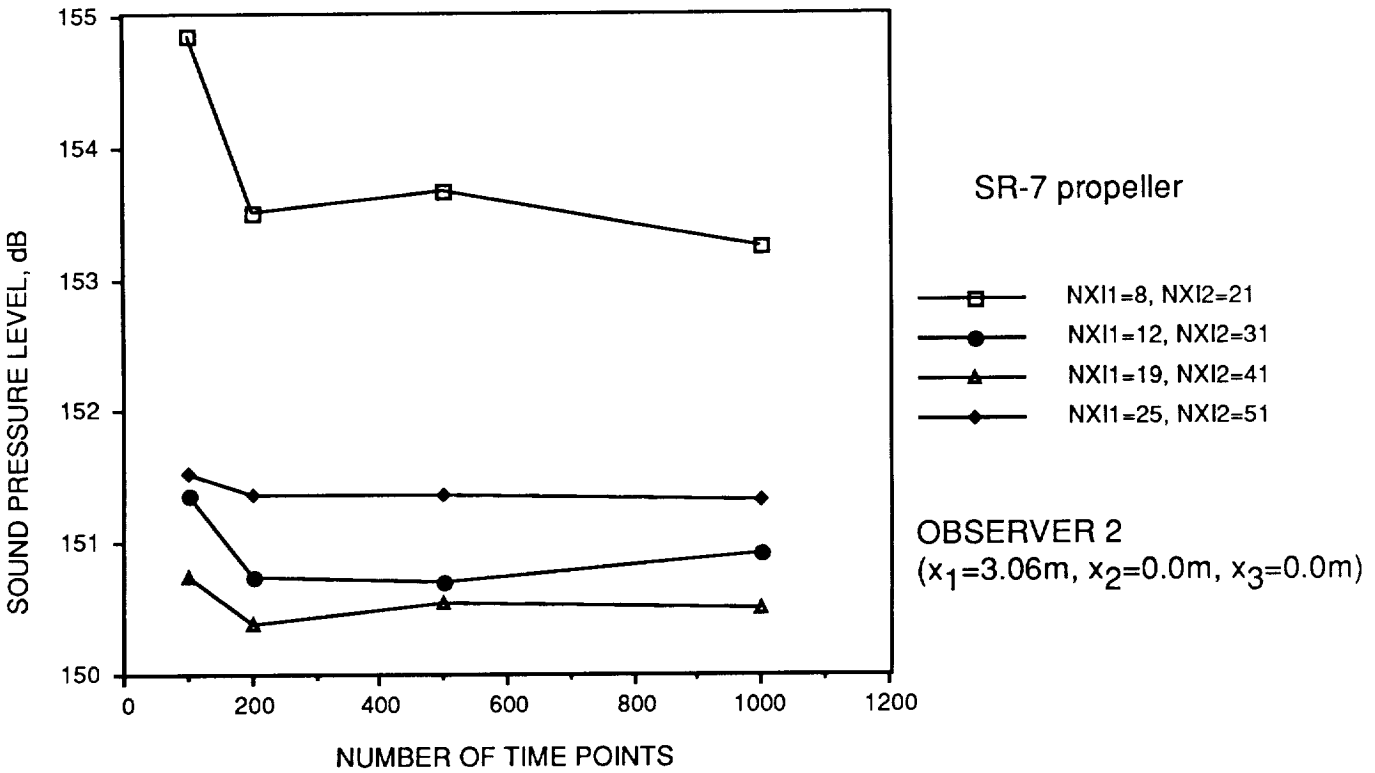
Figure 10.1 Noise comparison of the **first** harmonic for grid combinations.

79
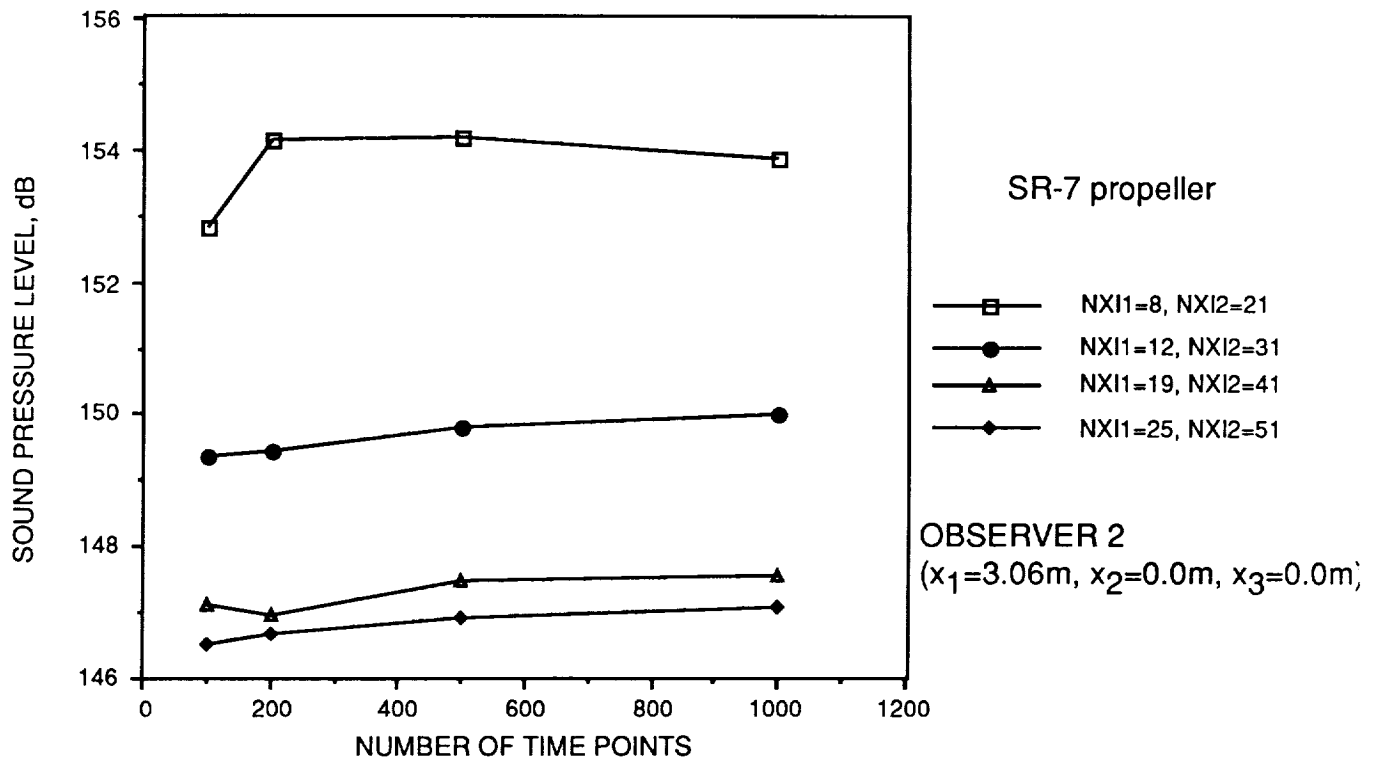
Figure 10.2 Noise comparison of the **second** harmonic for grid combinations.
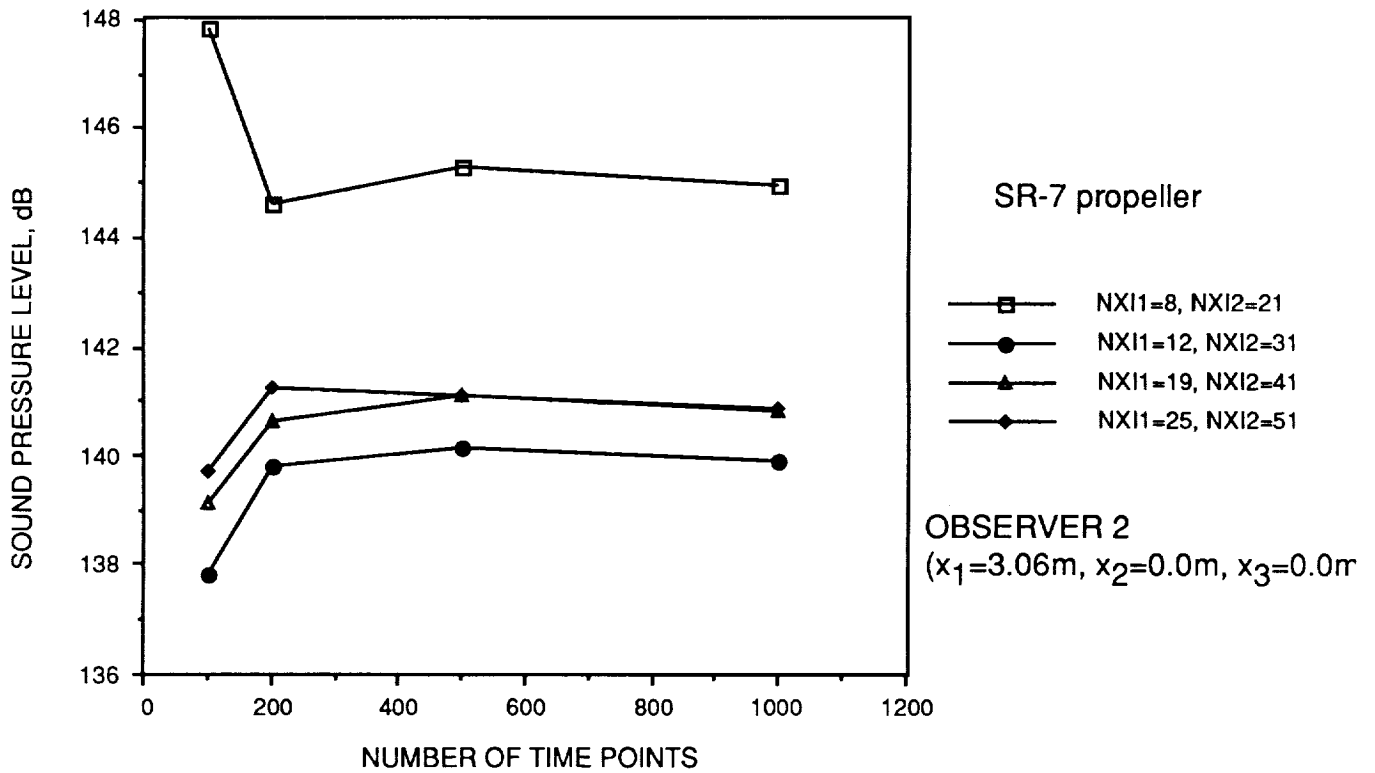
Figure 10.3 Noise comparison of **third** harmonic for grid combinations.

80
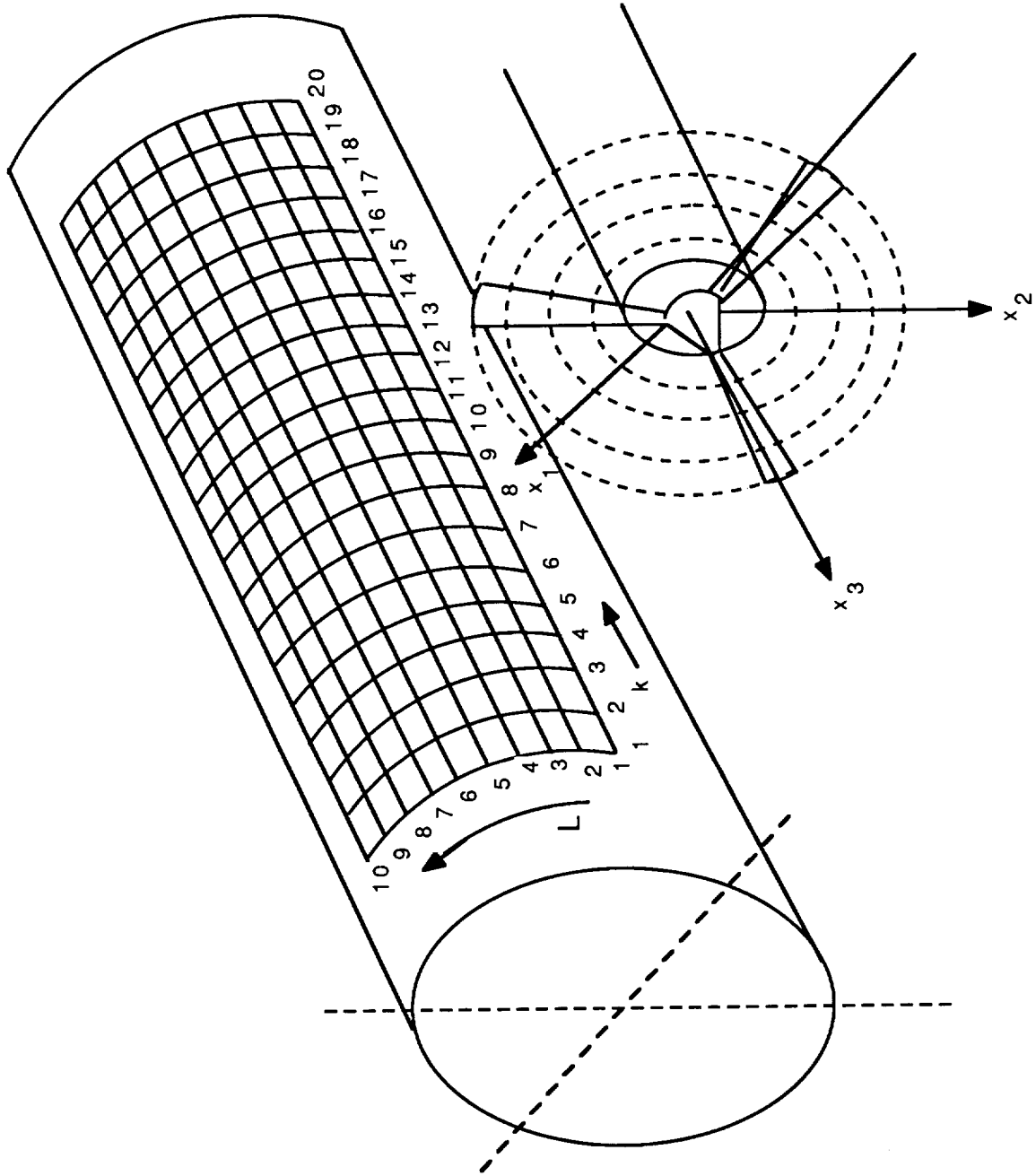
Figure 11.1 Grid used for propeller noise predictions for the support of the propeller noise interior program.

Figure 12.1 Comparison of ANOPP and DFP-ATP for the first harmonic.
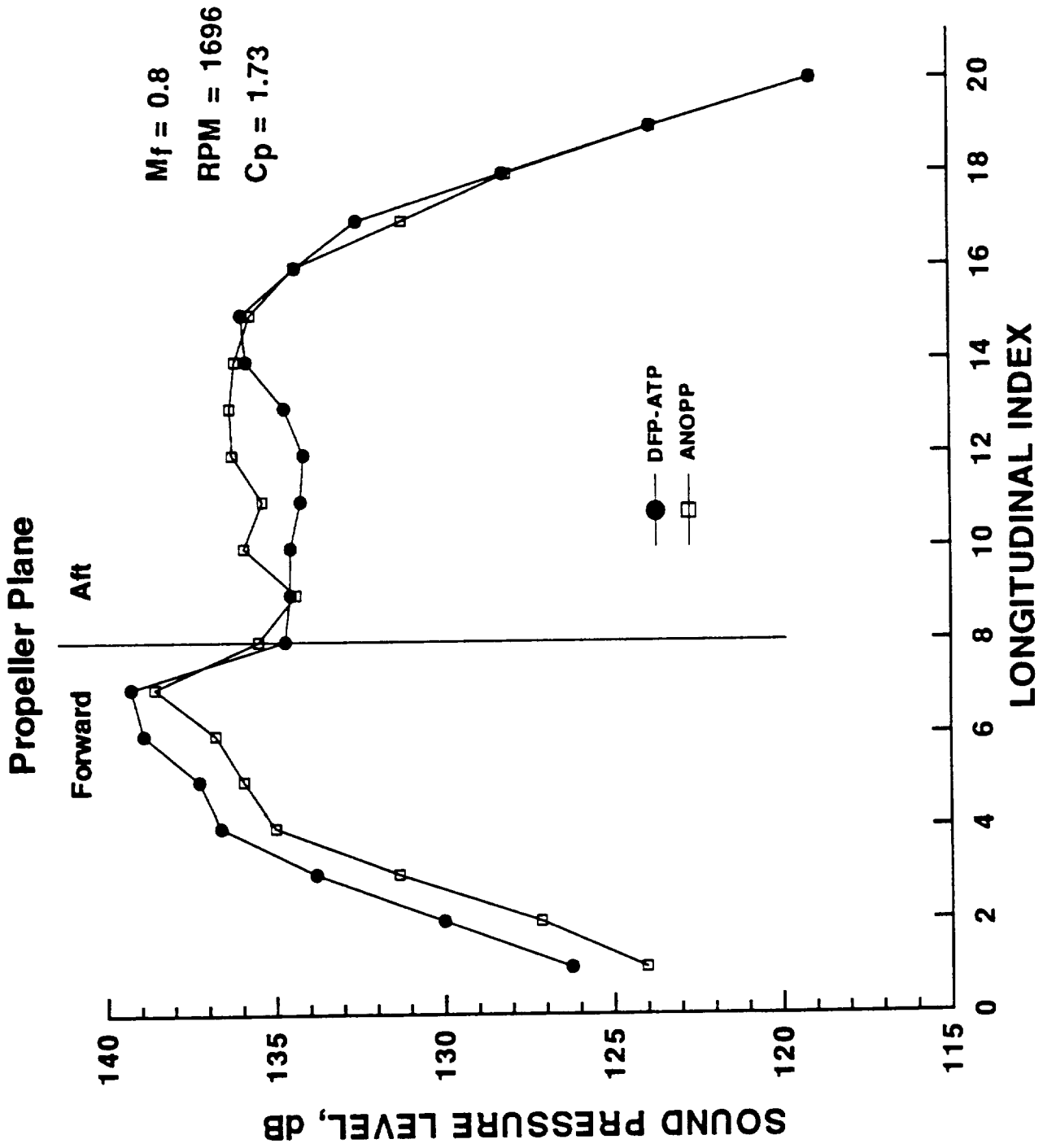
Figure 12.2 Comparison of ANOPP and DFP-ATP for the second harmonic.

83
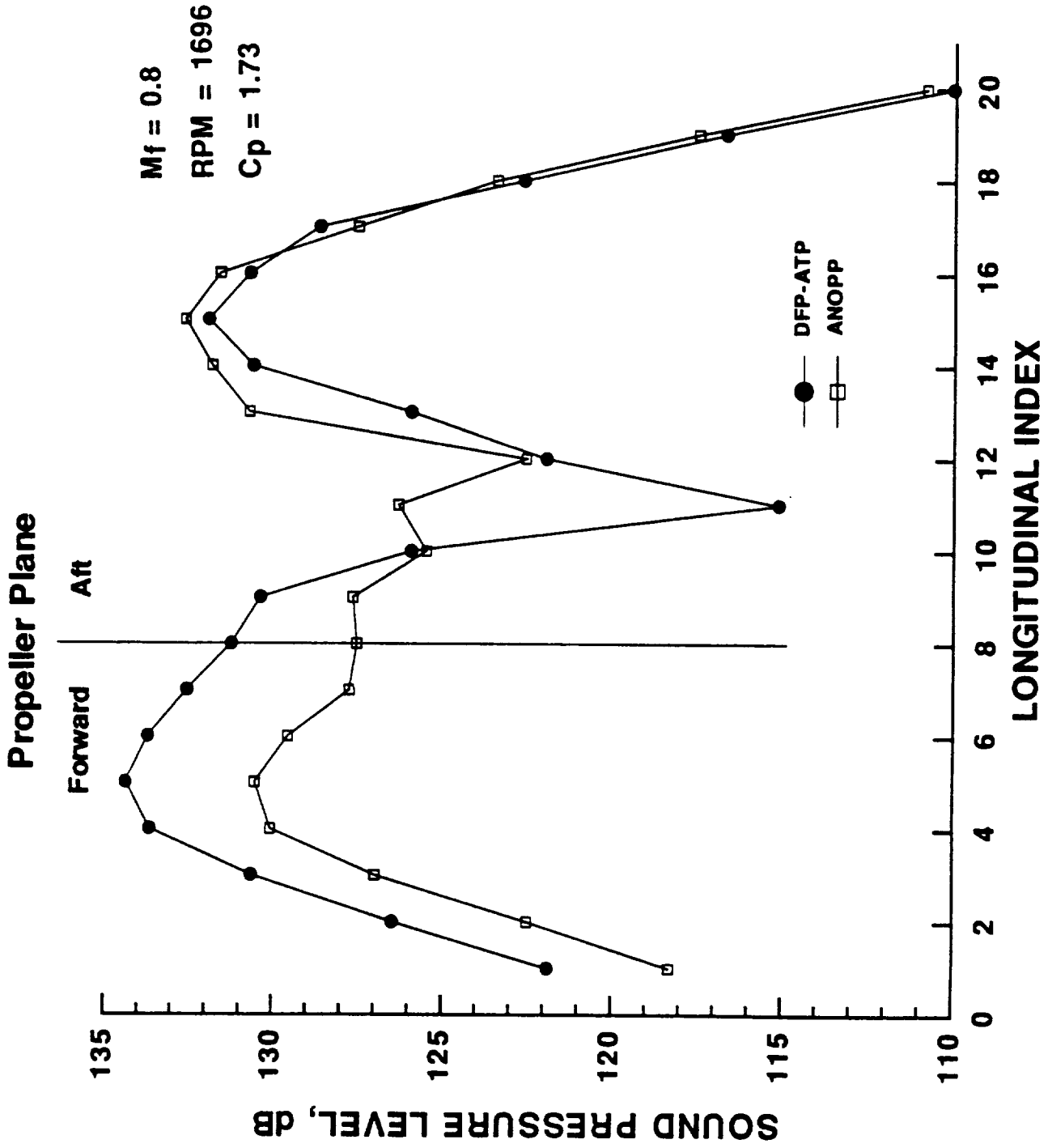
Figure 12.3 Comparison of ANOPP and DFP-ATP for the third harmonic.
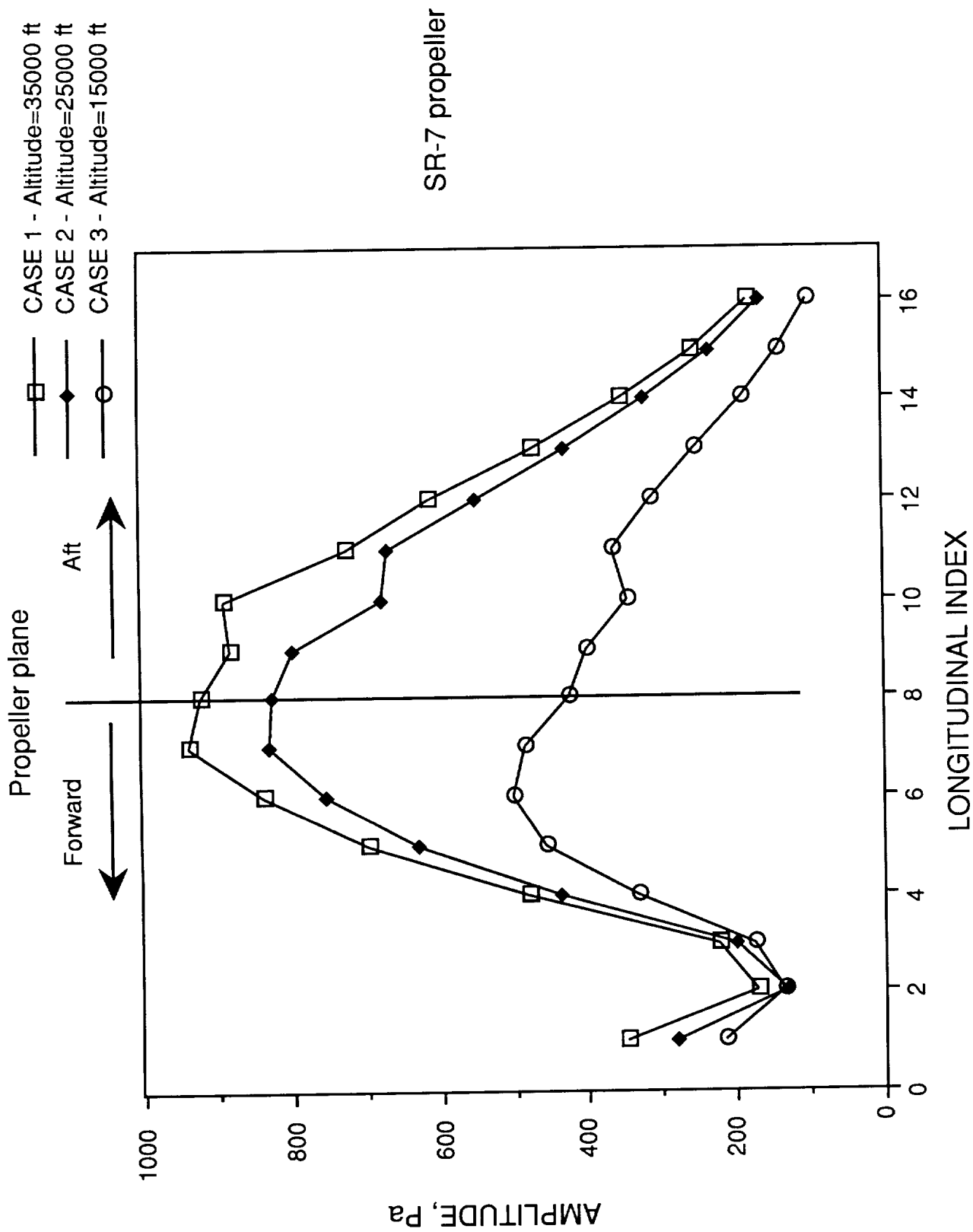
Figure 13.1   Amplitude of the first harmonic of the 3 cases at L=1 using ANOPP code.
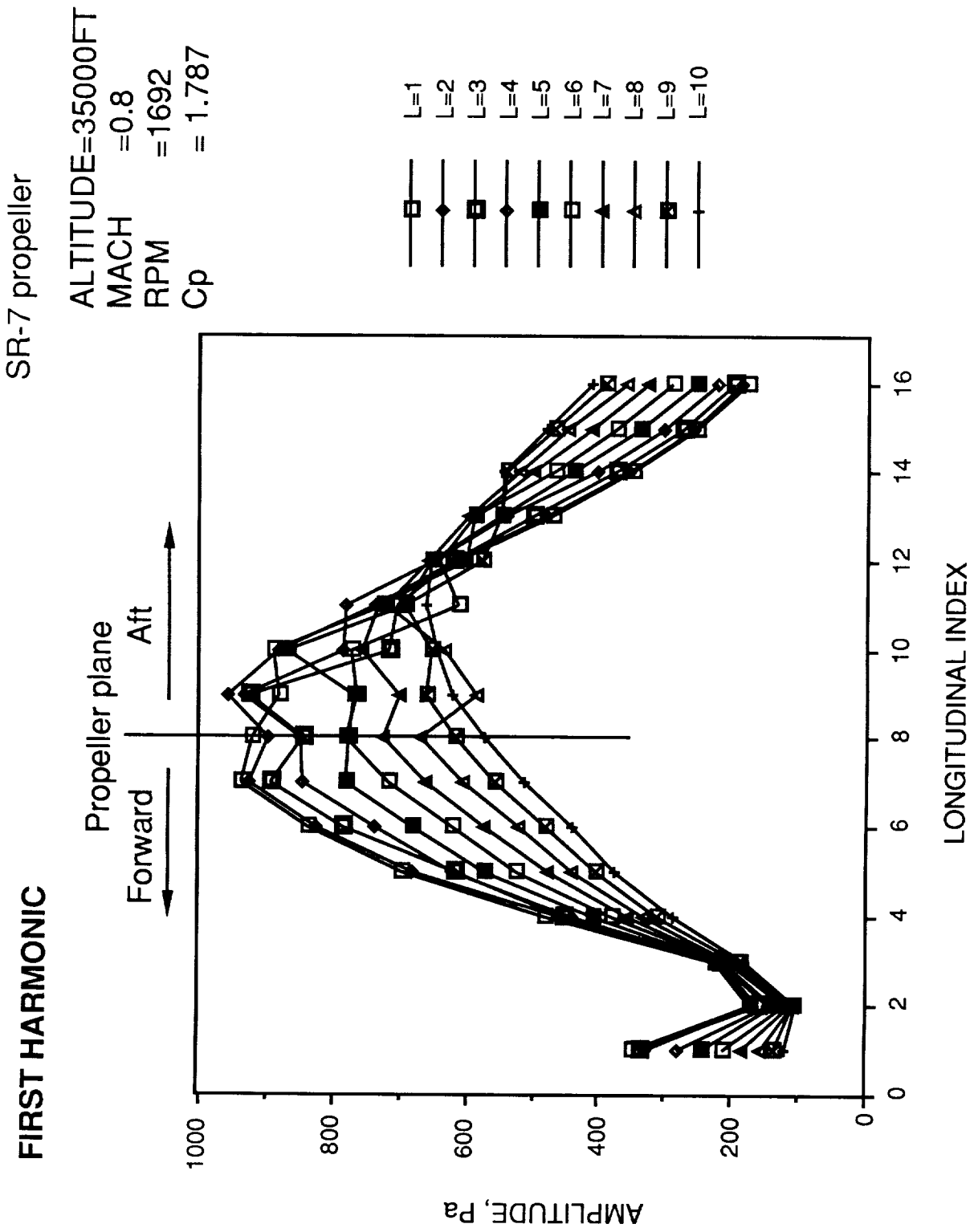
Figure 13.2   Amplitude of the first harmonic for the SR-7 ANOPP prediction.

FIRST HARMONIC

SR-7 propeller

ALTITUDE=25000FT
MACH   =0.8
RPM   =1777
Cp   = 1.56

L=1
L=2
L=3
L=4
L=5
L=6
L=7
L=8
L=9
L=10

Propeller plane

Forward Aft

AMPLITUDE, Pa

LONGITUDINAL INDEX
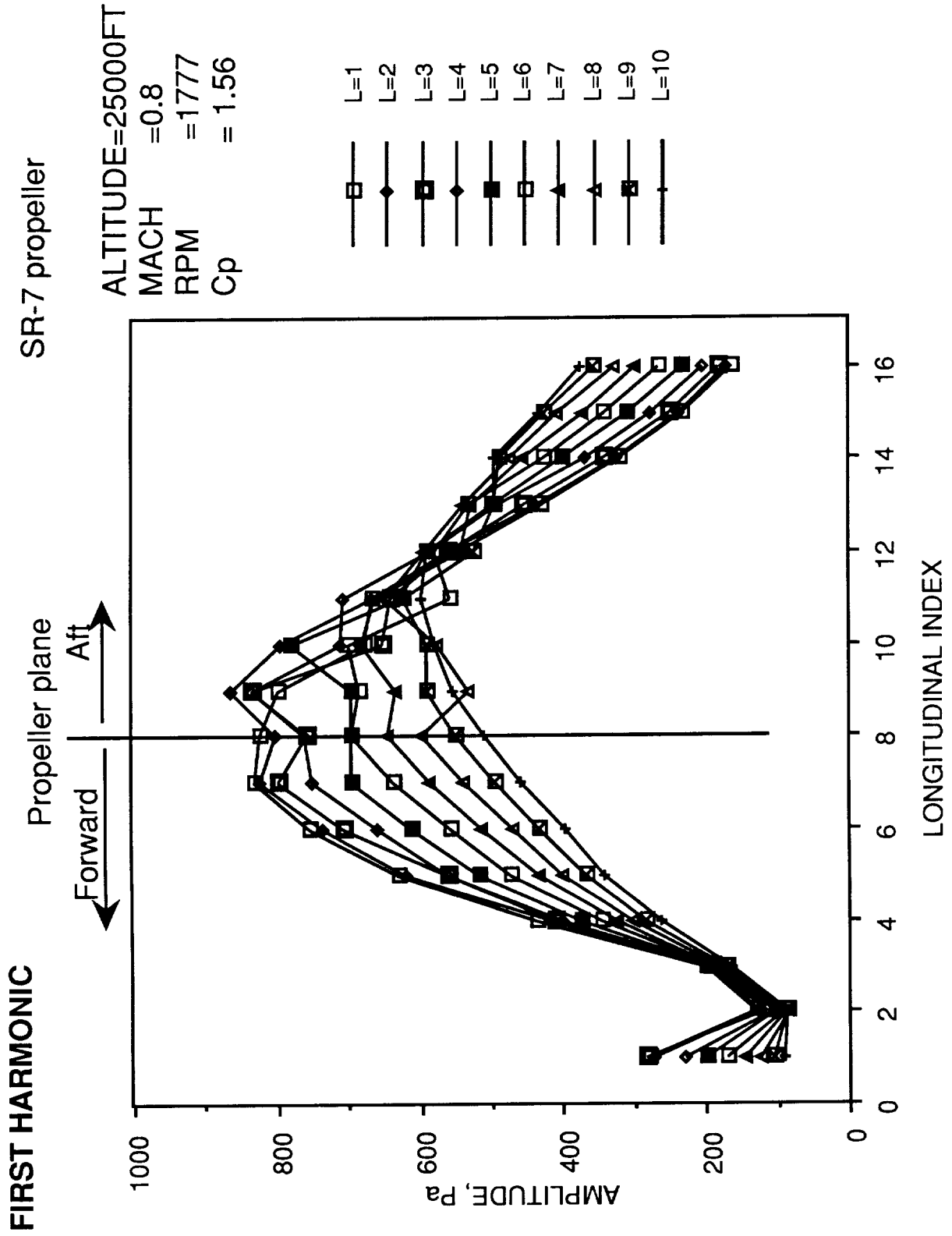
Figure 13.3   Amplitude of the first harmonic of the SR-7 ANOPP prediction.

FIRST HARMONIC

SR-7 propeller

ALTITUDE=15000FT
MACH =0.5
RPM =1692
Cp =1.33

L=1
L=2
L=3
L=4
L=5
L=6
L=7
L=8
L=9
L=10

Propeller plane

Forward   Aft
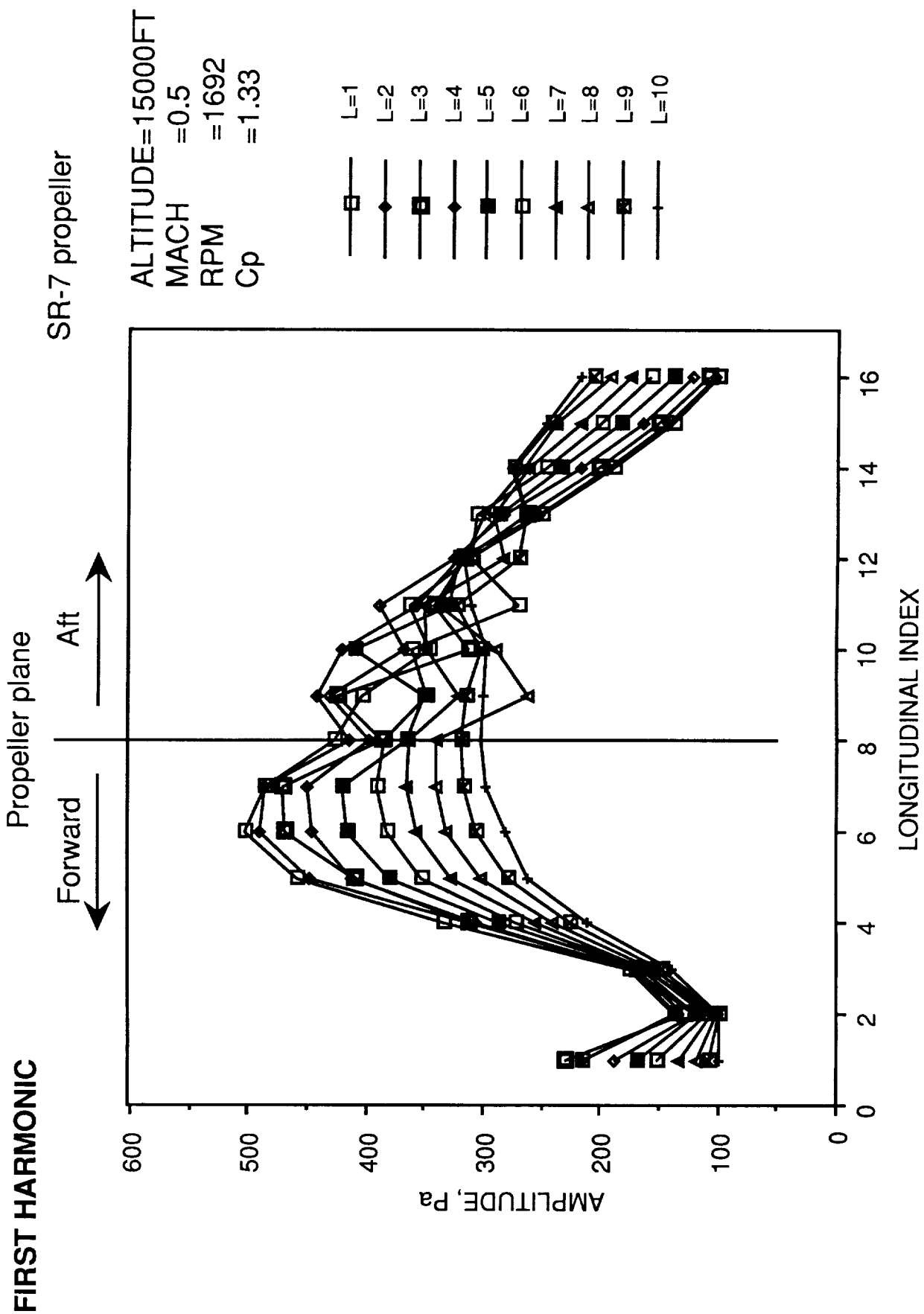
Figure 13.4   Amplitude of the first harmonic of the SR-7 ANOPP prediction.

88
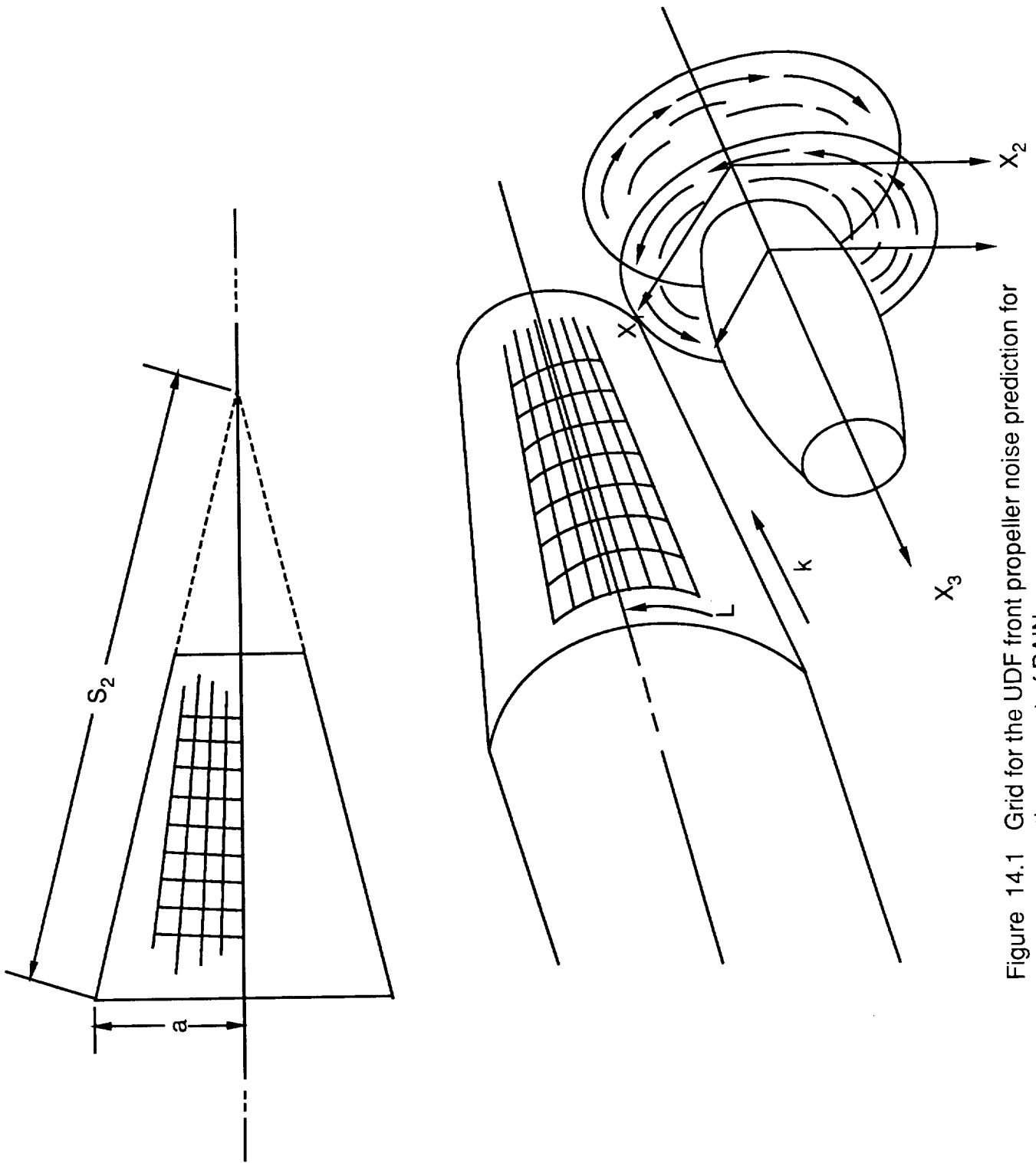
Figure 14.1 Grid for the UDF front propeller noise prediction for the support of PAIN.
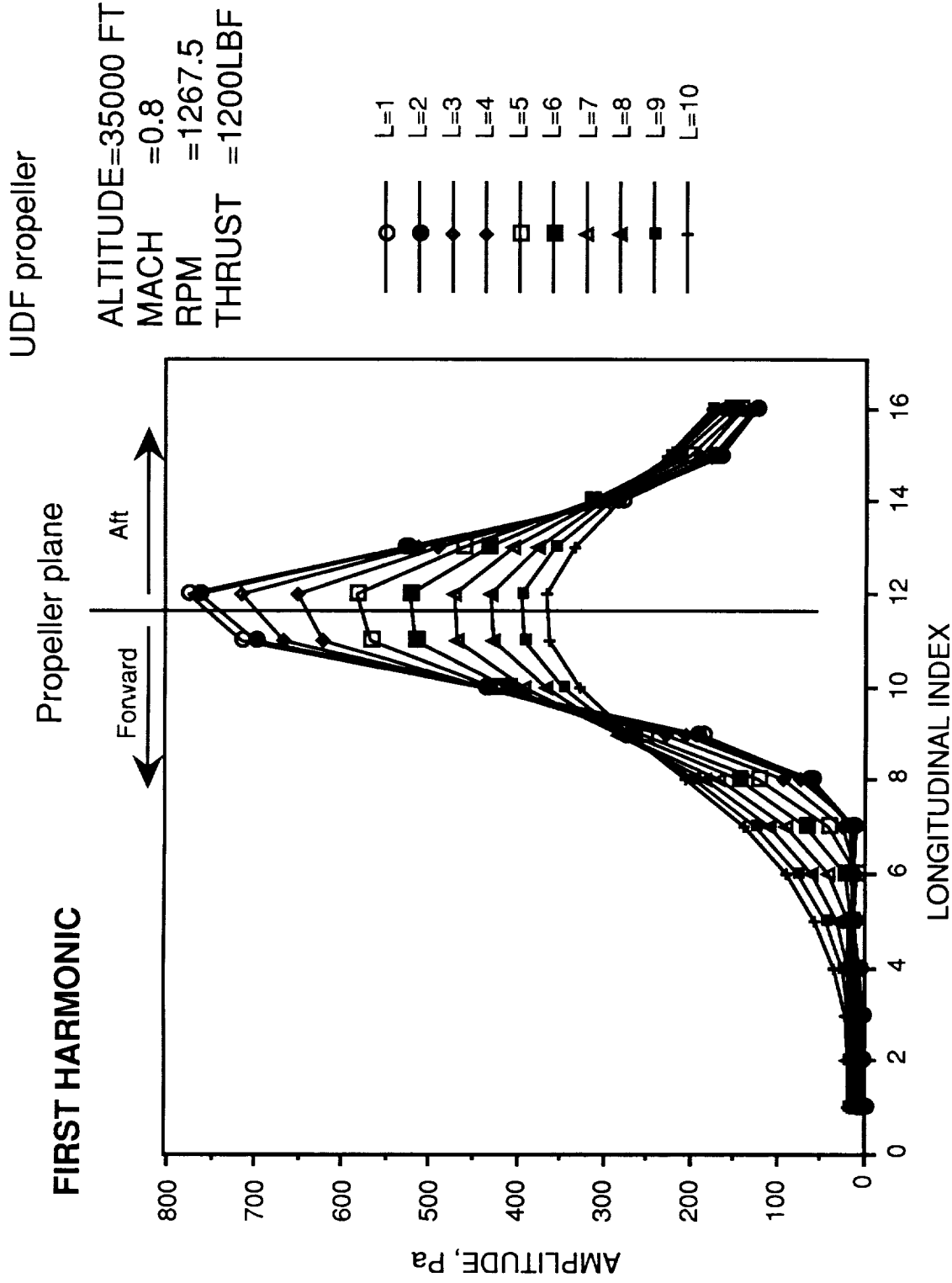
Figure 15.1 Amplitude of the first harmonic of the ANOPP prediction for UDF.
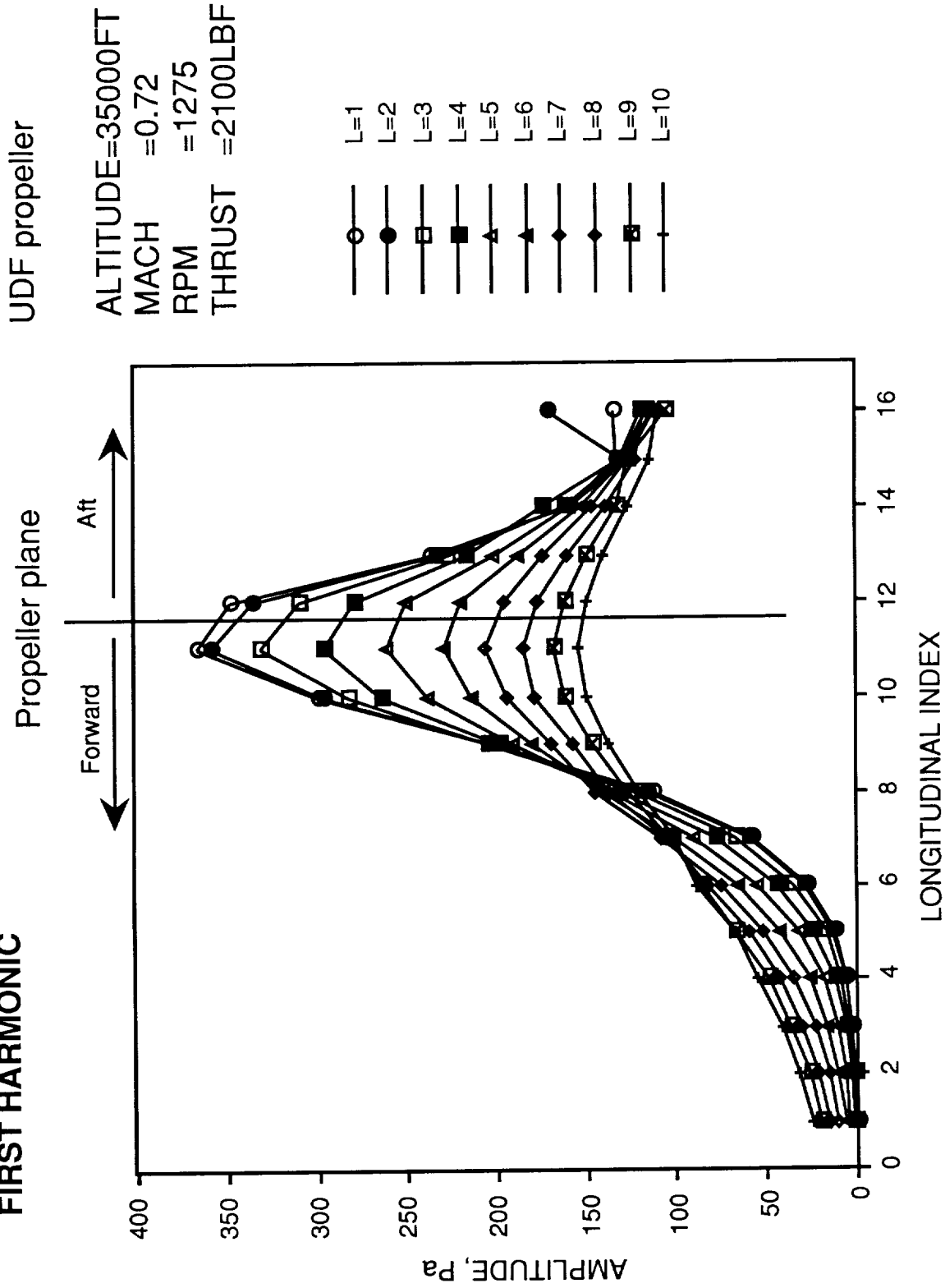
Figure 15.2   Amplitude of the first harmonic of ANOPP prediction for the UDF.
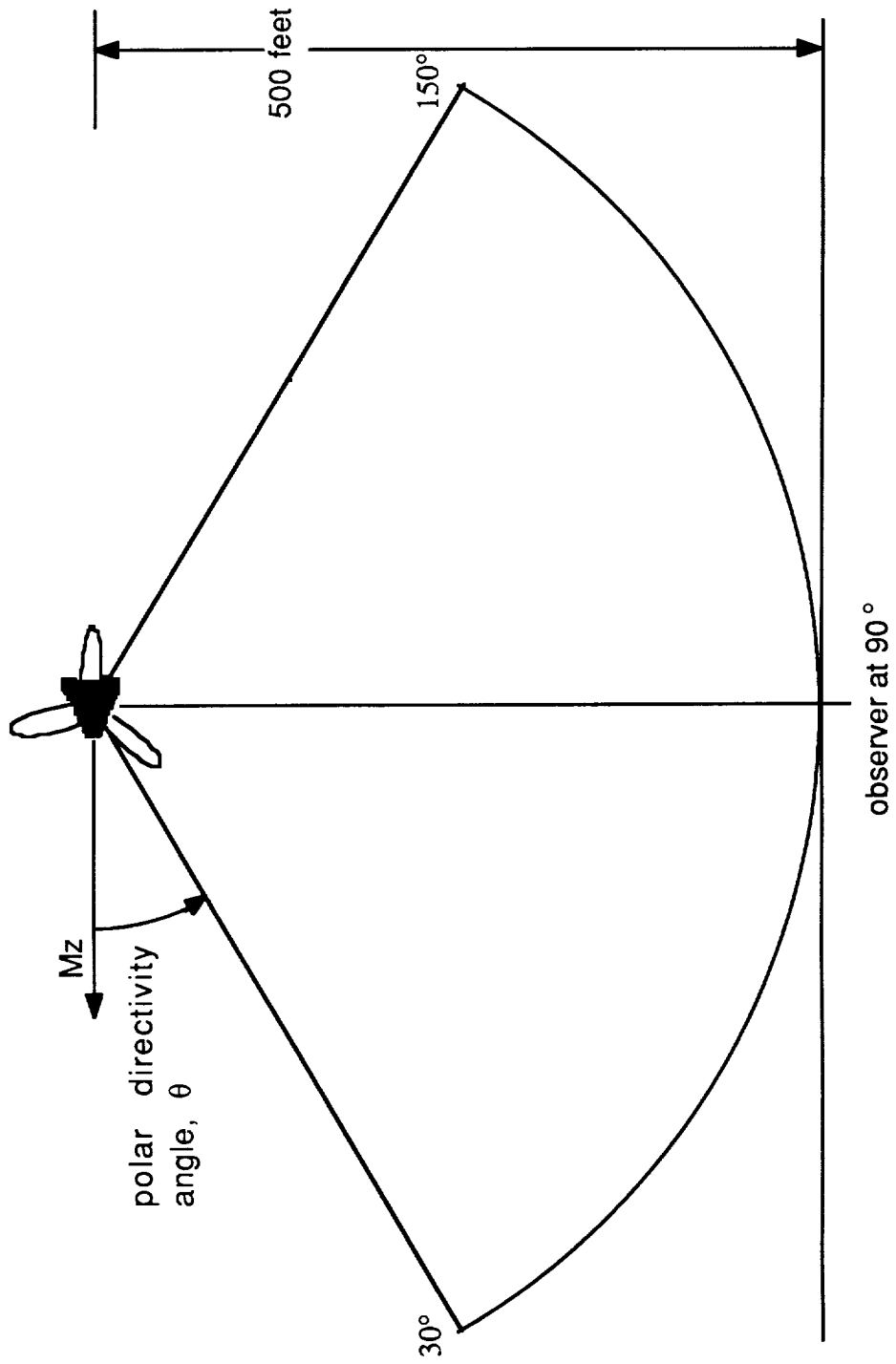
Figure 16.1　Source-to-observer positions used for the PTA propfan prediction.
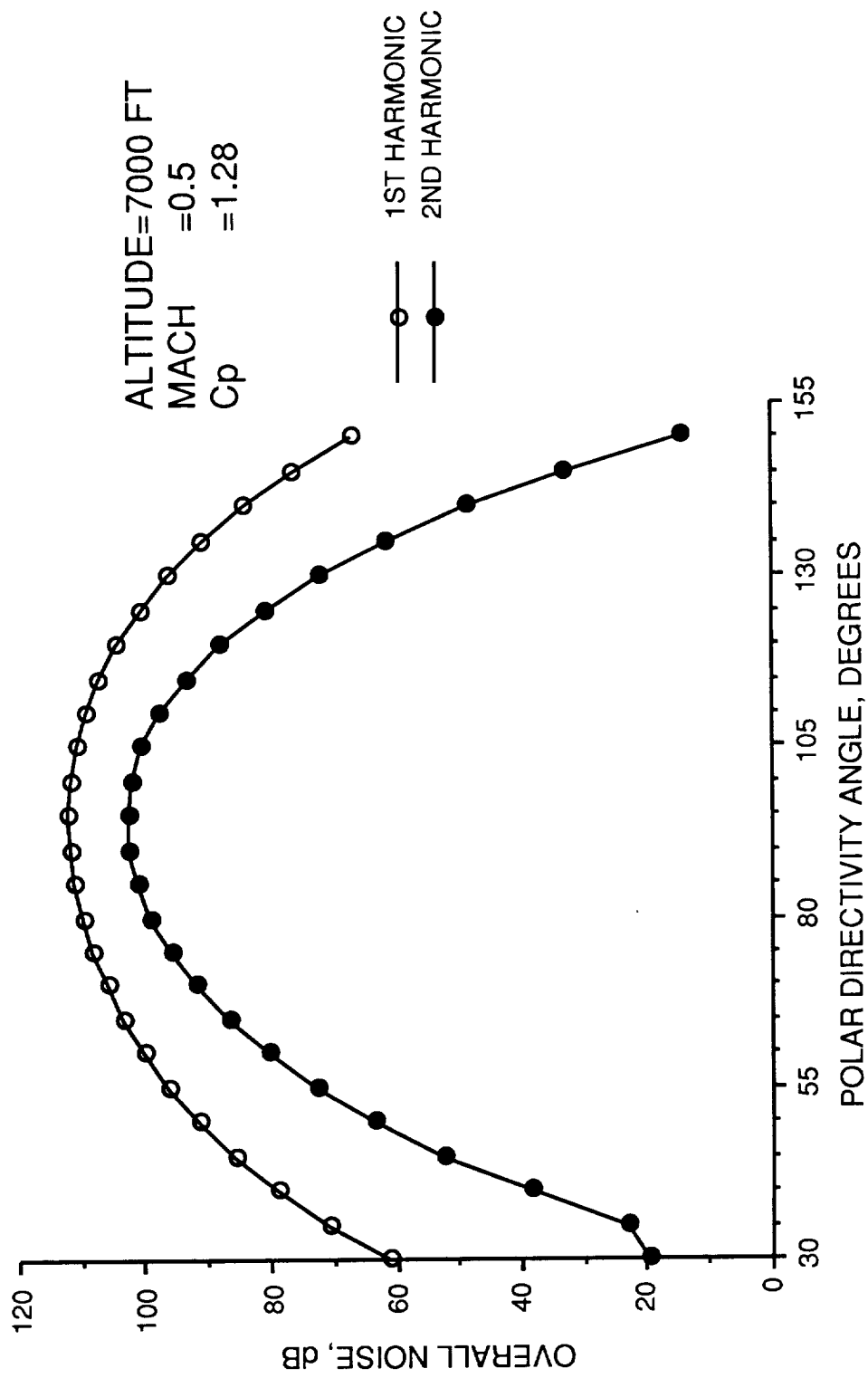
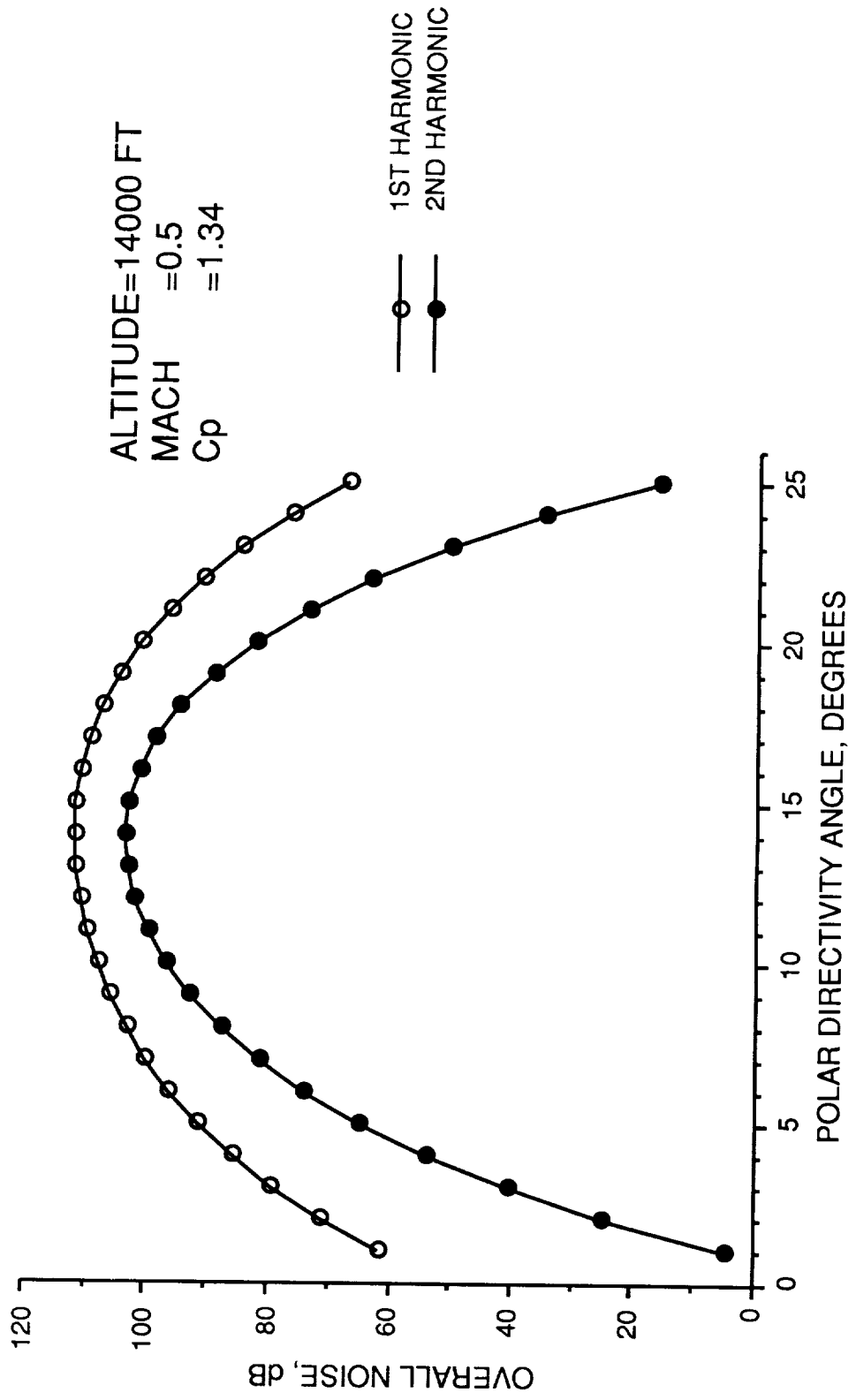Figure 17.1   Predicted noise level of the PTA propfan.
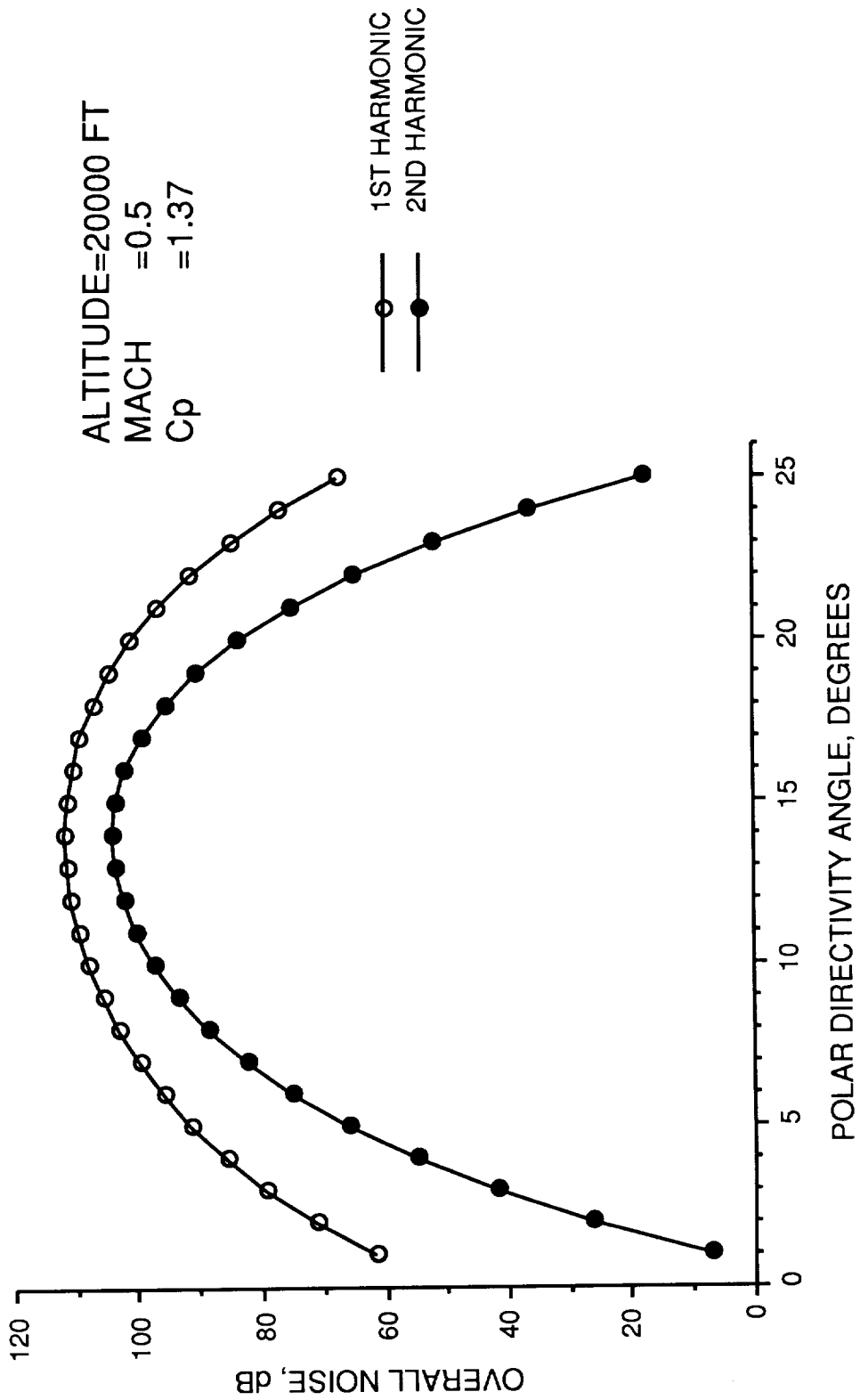
Figure 17.2 Predicted noise level of the PTA propfan.

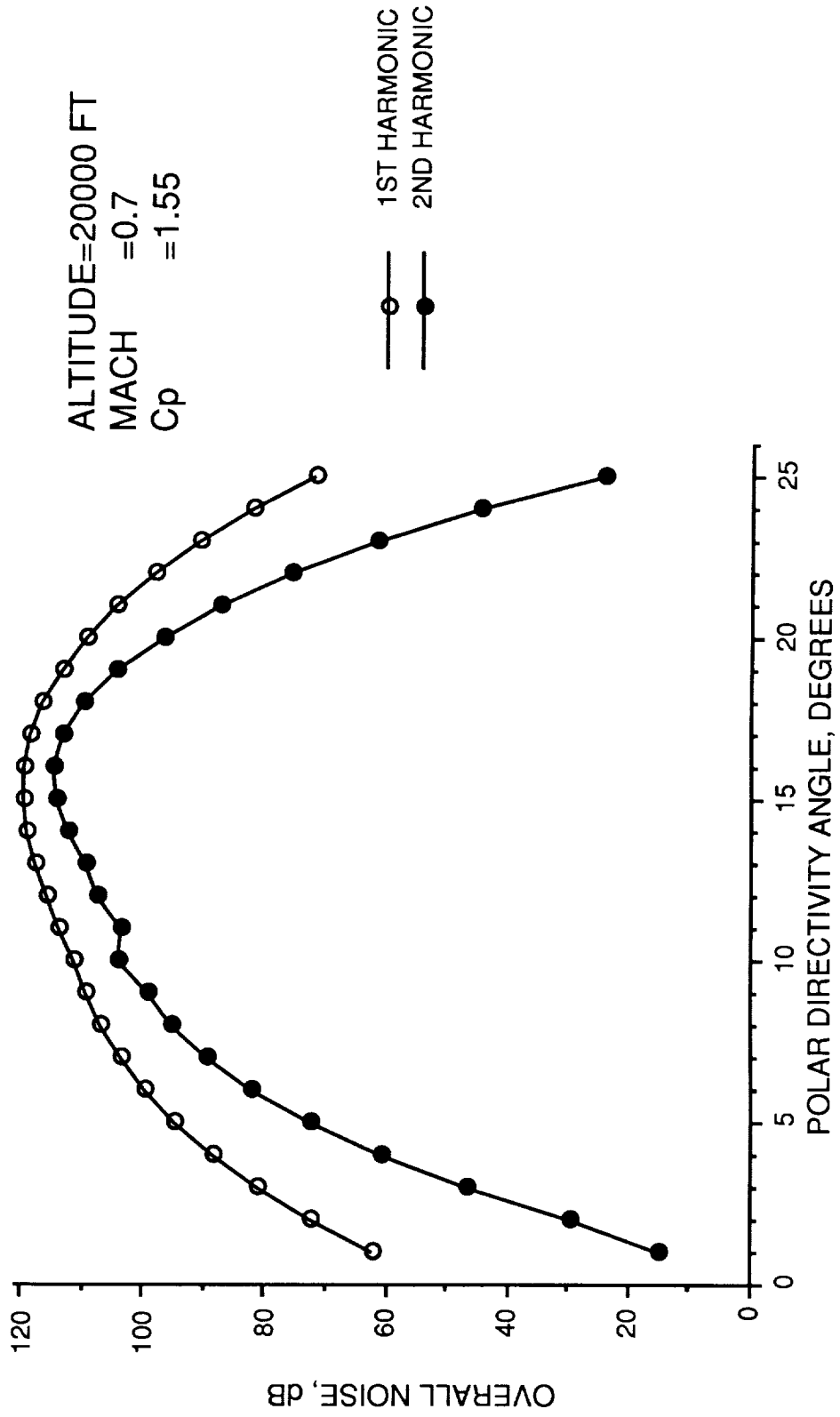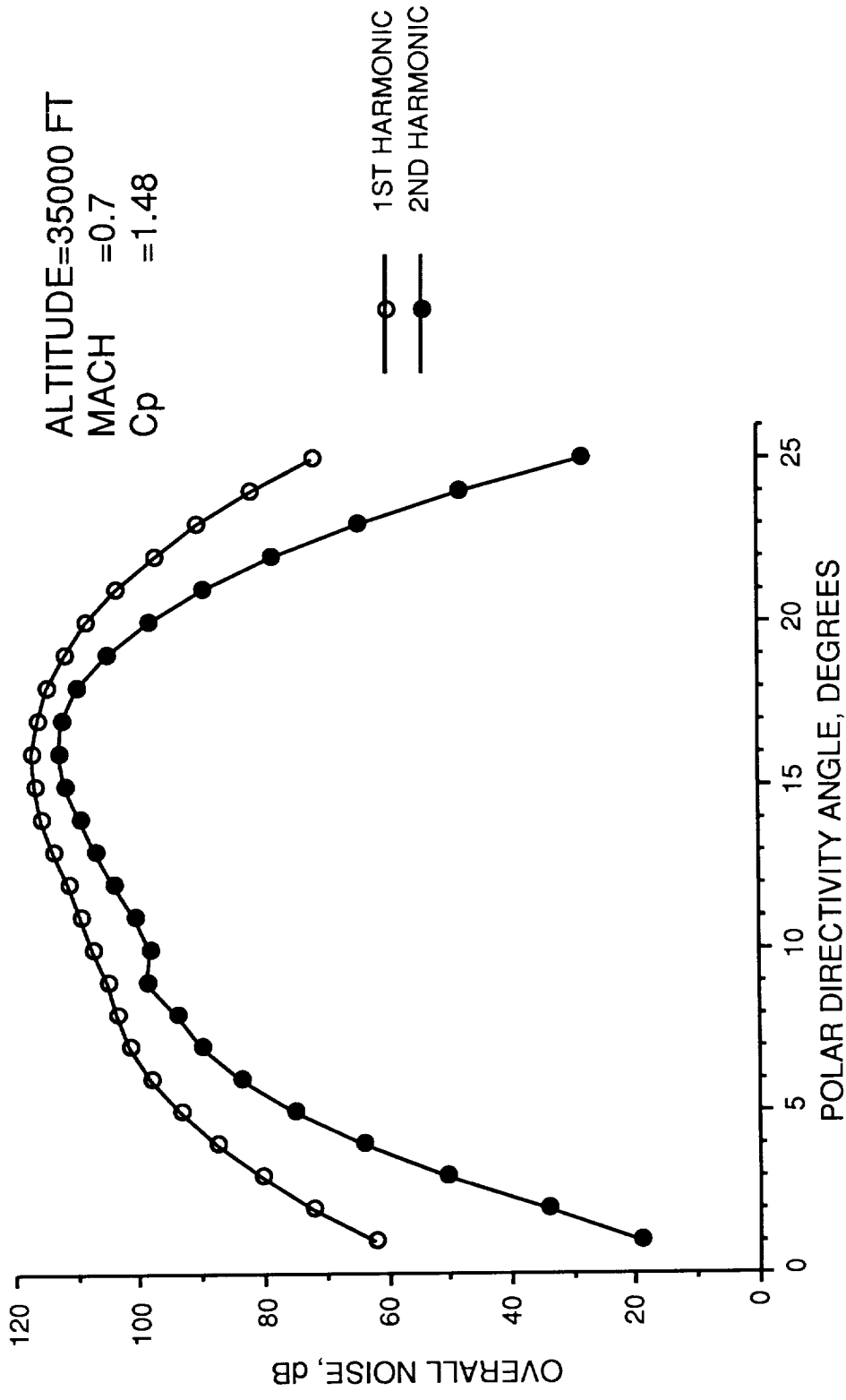Figure 17.3   Predicted noise level of the PTA propfan.

ALTITUDE=20000 FT
MACH   =0.5
Cp   =1.37

1ST HARMONIC
2ND HARMONIC

POLAR DIRECTIVITY ANGLE, DEGREES

OVERALL NOISE, dB

Figure 17.4   Predicted noise level of the PTA propfan.

ALTITUDE=20000 FT
MACH   =0.7
Cp   =1.55

1ST HARMONIC
2ND HARMONIC

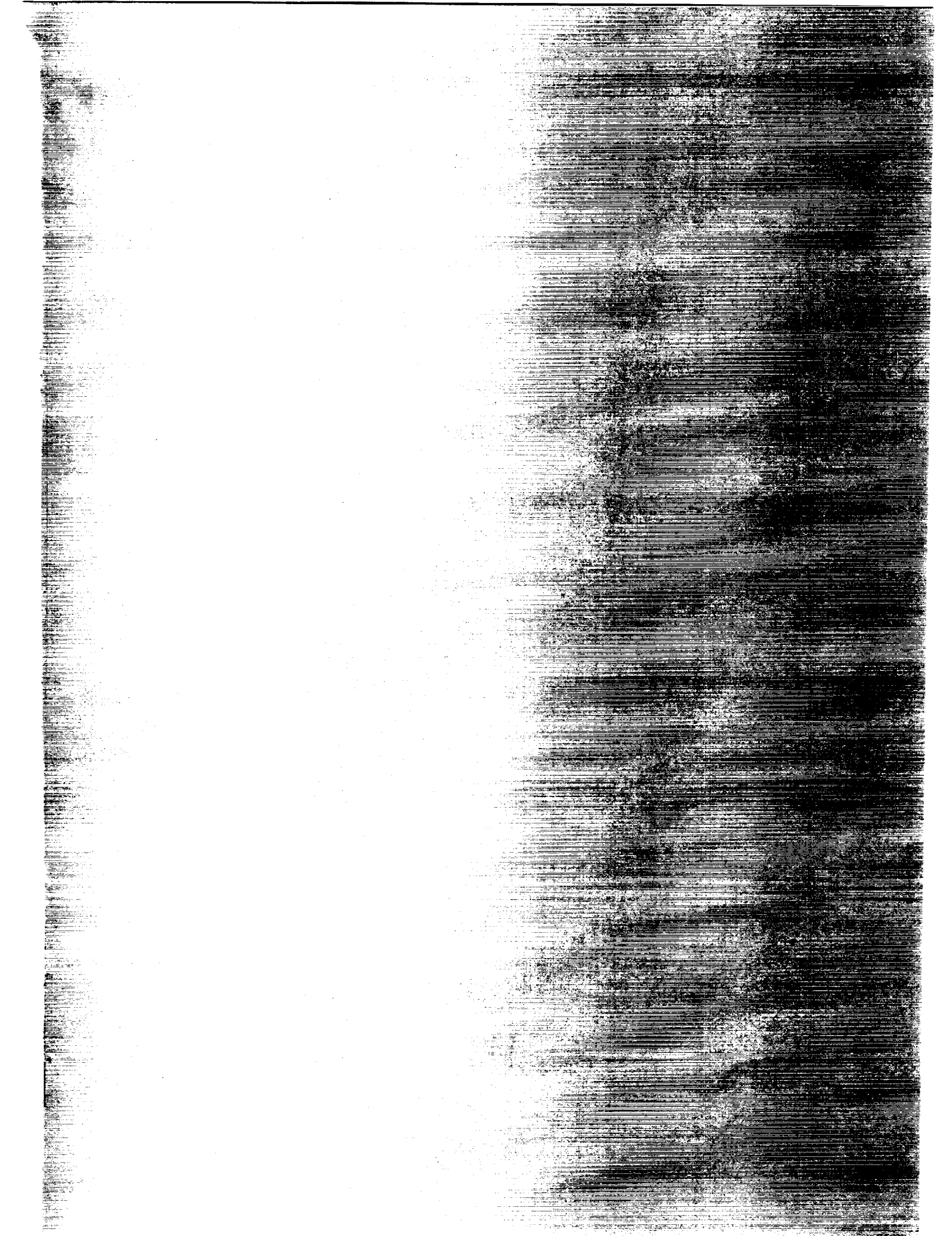POLAR DIRECTIVITY ANGLE, DEGREES

OVERALL NOISE, dB

Figure 17.5 Predicted noise level of the PTA propfan.

Report Documentation Page

1. Report No. NASA CR-4394	2. Government Accession No.	3. Recipient's Catalog No.

4. Title and Subtitle	5. Report Date September 1991
The NASA Aircraft Noise Prediction Program Improved Propeller Analysis System	6. Performing Organization Code

7. Author(s) L. Cathy Nguyen	8. Performing Organization Report No.
	10. Work Unit No. 532-06-37

9. Performing Organization Name and Address Lockheed Engineering & Sciences Company 144 Research Drive Hampton, VA 23666	11. Contract or Grant No. NAS1-19000
	13. Type of Report and Period Covered Contractor Report

12. Sponsoring Agency Name and Address National Aeronautics and Space Administration Langley Research Center Hampton, VA 23665-5225	14. Sponsoring Agency Code

15. Supplementary Notes

NASA Technical Monitor: Robert A. Golub, Langley Research Center

16. Abstract

This report describes the improvements and the modifications of the NASA Aircraft Noise Prediction Program (ANOPP) and the Propeller Analysis System (PAS). Comparisons of the predictions and the test data are included in the case studies for the flat plate model in the Boundary Layer Module, for the effects of applying compressibility corrections to the lift and pressure coefficients, for the use of different weight factors in the Propeller Performance Module, for the use of the improved retarded time equation solution, and for the effect of the number of grids in the Transonic Propeller Noise Module. The DNW tunnel test data of a propeller at different angles of attack and the Dowty Rotol data are compared with ANOPP predictions. The effect of the number of grids on the Transonic Propeller Noise Module predictions and the comparison of ANOPP TPN and DFP-ATP codes are studied. In addition to the above impact studies, the transonic propeller noise predictions for the SR-7, the UDF front rotor, and the support of the enroute noise test program are included.

17. Key Words (Suggested by Author(s)) Propeller noise prediction, ANOPP, Propeller analysis system, Transonic propeller noise prediction	18. Distribution Statement Unclassified-Unlimited Subject Category: 71

19. Security Classif. (of this report) Unclassified	20. Security Classif. (of this page) Unclassified	21. No. of pages 104	22. Price A06

NASA FORM 1626 OCT 86